R82-09 OSP 89184

SUBSCALE STEAM TESTS OF VAPOR SUPRESSION POOL MIXING AND CIRCULATION WITH APPLICATION TO THE SHOREHAM NUCLEAR POWER STATION

by
E. Eric Adams
and
Richard M. Baker

RALPH M. PARSONS LABORATORY
HYDRODYNAMICS AND COASTAL ENGINEERING

Report No. 273

Prepared for
Stone and Webster Engineering Corporation
Boston, Massachusetts
and
Long Island Lighting Company
Hicksville, New York

December, 1981

MIT

DEPARTMENT
OF
CIVIL
ENGINEERING

SCHOOL OF ENGINEERING
MASSACHUSETTS INSTITUTE OF TECHNOLOGY
Cambridge, Massachusetts 02139

R82-09

OSP 89184

SUBSCALE STEAM TESTS OF VAPOR SUPRESSION POOL MIXING AND CIRCULATION WITH APPLICATION TO THE SHOREHAM NUCLEAR POWER STATION

by

E. Eric Adams

and

Richard M. Baker

RALPH M. PARSONS LABORATORY

HYDRODYNAMICS AND COASTAL ENGINEERING

Report No. 273

Prepared for

Stone and Webster Engineering Corporation

Boston, Massachusetts

and

Long Island Lighting Company

Hicksville, New York

DECEMBER, 1981

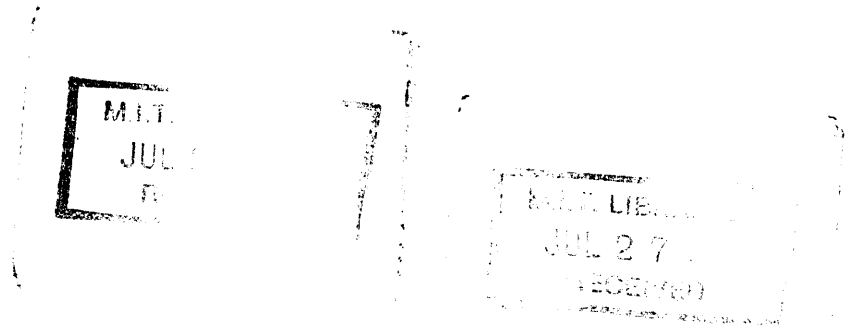
JUL 27

ABSTRACT

This report addresses the temperature distribution induced within a suppression pool by a steam discharge. The problem is first examined theoretically to identify the dominant zones and to estimate circulation and mixing occuring within each zone. This analysis is then used to justify physical model tests using a 1/17 Froude scale model employing an actual steam source. Results complement earlier sub-scale tests at MIT performed by Soliva (1980) using hot water in place of steam.

Experiments were performed to test sensitivity to the number of quencher ports, the fractional area of basin flow resistance, the initial water depth and the quencher orientation and location within the pool. Model results can be used to help understand the physical processes underlying pool mixing and circulation and to help extrapolate prototype temperature measurements from one site to another.

ACKNOWLEDGMENTS

This study was sponsored by Stone and Webster Engineering Corporation, Boston, Massachusetts, under Stone and Webster ESSOW No. SH1-474 and MIT OSP No. 89184. The authors wish to thank Mr. Jim Metcalf and Mr. Don Desmarais of Stone and Webster for their cooperation throughout the study.

The experiments were conducted by Mr. Richard Baker, Graduate Research Assistant under the supervision of Dr. Eric Adams, Principal Research Engineer, MIT Energy Laboratory, and Lecturer, Department of Civil Engineering. The report was typed by Mrs. Carole Solomon and Ms. Carol Erickson.

This study has been a follow-up to a previous theoretical study by Dr. Adams and Professors Keith Stolzenbach and Donald Harleman of the Department of Civil Engineering and previous experimental study by Mr. Jean-Charles Soliva, Graduate Research Assistant. Appreciation is expressed to Mr. David Kubiak, Graduate Research Assistant, and Mr. Roy Milley, Machinist, for their assistance in helping adapt the experimental set-up of Mr. Soliva for the present tests.

TABLE OF CONTENTS

I. INTRODUCTION

1.1 Suppression Pool Mixing and Circulation

The problem to be investigated concerns the mixing and circulation which is induced by steam discharge into a pool of water. The specific motivation concerns the performance of the vapor suppression pool of a GE MK II BWR as the result of the operation of one or more safety relief valves. In such a case steam is vented through a quencher to the vapor suppression pool where condensation occurs. The pool and a quencher used at the Shoreham Nuclear Station are illustrated in Figures 1 and 2.

In order to guarantee smooth continuous condensation, a local temperature limit is placed on the suppression pool water in the immediate vicinity of the quencher. As a condition for obtaining an operating license, a utility must demonstrate that this temperature limit will not be exceeded during various plant transients including a stuck open relief valve (SORV). The focus of this study, then, has to do with the local temperature rises near, but not within, the condensing steam plume. Detailed data regarding quencher condensation performance as a function of the local temperatures have been generated at (quencher) vendor facilities. Pool-wide (bulk) temperatures can be analytically predicted for various plant transients including SORV through the use of a thermal energy balance. Thus knowledge of the local-to-bulk temperature differences as a function of time would allow one to evaluate the performance of the quencher under particular loading conditions.

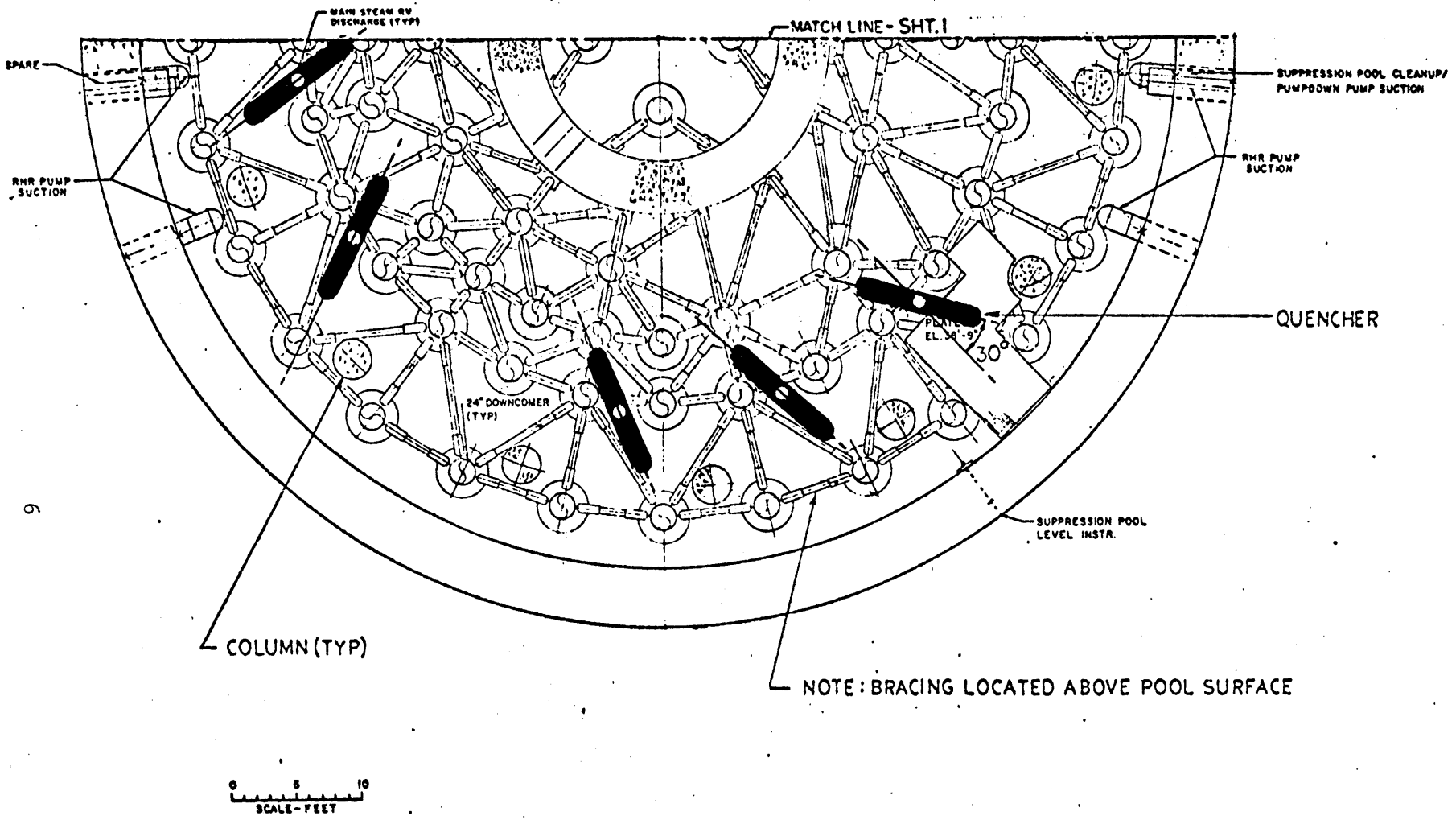

Figure 1 Sketch of Suppression Pool

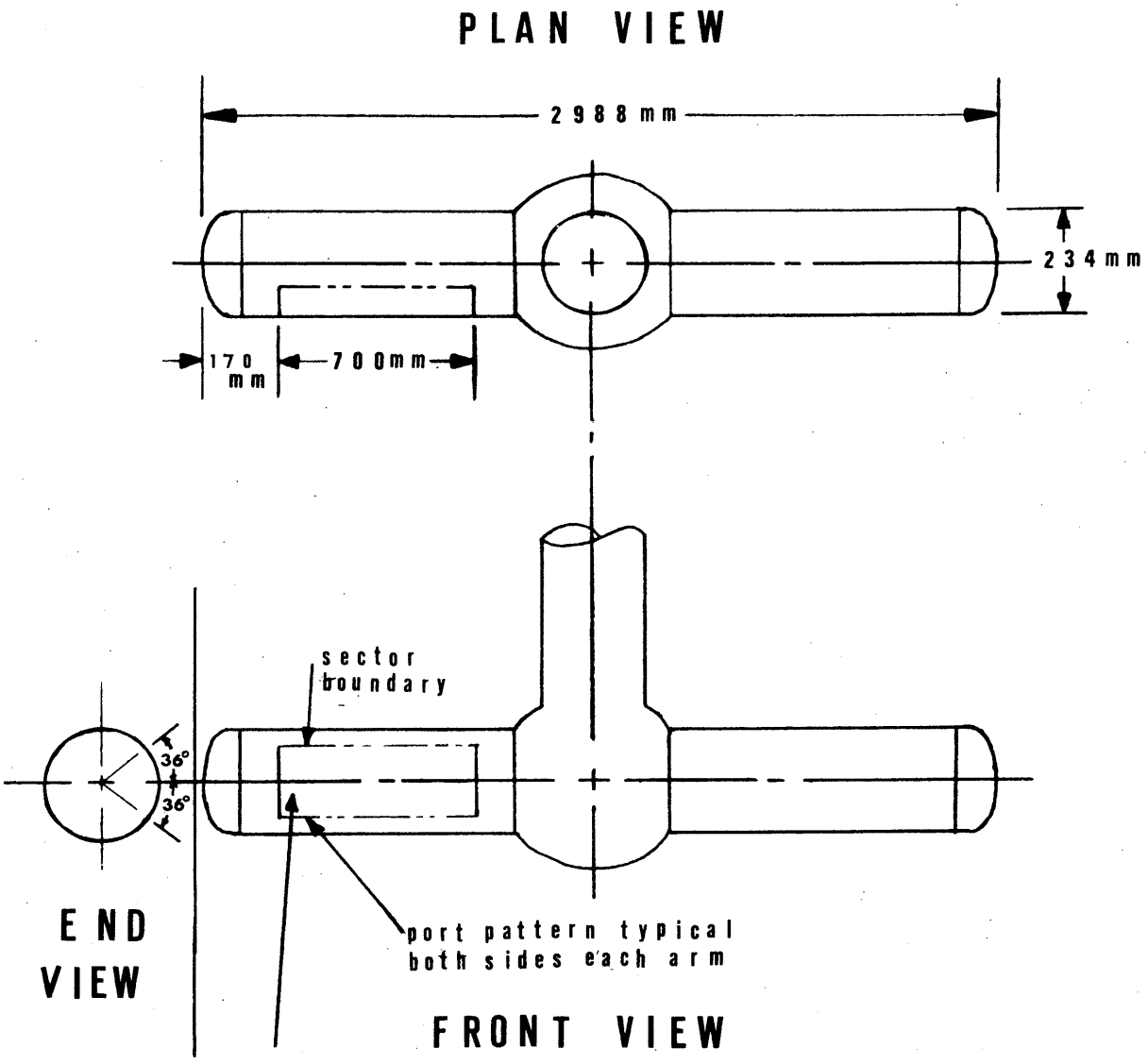

Figure 2: KWU T-Quencher (not to scale)

The present practice with respect to the local-to-bulk temperature difference is to rely on prototype tests conducted prior to commercial operation of the power plant. Because of safety specifications, these tests can only be conducted at low bulk temperatures and thus they can only be conducted for short durations (order of 10 to 15 minutes). By observing the convergence of the local and bulk temperatures during the latter portions of these in-plant tests, it has been assumed that the maximum local-to-bulk temperatures observed during the short duration of the prototype test would not be exceeded for long durations. By subtracting this maximum local-to-bulk temperature from the local limit one can establish an acceptable upper limit for bulk temperature.

1.2 Desirability of a Sub-scale Model

There are several general reasons why it would be desirable to use a sub-scale physical model to help assess these local temperatures. First, results from a sub-scale model could be used to help extrapolate the results of full-scale tests conducted at existing stations to represent conditions which would be expected at future stations, thus reducing the need for additional costly full-scale tests at the new stations. Second, because sub-scale tests are not limited by safety considerations existing in operating nuclear power plants, they may be used to simulate higher temperatures (and thus longer test durations) than prototype tests. Third, such tests could be used to help understand the physical processes underlying pool mixing and circulation. This understanding, in turn, could be used to help develop, calibrate or verify mathematical models of these processes. Experimental results could also be used

directly to suggest improvements in quencher design,location and orientation.

1.3 Application to Shoreham Nuclear Power Station

The experiments discussed in this report pertain to the 850 MWe Unit 1 of the Shoreham Nuclear Power Station. The station is located in the Town of Brookhaven on the north shore of Long Island and is being constructed for Long Island Lighting Company (LILCO) by Stone and Webster Engineering Corporation of Boston, Massachusetts.

Figure 1 shows a plan view of the Shoreham Unit 1 suppression pool highlighting the locations of a number of the eleven KWU T-Quenchers which will be used. LILCO and Stone and Webster plan to address the question of local-to-bulk temperature differences by a combination of physical model study and use of prototype data, Specifically, by the time fuel is loaded at Shoreham, LILCO and Stone and Webster expect that prototype data will be available from the LaSalle County Nuclear Station in Illinois. While the Shoreham and LaSalle units are similar (both GE MK II BWR's), the pool geometries (especially operating water depths) and quencher orientations are different. These differences are illustrated in Figure 3. The purposes of the sub-scale tests reported herein are (1) to justify the general validity of sub-scale model tests and (2) to explore the sensitivity of pool temperature distribution to the variables of water depth and quencher orientation. The results of this sensitivity test will then be used by Stone and Webster to rescale the LaSalle prototype results for use at Shoreham.

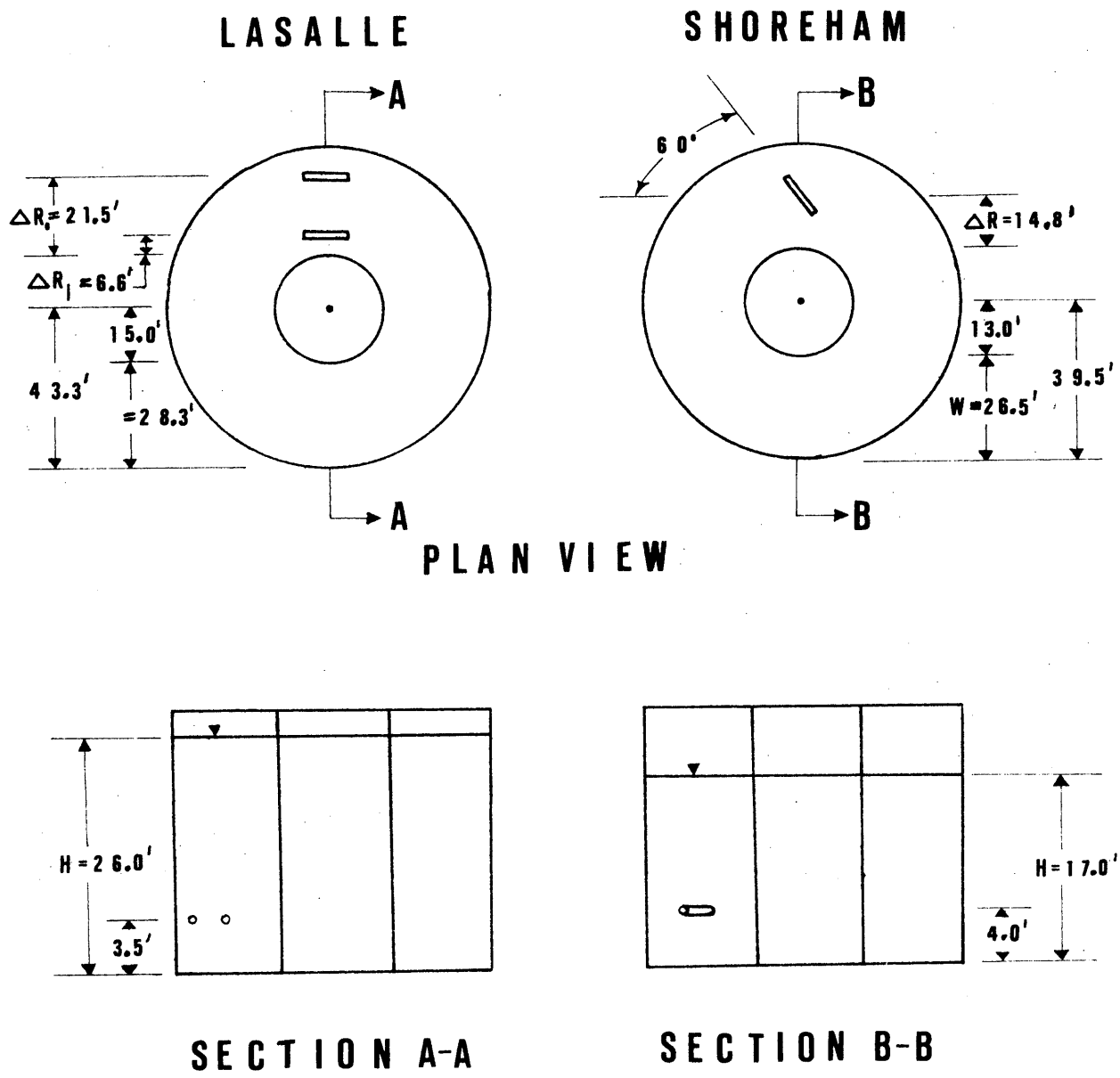

Figure 3: Schematic Comparison of Suppression Pools and Quencher Configurations at LaSalle and Shoreham

1.4 Outline

The report proceeds as follows. In Chapter II the problem of mixing is broken into various zones which are associated with particular physical processes. The behavior of each zone and the limitations of various scaling approaches are analyzed. In Chapter III a dimensional analysis is performed which leads to the derivation of various dimensionless parameters which must be maintained from prototype to model in order that dynamic, kinematic, thermodynamic and geometric similarity be maintained. Chapter III also includes the description of the model tank built to verify these approaches and to explore the required sensitivities. In Chapter IV test results are presented and analyzed. Conclusions based on the test results are summarized in Chapter V.

1.5 Relationship to Previous Sub-scale Tests at MIT

The tests reported herein were conducted using actual steam as the source. These tests complement some preliminary tests performed at MIT using hot water as an analog for the steam source. The report describing these tests (Soliva, 1980) also includes development of several simple mathematical models of pool mixing and circulation. Because much of the theoretical justification for the use of a steam source and a hot water source is similar, this discussion has been taken largely from the earlier report. However, for details of the mathematical analysis or the results of the hot water tests the reader is referred to Soliva (1980).

II. THEORETICAL CONSIDERATIONS

Figure 4 is a sketch of the various zones which are thought to characterize the problem. These zones include:

1. Condensation zone
2. Individual jet merging zone
3. Buoyant jet zone
4. Near field circulation zone
5. Far field circulation zone

It is clear from the discussion of objectives that interest centers around temperatures in Zone 4 and in particular on the temperature within that part of Zone 4 which provides the entrainment for Zones 1 and 2. Because the zones are interrelated, however, it is necessary to discuss all of them.

2.1 Condensation Zone

An actual quencher has a large number of small holes; their arrangement has been designed by the vendor so that condensation occurs for each jet, before substantial interaction between jets takes place. Thus there are many condensation zones. Only one such zone is illustrated in Figure 4. The length of this zone (distance from the quencher manifold) will vary with the degree of subcooling (local temperature of the receiving water below the temperature of steam saturation) but is expected to be of the order of 10 jet diameters (Stanford and Webster, 1972). This is confirmed by movies of the quencher operation. Within this distance, the

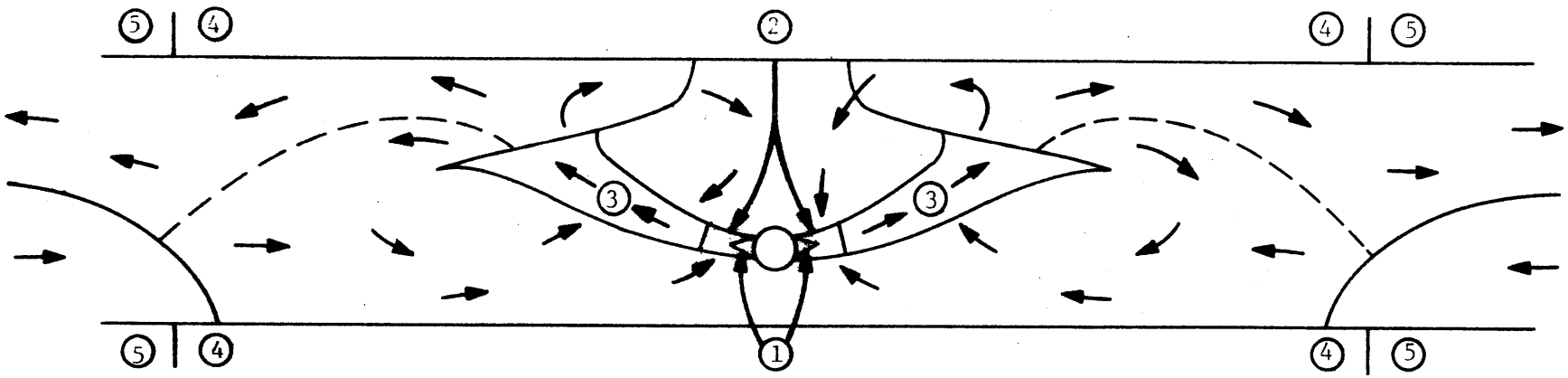

a) Qualitative Flow Field Description

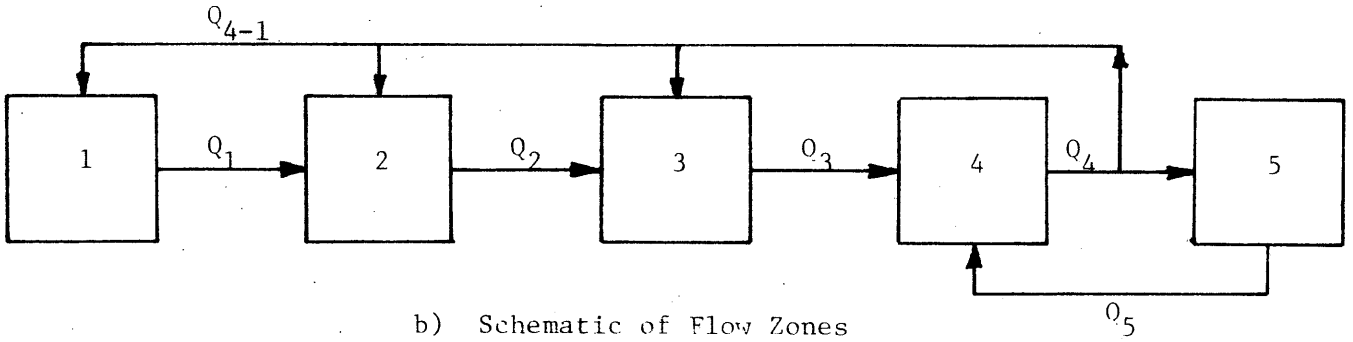

b) Schematic of Flow Zones

Figure 4 Zones of Analysis

aggregate mass flux from the individual jets increases due to entrainment. If the flow is assumed to be isenthalpic (i.e., negligible conversion of steam kinetic energy to sensible or latent thermal energy) then

$$\rho_1 Q_1 h_1 = \rho_s Q_s h_s + \rho_4 Q_{4-1} h_4 \qquad (2.1)$$

where ρ is the fluid density, Q is the volumetric flow rate (e.g., ft^3/s), h is the enthalpy and the subscripts refer to the various zones. Thus, for example, $\rho_s Q_s$ represents the mass rate of steam G_s leaving the quencher, $\rho_1 Q_1$ represents the mass rate of liquid leaving Zone 1 and $\rho_4 Q_{4-1}$ represents the mass flow rate of liquid entrained from Zone 4 towards Zone 1. The dilution at the end of Zone 1 is defined as

$$S_1 = \frac{\rho_1 Q_1}{\rho_s Q_s} \qquad (2.2)$$

For a given mass rate G_s, density ρ_s and flow rate Q_s will vary according to the steam state. Therefore it is convenient to define the source mass rate in terms of the density of water ρ_o and an "equivalent water" volumetric flow rate Q_o such that $\rho_s Q_s = \rho_o Q_o$. Because water can be treated as incompressible, $\rho_o = \rho_1 = \rho_2 = \rho_3 = \rho_4 = \rho_5 = \text{const}$. Equation (2.2) thus reduces to

$$S_1 = \frac{Q_1}{Q_o} \qquad (2.3)$$

S_1 will be a function of the degree of sub-cooling. Table 1 lists the approximate values of S_1 needed to just condense the entire steam jet at the end of Zone 1 based on a steam enthalpy of 1200 BTU/lbm (typical steam loading conditions; Stone and Webster, personal communication). Because the edges of

TABLE 1

MINIMUM DILUTION S_1 AT THE END OF ZONE 1 NEEDED TO QUENCH STEAM AS A FUNCTION OF THE LOCAL TEMPERATURE T_4

(assumes h_s = 1200 BTU/lbm, T_1 = 220°F)

T_4 (°F)	h_4 (BTU/lbm)	$S_1 = \frac{h_s - h_4}{h_1 - h_4}$
32	0	6.4
60	28	7.3
100	68	9.4
140	108	13.6
180	148	26.3
220	188	∞

the entrained liquid will be sub-cooled before the core of the steam jet has condensed, the actual dilutions at the end of the condensation zone will be higher.

The condensation of a steam jet is expected to depend on the exit velocity, as characterized by the Mach number. Because it is not feasible to simultaneously model Mach number along with the other parameters which characterize the remaining zones, Zone 1 will not be modeled accurately in a sub-scale model. However, replacing this zone with an "equivalent" zone should be adequate as long as the characteristic temperatures in Zone 4 are unaffected.

2.2 Individual Jet Merging Zone

This zone incorporates Zone 1 and is the region in which the individual jets merge to form coherent plumes. The length of this zone (distance from the quencher) depends on the rate of liquid jet spreading and is estimated as approximately ten times the lateral jet spacing. Within this distance it is expected, based on analysis of free liquid jets, that the dilution will be approximately double. If S_{1-2} represents this additional dilution and S_2 represents the overall dilution at the end of Zone 2 then

$$S_2 = \frac{Q_2}{Q_o} \tag{2.4}$$

At a local temperature $T_4 = 100^{\circ}F$, the value of S_2 would be about 20. As with Zone 1 it is not possible (due to Reynolds number effects) or practical (because the holes would be too small) to model Zone 2 precisely. However, this would not be necessary as long as the influence on the remaining zones is preserved. In this regard, what is important is the

TABLE 2 APPROXIMATE CONDITIONS AT THE QUENCHER ORIGIN (SUBSCRIPT s or o USED IN TEXT) AND AT THE END OF ZONE 2 (SUBSCRIPT 2 USED IN TEXT)

Variable	Symbol	Units	Value at Quencher	Value at End of Zone 2	Comments
mass flux	G	$\frac{lbm}{s}$	240	4800	assumes dilution $S_2 = S_1 \cdot S_{1-2} = (10)(2) = 20$
energy flux (above ambient)	$E = G(h-h_4)$	$\frac{BTU}{s}$	2.9×10^5	2.9×10^5	assumes enthalpy of steam, $h_s = 1200 \frac{BTU}{lbm}$
kinematic momentum flux	$M(=\frac{Gu}{\rho_w})$	$\frac{ft^4}{s^2}$	6130	6130	assumes sonic exit velocity, $u_o = 1600 \frac{ft}{s}$
characteristic jet temperature	T	^oF	330	150	assumes $T_4 = 100^oF$ and $S_2 = 20$
characteristic source density	ρ	$\frac{lbm}{ft^3}$	.16	61.999	assumes pressure at quencher port = 60 psia
volumetric flow rate (water equiv.)	$Q(=G/\rho_w)$	$\frac{ft^3}{s}$	3.85	77	
kinematic buoyancy flux	B	$\frac{ft^4}{s^3}$	42 21	42 21	from eqn.(2.12) using $\Delta h_{s_1} = 1130$ BTU/lbm and $\beta_1 = .0003^oF^{-1}$ (top) and $.00015^oF^{-1}$ (bottom)
characteristic jet velocity	u	$\frac{ft}{s}$	1600	79	
aggregate jet cross-section area	A	ft^2	.94 .0024	.97	actual port area (top) and water equivalent area, Q_o/u (bottom)
characteristic jet dimension	$\ell(=\sqrt{A/4})$	ft	.48 .025	.49	assumes two equivalent round jets on either side of quencher

TABLE 2 (Continued)

Variable	Symbol	Units	Value at Quencher	Value at End of Zone 2	Comments
jet densimetric Froude number	$\mathbb{F}$ ($\mathbb{F}^2=u^2/g\,\frac{\rho_4-\rho}{\rho_4}\,\ell$)	N.D.	---	~250	
relative water depth	$\frac{H}{\ell}$	N.D.	---	38	based on water depth of 17 feet
relative jet submergence	$\frac{Y}{\ell}$	N.D.	---	26	assumes quencher is 4 feet off of floor
momentum-buoyancy parameter	$M^{3/4}/B^{1/2}H$	N.D.	5.3 7.5	5.4 7.5	based on β = $.0003^{o}F^{-1}$ (top) and $.00015^{o}F^{-1}$ (bottom)
source flow parameter	$Q/M^{1/2}H$	N.D.	.0025	.049	

gross flow properties into and out of Zone 2. Because of the importance of these flows, the condtions at the end of Zone 2 are computed and presented in Table 2 along with the relevant values of the same parameters at the source.

2.3 Buoyant Jet Zone

Within this zone the plume travels horizontally due to its initial momentum and rises vertically (somewhat) due to buoyancy. In addition, its trajectory may be influenced by the presence of obstacles within the suppression pool. The volume flow rate within the jet increases along the trajectory due to liquid entrainment and the overall dilution at the top of the zone may be defined as

$$S_3 = S_2 \cdot S_{2-3} = \frac{Q_3}{Q_o} \tag{2.5}$$

The value of S_{2-3} is not easily determined analytically due to the complex source shape and orientation and the confining nature of the pool. However, bracketing estimates can be obtained by considering the dilutions reported in the literature for jets under more idealized conditions. Because of the high discharge Froude number indicated in Table 2 the jet may be approximated as non-buoyant. Two conditions are considered: an axisymmetric (circular port) horizontal discharge and a 2-D plane (slot) horizontal discharge. Dilutions are estimated using formulas from Albertson et al. (1950).

For the 2-D plane jet, dilution is estimated as

$$S_{2-3} = .62\left(\frac{s}{b_2}\right)^{1/2} \tag{2.6}$$

where s is the trajectory length and b_2 is the equivalent slot width at the end of Zone 2. Assuming two slot jets (one on either side of the quencher), $b_2 = A_2/2W$ where W is the annular width (26.5' for Shoreham) and A_2 is the aggregate jet cross section area (~ 1 ft^2). Assuming that the trajectory in Zone 3 is of the order s=w, the predicted dilution is about 23. For the 3-D axisymmetric jet, dilution is estimated by

$$S_{2-3} = .32 \frac{s}{D_2} \tag{2.7}$$

where D_2 is the equivalent jet diameter at the end of Zone 2. Assuming four horizontal jets (two on either side of the quencher) $D_2 = (A_2/\pi)^{1/2} = .56$ and the dilution S_{2-3}, evaluated at $s = 26.5'$ is about 15. Allowing for the influence of the basin obstacles in reducing dilution, and considering that the prototype quencher is intermediate between an idealized 2-D and 3-D source, a reasonable estimate for dilution in Zone 3 is $S_{2-3} = 15$, for which the flow Q_3 is about 1200 cfs.

It can be noticed from the Equations (2.6) and (2.7) that the total mass flux estimated at the end of Zone 3 depends only on the jet momentum and the trajectory. For the 2-D jet approximation, for example, the induced flow per unit width can be expressed as

$$\frac{Q_3}{W} = S_{2-3} \frac{Q_2}{W} = \frac{.62}{2^{\frac{1}{2}}} s^{\frac{1}{2}} \left(\frac{M}{W}\right)^{\frac{1}{2}} \tag{2.8a}$$

while for the 3-D jet approximation, the induced flow can be expressed as

$$Q_3 = S_{2-3} Q_2 = \frac{.32\pi^{\frac{1}{2}}}{4} s M^{\frac{1}{2}} \tag{2-8b}$$

In equations (2-8 a and b) the momentum flux M refers to the total quencher momentum rather than the momentum associated with each equivalent jet.

Except for drag forces due to basin obstacles, momentum flux will be essentially conserved within Zone 3 and thus can be approximated by its value at the source, or

$$M_o = Q_o u_o \qquad (2\text{-}9)$$

See Table 2 for a typical value of M_o. The fact that the induced flow rate at the end of Zone 3 does not depend strongly on the flow at the end of Zone 2, but only on the discharge momentum, suggests that the source momentum needs to be properly scaled in a sub-scale manner, but that the exact nature of the source is not important.

2.4 Near Field Circulation Zone

As the flow reaches the top of Zone 3 it spreads horizontally due to the presence of the free surface. It is also buoyant relative to its surroundings. If the water were deep enough or the buoyancy great enough, a stable stratification would be created with a warm surface density current flowing away from the quencher and a relatively cool bottom layer flowing toward the quencher. These flows would be superimposed on any gross pool circulation. However Q_5, the flow rate in the far field, will be determined in the next section to be less than Q_3, which indicates that near field recirculation takes place since all of the entrainment flow cannot be supplied from "far field" lower layer water. The recirculated water from Zone 3, along with the far field water which is able to be

exchanged in Zone 5, mix in Zone 4 as indicated in Figure 3.

At this point it is important to emphasize that the recirculation in Zone 4 is caused by the fact that the aggregate entrainment demand in Zones 1, 2 and 3, Q_3-Q_o, exceeds that which can be supplied by gravitational convection. The fact that Q_3 and Q_5 are governed by momentum, buoyancy and water depth suggests that this recirculation is relatively insensitive to the exact flow near the source (i.e., Q_o, Q_1 or Q_2). It is thus anticipated that if the flow conditions leaving Zone 2 were changed by approximating the steam source the basic behavior or Zone 4 would remain unchanged.

2.5 Far Field Circulation Zone

The flow which does spread on the water surface is ultimately downwelled to become the lower layer return flow and/or is returned as gross pool circulation. The dilution between Zones 2 and 5 can be defined as

$$S_{2-5} = \frac{Q_5}{Q_2} \tag{2.10}$$

and has been studied for the case of a 2-D vertical jet discharging into a rectangular channel by Jirka et al. (1973). See Figure 5. Since we are interested in the far field circulation which is expected to depend largely on buoyancy rather than momentum, the 2-D vertical jet is an acceptable approximation. Jirka's formula for S_{2-5} can be written as:

$$S_{2-5} = \frac{4^{1/3}\, \mathbb{F}_{HC}^{2/3}\, (B/W)^{1/3}\, HW}{Q_2} \tag{2-11}$$

where B is the buoyancy flux and $\mathbb{F}_{HC}$ is a function of flow resistance

2D Channel (After Jirka et al. 1973)

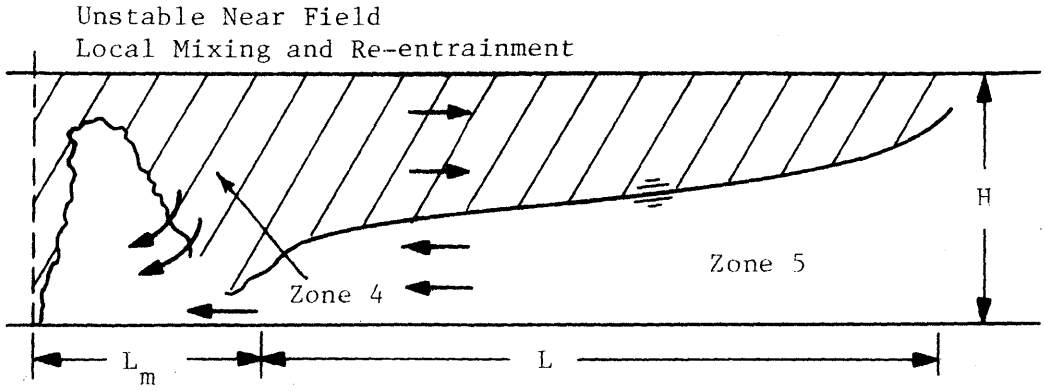

$L_m \simeq 2.5H$

Suppression Pool Plane View

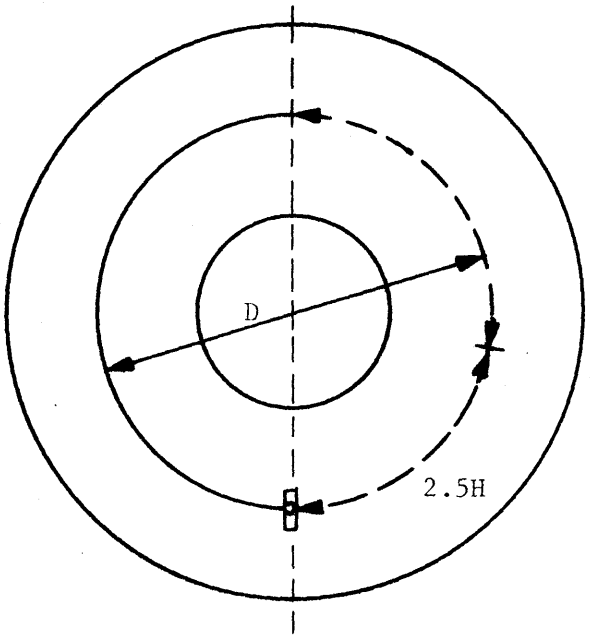

$L = \frac{\pi D}{2} - 2.5H$

prototype values

$D \sim 52$

$H \sim 16$

Figure 5 Definition Sketch for Far Field Analyses

ranging from $F_{HC} = 0.25$ (no resistance) to 0.0 (total resistance).

The buoyancy flux is derived from the thermal energy of the steam discharge. It may be defined in terms of an equivalent water source (or the actual steam source after condensation takes place) having the same excess enthalpy, Δh_s, above that of the ambient. Designating condensed quantities with a subscript c, the source buoyancy can be written

$$B_o = Q_c \frac{\Delta\rho_c}{\rho} g = Q_o \beta \frac{\Delta h_s}{c_p} g \qquad (2.12)$$

where β is the coefficient of thermal expansion of water. Because β is a function of temperature which varies along the jet trajectory, B_o is not strictly constant; it is evaluated in Table 2 for two different values of β.

Jirka defines F_{HC} as a function of boundary resistance given by f_o L/H where f_o is a boundary friction coefficient and L is a function of channel length. In our case, resistance due to pressure drag must be incorporated into F_{HC} and the value of L for our annular channel should be interpreted as indicated in Figure 5.

The friction coefficient f_o can be determined from a Moody chart as a function of channel Reynolds number and boundary roughness. Assuming $Q_5 \simeq Q_3$ and estimating the roughness length ε as .08" (concrete), a value of $f_o = .07$ is estimated. In addition to the viscous drag exerted by f_o, the support columns (approximately 14 of 3 ft diameter) and the downcomers (approximately 84 of 2 ft. diameter) exert pressured drag. See Figure 1.

A drag coefficient C_{D_i} may be defined for each obstacle as

$$C_{D_i} = \frac{F_i}{\frac{1}{2}\rho v_5^2 H_i D_i} \tag{2.13}$$

where F_i is the drag exerted by each cylinder of diameter D_i and height H_i and v_5 is a representative velocity in Zone 5. Values of C_{D_i} are a function of cylinder Reynolds number (based on D_i and v_5) and are estimated (Schlichting, 1979) as 0.4 for the columns and 0.5 for the downcomers.

The total force exerted on the fluid is

$$F_{Tot} = F_{Boundary} + F_{Drag} = \rho v_5^2 \{\frac{f_o}{8} xL + \sum_{i=1}^{N} \frac{C_{D_i}}{2} D_i H_i\} \tag{2.14}$$

where x is the wetted perimeter, xL is the wetted area of the pool, and N is the number of obstacles. An equivalent friction coefficient can thus be calculated as

$$f_e = f_o + \frac{4}{xL} \sum_{i=1}^{N} C_{D_i} D_i H_i \tag{2.15}$$

Using $f_o = .07$, x = 60.5 ft, L = 40 ft, $H_i = 17$ ft and N = 98, values of $f_e \simeq .76$ and f_e L/H = 1.78 are computed. Then one finds on the chart of F_{HC} vs f_o L/H (Jirka, 1973 p. 137) the value $F_{HC} = .15$. Using values from Table 2, Equations (2.10-11) yield $S_{2-5} \simeq 3$ and $Q_5 \simeq 230$ ft ^{3}/s. Note that $Q_5 < Q_3$ ($S_{2-5} < S_{2-3}$) corroborating our previous assumption concerning recirculation.

2.6 Summary

From the preceding discussion it is apparent that the desired

temperature field in Zone 4 reflects the flow of heated water into Zone 4 from Zones 3 and 5 and out of Zone 4 into Zones 1, 2, 3 and 5. These flows can be accurately modeled, in turn, if the flows into and out of Zone 2 are correctly modeled. These have been indicated schematically in Figure 4-b. The discussion in the following chapters is based on the assumption that the flows in Zones 2, 4 and 5 are to be modeled accurately but that it may be necessary to schematize the source so that Zones 1 and 2 are modeled only with respect to the gross flow into and out of the zones.

III. EXPERIMENTAL DESIGN

3.1 Model Scaling

In order to properly model the flow fields in Zones 3, 4 and 5, it is necessary to insure that the relevant physical processes which take place within the zones and on the boundaries are accurately represented. This insurance is obtained, traditionally, by either of two formal procedures. The first is to normalize the relevant governing equations and their boundary conditions and then to identify the dimensionless coefficients which are then maintained from prototype to model. The second procedure is to identify the relevant physical variables which characterize the problem and then to utilize dimensional arguments (e.g. the Buckingham - Π theorem) to arrive at the dimensionless parameters which must be maintained. If performed correctly, these two procedures are equivalent. Because the discussion in Chapter 2 provides a head start on understanding the physical processes, the latter procedure is adopted in this study.

3.1.1 Dimensionless Groupings

The primary dependent variable of interest is the pool temperature T in Zones 3, 4, and 5. (At this point reference to the particular zone is omitted.) It is expected that the pool temperature rise above its initial value T_i could be a function of the source and pool geometry and a number of independent variables in the form:

$$T-T_i = \phi \{\vec{x}, t, Q_o, M_o, B_o, H, c, g, \nu, \alpha, k\} \qquad (3.1)$$

where the variables and their dimensions are:

$\vec{x}$ = spatial coordinates (L)

t = time from the start of discharge (T)

T_i = initial pool temperature (t)

Q_o = source volume flux (L^3t^{-1})

M_o = source momentum flux (L^4t^{-2})

B_o = source buoyancy flux (L^4t^{-3})

H = pool depth (L)

c = speed of the sound in the fluid (Lt^{-1})

g = acceleration of gravity (Lt^{-2})

ν = kinematic viscousity (L^2t^{-1})

α = thermal diffusivity (L^2t^{-1})

k = water surface kinematic heat exchange coefficient (Lt^{-1})

The bulk flow parameters Q_o, M_o, and B_o have been defined in Chapter 2. It should be remembered that specification of these quantities is equivalent to the specification of the source size, velocity and enthalpy excess.

$$u_o = \frac{M_o}{Q_o} = \text{source velocity} \tag{3.2}$$

$$A_o = \frac{Q_o^2}{M_o} = \frac{Q_o}{u_o} = \text{total source flow area} \tag{3.3}$$

$$\Delta h_s = \frac{B_o c_p}{Q_o \beta g} \tag{3.4}$$

The specification of the source area A_o along with the source shape

constitutes a complete description of the source geometry.

The functional dependence of the pool temperature T upon the specified parameters may be cast in dimensionless terms

$$\frac{T-T_i}{T_{bulk}-T_i} = \phi\left[\frac{\vec{x}}{H}, \frac{tM_o^{1/2}}{H^2}, \frac{Q_o}{M_o^{1/2}H}, \frac{M_o}{Q_oC}, \frac{M_o^{3/4}}{B_o^{1/2}H}, \right. \tag{3.5}$$

$$\left. \frac{M_o}{gH^3}, \frac{M_o^{1/2}}{\nu}, \frac{M_o^{1/2}}{\alpha}, \frac{kH}{M_o^{1/2}}\right]$$

where T_{bulk} is the bulk pool temperature which may always be computed from the total heat input to the basin, or from a spatial integration of the pool temperature T.

Equation (3.5) expresses a relationship between normalized induced temperatures and nine independent dimensionless parameters. The first independent parameter relates to geometric similitude (i.e. correct spatial scaling,) the second parameter relates to kinematic similitude (i.e. correct scaling of time) and the last seven parameters relate to dynamic and thermodynamic similitude (i.e. correct scaling of forces and heat transfer). The theory of scale modeling is that if each of the independent dimensionless parameters is maintained constant between model and prototype, then the dependent normalized temperatures will also be the same in the model and the prototype. Clearly, not all of these parameters can be satisfied in the sub-scale model. In the following each parameter is discussed to identify which are most important and to assess the consequences if certain parameters are not preserved.

3.1.2 Significance of the Groupings

3.1.2.1 Geometric Scaling $\left[\frac{\vec{x}}{H}\right]$

Precise geometric similitude requires that geometric features of the basin and the quencher be scaled according to a fixed undistorted scale ratio. Using the pool depth H as a characteristic length, the length scale ratio H_r (or the ratio of water depth in model to water depth in prototype) should be used to scale all model dimensions and the location of measurements. For example, a temperature measurement taken one foot in front of the quencher in the model should correspond to a measurement of a distance of one foot divided by H_r in front of the prototype quencher. While it is possible to scale the dimensions of the pool with reasonable precision, it is not possible to scale, precisely, the various details of the quencher-in particular the exact number and location of ports. However, the discussion in Chapter 2 suggests that this is not necessary because the jets from the individual ports merge and the primary interest is in the behavior of Zones 3, 4 and 5, which occur after merging. The degree to which it is possible to approximate the geometry of a prototype quencher with a model quencher of fewer ports is explored as part of the experimental program.

3.1.2.2 Time Scaling $\left[\frac{tM_o^{1/2}}{H^2}\right]$

Noting that $M_o^{1/2}/H$ is a characteristic velocity, proper scaling of time insures that lengths (scaled by H) are proportional to the product of velocity and time, thus insuring kinematic similarity.

3.1.2.3 Source Size/Flow/Shape Parameter $\left[\frac{Q_o}{M_o^{1/2} H} \right]$

The discussion in Chapter 2 suggests that the induced flow rates will be several orders of magnitude greater than Q_o and, in fact, that they will depend mainly on momentum flux M_o and buoyancy flux B_o rather than volume flux Q_o. This suggests that this parameter will not be significant. This conclusion can also be reached by interpreting this parameter as a length scale ratio

$$\frac{Q_o}{M_o^{1/2} H} = \frac{\ell_o}{H} = \text{ratio of source size to pool size.} \qquad (3.6)$$

For the prototype geometry under consideration $\ell_o \simeq .025$ ft and $H \simeq 20$ ft. Thus it is expected that the source flow will not be a significant quantity (Wright, 1977). A corollary to this conclusion is that the source shape is also not significant. This conclusion is supported by the studies of Yevdjevich (1966) involving jets in unbounded environments.

In his experiments with a hot water source, Soliva (1980) found it advantageous to use larger flow rates Q_o than would be implied by precise scaling of the parameter $Q_o/M_o^{1/2}H$. This allowed him to achieve greater resolution in his temperature measurements to compensate for the lower enthalpy rise of the (hot water) source. His use of the larger Q_o was defended by the above arguments. However, for the steam source used in the present experiments this is not necessary and the parameter $Q_o/M_o^{1/2}H$ can be preserved.

3.1.2.4 Source Momentum - Buoyancy Parameter $\left[\frac{M_o^{3/4}}{B_o^{1/2} H} \right]$

This parameter expresses the ratio of source momentum and buoyancy. As discussed in Chapter 2, both momentum and buoyancy will be significant to the flow and temperature distribution in the pool. Thus this parameter must be preserved in any sub-scale model.

It should be noted that the requirement of a constant (from model to prototype) momentum-buoyancy parameter $M_o^{3/4}/B_o^{1/2}H$ and a constant source flow parameter $Q_o/M_o^{1/2}H$ is equivalent to the requirement of a constant densimetric Froude number. This can be seen by taking the ratio of the two parameters,

$$\frac{M_o^{3/4}/B_o^{1/2}H}{Q_o/M_o^{1/2}H} = \frac{M_o^{3/4}}{B_o^{1/2}Q_o} = \frac{u_o}{(g\beta\frac{\Delta hs}{c_p})^{1/2} A_o^{1/4}} \qquad (3.7)$$

The last term in the above equation can be related to a discharge densimetric Froude number by noting the relationship between discharge enthalpy rise Δh_s and normalized density difference $\frac{\Delta\rho}{\rho}$ within the condensed flow region as given by Equations (2.12).

3.1.2.5 Mach Number $\mathbb{M} = \left[\frac{M_o}{Q_o c} \right]$

This parameter is clearly equivalent to the conventional Mach number based on the source velocity, i.e. $\mathbb{M} = u_o/c$. The prototype steam discharge is expected to be sonic $\mathbb{M} = 1$. As discussed in Chapter 2, previous experiments have shown that the configuration of the steam condensation zone is dependent on whether the source flow is sonic or subsonic. However,

as indicated by Table 1, the net dilution associated with condensation is not, to the first order, a function of the source Mach number. In addition, the length scale of the condensation zone is considerably smaller than the scale of the suppression pool and of the flow region whose temperature is of interest. Accordingly the Mach number of the source will not be a significant parameter and thus a non-sonic steam source, or even a heated water source could be used in a sub-scale model.

3.1.2.6 Free Surface Froude Number $\left[\frac{M_o}{gH^3}\right]$

This parameter governs the correct scaling of free surface motion (i.e. waves). Because these are not expected to be significant, this parameter may be neglected in the sub-scale model.

3.1.2.7 Reynolds Number $\left[\frac{M_o^{1/2}}{\nu}\right]$

The parameter $M_o^{1/2}/\nu$ may be interpreted in terms of the conventional Reynolds number by noting that $M_o^{1/2}/\nu = \frac{u_o\sqrt{A_o}}{\nu}$. For the full scale pool the Reynolds number is expected to be on the order of 10^7, indicating that fluid viscosity will have minimal effect on the flow. Model Reynolds numbers may be estimated by noting that in a Froude scale model, the following relationship between scale ratios must hold

$$u_{or} = \left[\Delta h_{sr} \; H_r\right]^{1/2} \tag{3.8}$$

where the subscript r denotes the ratio of a sub-scale to a full scale quantity. It then follows that the Reynolds number ratio is

$$\mathbb{R}_r = \frac{u_{or} H_r}{\nu_r} = \frac{\Delta h_{sr}^{1/2} H_r^{3/2}}{\nu_r} \tag{3.9}$$

For a sub-scale model with a length scale ratio of 1/17 (the approximate value chosen for our experiments) and for a steam source ($\Delta h_{sr} \simeq 1, \nu r \simeq 1$), Equation (3.9) suggests $\mathbb{R}_r \simeq 1/70$ or that the model Reynolds number will be of under 10^5. Buoyant jet experiments by Ungate (1975), suggest that jet mixing is independent of Reynolds number for Reynolds number greater than about 1500 so that lack of Reynolds number scaling should be no problem in the near field of a sub-scale test.

The Reynolds number also may influence the viscous and form drag which the flow experiences in Zones 4 and 5, as expressed in Equation (2.14). The viscous forces will be properly scaled in a densimetric Froude scale model if the interfacial and boundary friction factors are independent of Reynolds number over the range between model and prototype. Interfacial friction factors are usually taken as a fraction (0.5 - 1.0) of the boundary friction factor (Jirka et al., 1975), and the boundary friction factor, within the turbulent range, is an asymptotically decreasing function of Reynolds number. Since the model Reynolds number may be two orders of magnitude smaller than the prototype value, it is expected that model friction factors may be approximately twice as large as in the prototype (Daily and Harleman, 1966). The experimental results will thus be conservative in the sense that this increased friction will result in a decrease of far field circulation and thus a decrease in the rate at which heat may be removed from the source. This effect could be reduced by choosing a larger model length scale, smoother walls, or vertical scale distortion, but because viscous drag is not expected to provide the major flow resistance, this is not considered necessary.

Form drag is associated with pressure forces incurred as the flow in Zone 5 travels around the various structures within the basin. The discussion in Section 2.5 indicates that for this problem, form drag, as opposed to viscous drag, provides the dominant flow resistance. This resistance will be properly scaled in a densimetric Froude model if the drag coefficients associated with these obstacles are similar from model to prototype. The drag coefficient is expected to depend on a Reynolds number based on the velocity in Zone 5 and a characteristic dimension of each obstacle. For prototype conditions the Reynolds number would be approximately 10^5 while the Reynolds number for a 1/17 model would be of order 10^3. Within this range of Reynolds numbers, the drag coefficient shows some variation due to the transition between laminar and turbulent boundary layers suggesting that the resistance may be somewhat different from model to prototype. The sensitivity of the measured temperatures to this resistance could be tested in a sub-scale model by varying the number of obstacles or their size.

3.1.2.8 Reynolds-Prandtl Number $\left[\frac{M_o^{1/2}}{\alpha}\right]$

Molecular diffusion of heat is represented by the parameter $\frac{M_o^{1/2}}{\alpha}$ which is equivalent to the product of a Reynolds number and a Prandtl number and, again, must be considered in Zones 3, 4, and 5. In Zone 3 the role of thermal diffusion is similar to that of viscous diffusion of momentum, and is regarded as insignificant for sufficiently large Reynolds number.

The significance of the vertical diffusion of heat (either by

molecular or turbulent transport) in Zone 5 can be expressed by the ratio of the time scale of the experiment divided by the time scale for vertical diffusion, or

$$\frac{\text{experimental time}}{\text{diffusion time}} = \frac{\alpha t}{H^2} \tag{3.10}$$

(Horizontal diffusion of heat is not considered significant due to smaller temperature gradients.) To properly scale vertical diffusion, either this parameter would be equal in model and prototype (requiring the value of α to be a factor of 289 smaller in a 1/17 model) or the parameter should be negligible in both model and prototype. At least the latter should be true. For example, in the model α should be characterized by its molecular value (about 10^{-6} ft^2/sec). Thus a model with a one foot water depth could be run for the order of $t = 1^2/10^{-6} = 10^6$ sec, before this diffusion became important. Even if diffusion should be overstated in the model, the effect would be conservative in the sense that it would lead to greater ambient temperatures near the bottom of the basin in the area in which entrainment to the steam jet takes place.

3.1.2.9 Surface Heat Loss Parameter $\left[\frac{kH}{M_o^{1/2}}\right]$

The parameter $\frac{k\beta gH^2\Delta T_{bulk}}{B_o}$ provides an indication of the importance of surface heat exchange (by conduction, evaporation and radiation) to the problem. Assuming geometric scaling, the ratio of this parameter in model and prototype would be $k_r H_r / M_{o_r}^{1/2}$ which would be increased

(a non-conservative trend) unless the model value of k_r could be significantly reduced (e.g., by controlling the atmosphere above the model). However, for k = 10^{-5} ft/sec (Ryan et al., 1974) it is expected that the value of this parameter is sufficiently small (order of 10^{-3} in the model) to be insignificant.

3.1.2.10 Temperature Scaling

For a constant heat input (and associated buoyancy flux B_o), the bulk temperature rise for a volume H^3 will be $T_{bulk}-T_i \sim B_o t/H^3 \beta g$, or, using the relationship for time scaling, $T_{bulk}-T_i \sim \frac{B_o}{\beta g M_o^{1/2} H}$.

This provides a means for properly scaling the temperatures observed in a sub-scale model. That is, the normalized temperatures on the left side of Equation (3.5) can be expressed as

$$\frac{T-T_i}{\frac{1}{\beta g}\frac{B_o}{M_o^{1/2}H}} = \phi \text{ (dimensionless independent parameters)} \qquad (3.11)$$

Note that if densimetric Froude scaling is employed, i.e. if the momentum-buoyancy and source flow parameters are preserved, and if a steam source is used, i.e. $\Delta h_{sr} \simeq 1$, then the parameter $B_o/M_o^{1/2}H$ will also be preserved. Since β and g will be the same in model and prototype, this means that temperature differences measured in the model will correspond directly to those occuring in the prototype.

3.1.2.11 Summary

The above discussion suggests that momentum and buoyancy are the dominant forces governing motion and that these may be properly scaled by maintaining geometric and kinematic (time) similarity and maintaining a

constant ratio of the source momentum-buoyancy parameter in the model and the prototype. A number of other factors, including source size and shape, free surface effects, viscous forces, vertical (thermal) diffusion and surface heat loss may be shown to be insignificant or to be conservatively represented. With these assumptions, Equation (3.9) may be rewritten as

$$\frac{T-T_i}{\frac{1}{\beta g}\frac{B_o}{M_o^{1/2}H}} = \phi\left(\frac{\vec{x}}{H}, \frac{tM_o^{1/2}}{H^2}, \frac{M_o^{3/4}}{B_o^{1/2}H}\right) \qquad (3.12)$$

Note that this expression is valid for the use of either a steam or a hot water source. The next section discusses the use of this relationship in the conduct of a sub-scale experiment using a steam source.

3.1.3 Scaling for a Steam Source

The experimental tests were performed in a basin with an undistorted scale ratio of 1/17. This scale was dictated by the size of the available basin and the available steam flow. The steam source was characterized by similar enthalpy difference as prototype, and by correctly reproduced source flow and momentum-buoyancy parameters. These conditions correspond to the following constraints on the ratios of source variables in model and prototype:

$$\Delta h_{sr} = 1 \qquad \text{(enthalpy ratio)} \qquad (3.13)$$

$$\frac{G_{sr}^{1/4} u_{sr}^{3/4}}{\Delta h_{sr}^{1/2} H_r} = 1 \text{ (momentum-buoyancy parameter)} \qquad (3.14)$$

$$\frac{G_{sr}^{1/2}}{u_{sr}^{1/2} H_r} = 1 \quad \text{(source-flow parameter)} \tag{3.15}$$

$$H_r = 1/17 \quad \text{(scale ratio)} \tag{3.16}$$

These constraints lead to the requirement that

$$u_{sr} = H_r^{1/2} = 0.24 \tag{3.17}$$

$$G_{sr} = H_r^{5/2} = .00084 \tag{3.18}$$

Assuming a prototype discharge velocity of 1600 ft/sec and a mass flux of 240 lbm/s (see Table 2), the corresponding model values are 384 ft/sec and 0.20 lbm/s. The required velocity is achieved by having the total port area scaled in proportion to the length ratio squared or

$$A_{or} = H_r^2 = .0035 \tag{3.19}$$

The required total model port area is thus .0032 ft^2.

Recalling the discussion in Section 3.1.2.10, measured temperature rises correspond directly to prototype temperature rises, i.e.

$$(T-T_i)_r = 1 \tag{3.20}$$

while from Section 3.1.2.2, time scales as

$$t_r = H_r^2/M_{or}^{1/2} = H_r^{1/2} = 0.24 \tag{3.21}$$

Thus a temperature rise measured in the model one minute after the start of steam injection would correspond to the same temperature occurring in the prototype approximately four minutes after start-up.

3.2 Experimental Set-up and Procedures

3.2.1 The Basin

The pool model has been built in the shape of an octagonal annulus

inside an existing experimental channel; the channel width determined the geometric ratio $H_r = 1/17$. Figure 6 represents the side view and top view of the basin. A false floor hides the steam feed pipe and by-pass piping. Only the quencher traverses the floor through a manhole of about 1 ft^2 provided to allow changes of quencher model and orientation between the experiments. The walls of the basin are plywood except for the two outside lengths corresponding to the experimental channel. One of the lengths is glass allowing us to visualize the flow. The height of glass is about 2' allowing us to model prototype water depths up to about H = 34' with a length scale rate of $H_r = 1/17$. The pool is designed to be water tight so that it is not necessary to flood the outer portions of the channel. In this way the times required to fill and drain the basin and the heat loss from the steam feed pipe are minimized.

The form drag in the prototype is caused mainly by the downcomers of 2 ft diameter and for a less important part by structural columns whose size is always less than 3 ft diameter. The resistance of these obstacles to the flow can be characterized by the ratio of their area to the total pool area. This ratio is about 8% in the prototype (See Figure 1). To simulate flow resistance in the model we have chosen to place in the pool a certain number of PVC bars of nominal diameter 1" (for about 1.9% of the pool area) and 2" (for about 6%) for a total area of about 8%. The capability exists to remove the bars or to increase the number of bars by a factor of two to an area of about 16%. The detail of the bars' arrangement is given by Figure 7. The bars are held loosely in place from the top by an array of slats fixed to the basin walls with C-clamps.

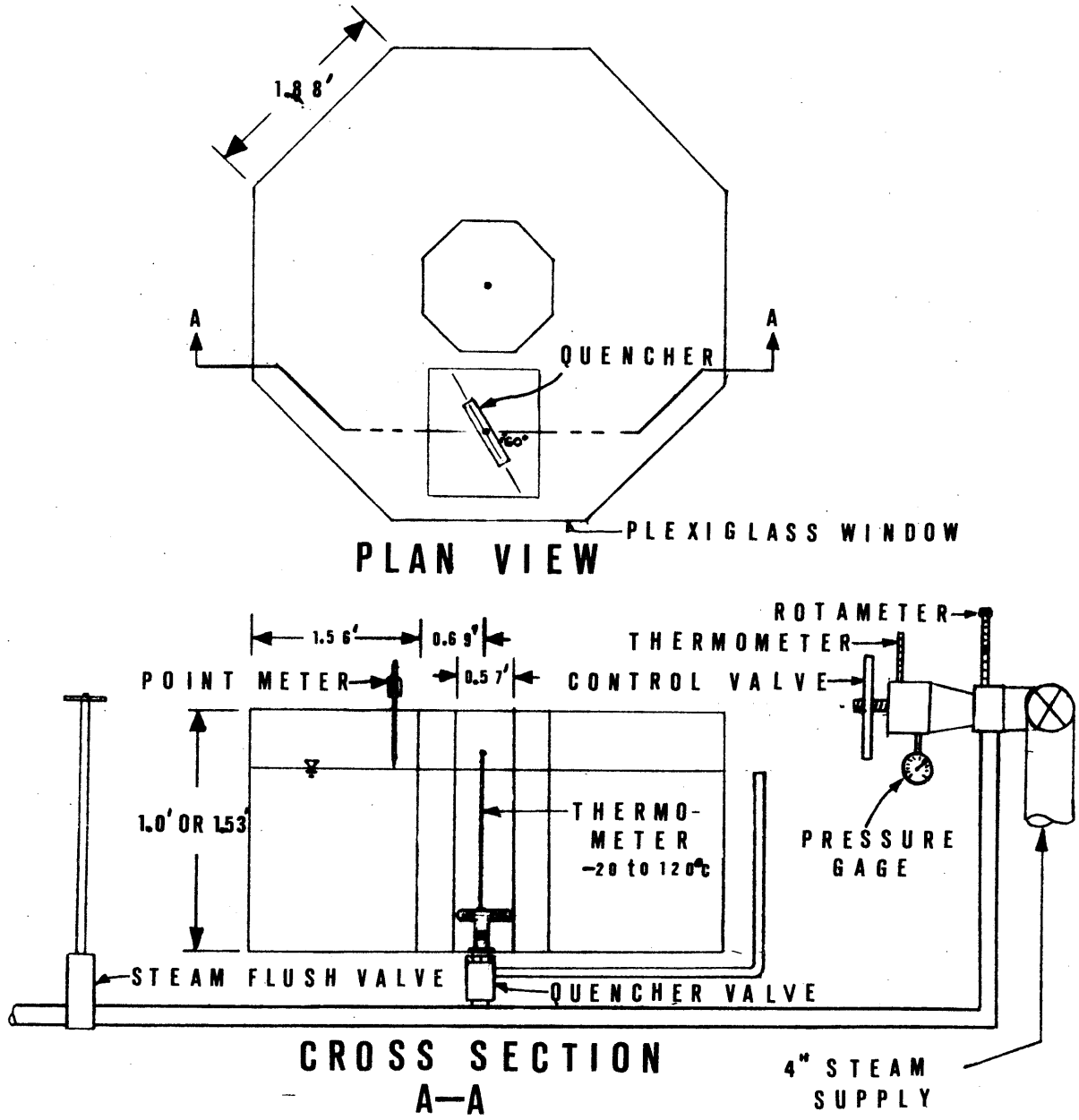

Figure 6: Subscale Test Basin with Steam Supply System

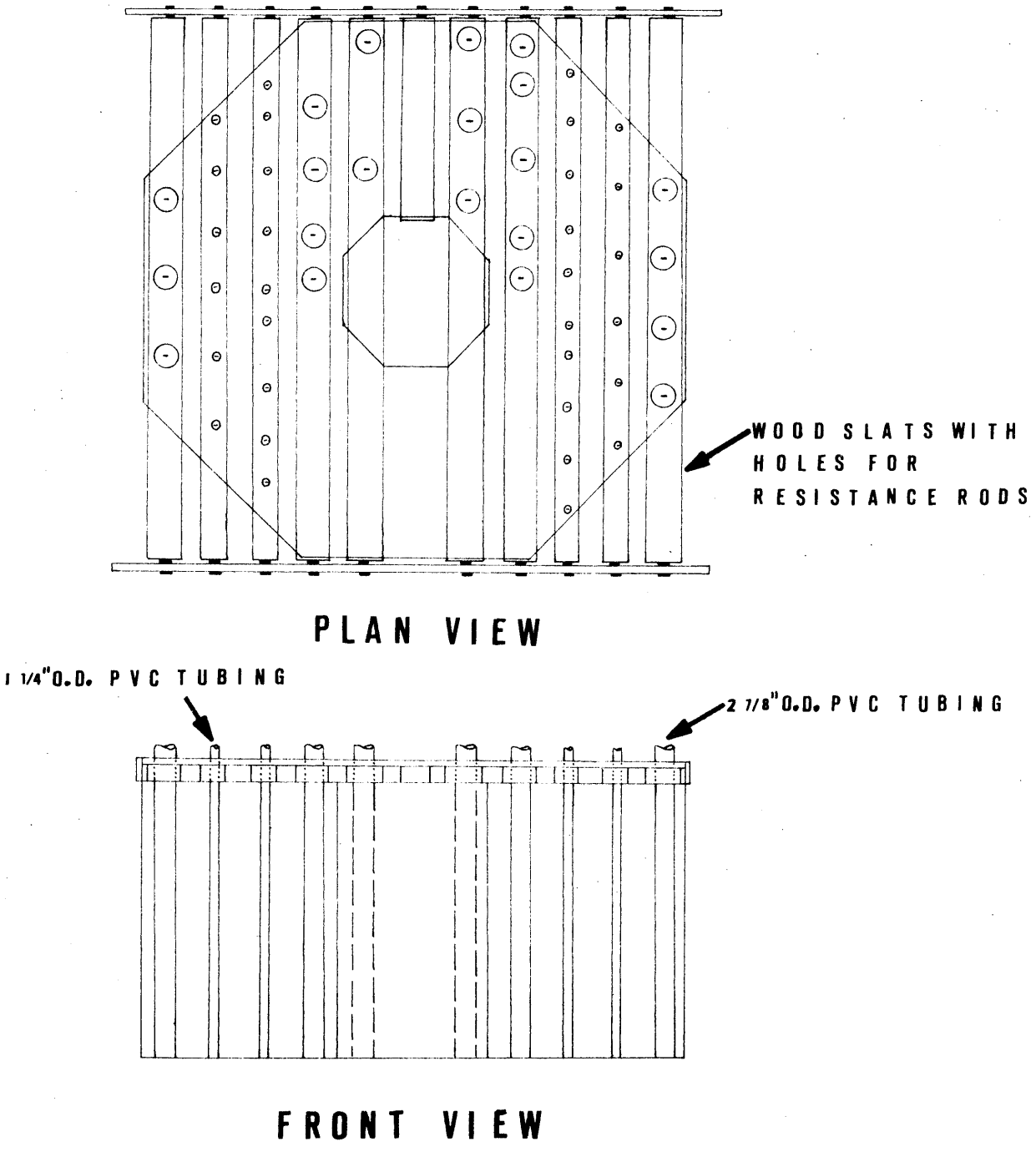

Figure 7: Basin with 8% of Volume Filled by Flow Resistance Rods

This solution allows us to vary easily the number of obstacles in the pool to model different magnitudes of drag force.

3.2.2 The Quenchers

Three quenchers have been designed and are illustrated in Figure 8. The three quenchers differ in the number of ports (35, 17 and 9) but in other respects are identical. The total port area is kept constant (scaled to the prototype by H_r^2) and the port spacing and orientation are designed to correspond closely to prototype arrangements.

3.2.3 Steam Delivery

Steam was supplied by a 4" line from the building heating system. Flow rate was controlled principally by a gate valve upstream of the quencher and measured by a rotameter as shown in Figure 6. The rotameter was calibrated using heat balances performed prior to the start of testing and the calibration was checked by performing a heat balance for each experiment. The state of the steam could be estimated by upstream measurement of temperature and pressure near the rotameter. At the location of quencher ports steam state could be determined by a mercury thermometer penetrating the quencher wall (see Figure 6) and the known hydrostatic pressure corresponding to the quencher depth below the surface. In order to approach an equilibrium state before beginning an experiment a by-pass, or flush line, was introduced near the quencher. When equilibrium was reached, flow could be diverted to the quencher by closing the flush valve and opening the quencher control valve.

3.2.4 Temperature Measurement

Thirty YSI Series 700 thermistor probes (time constant = 1 sec)

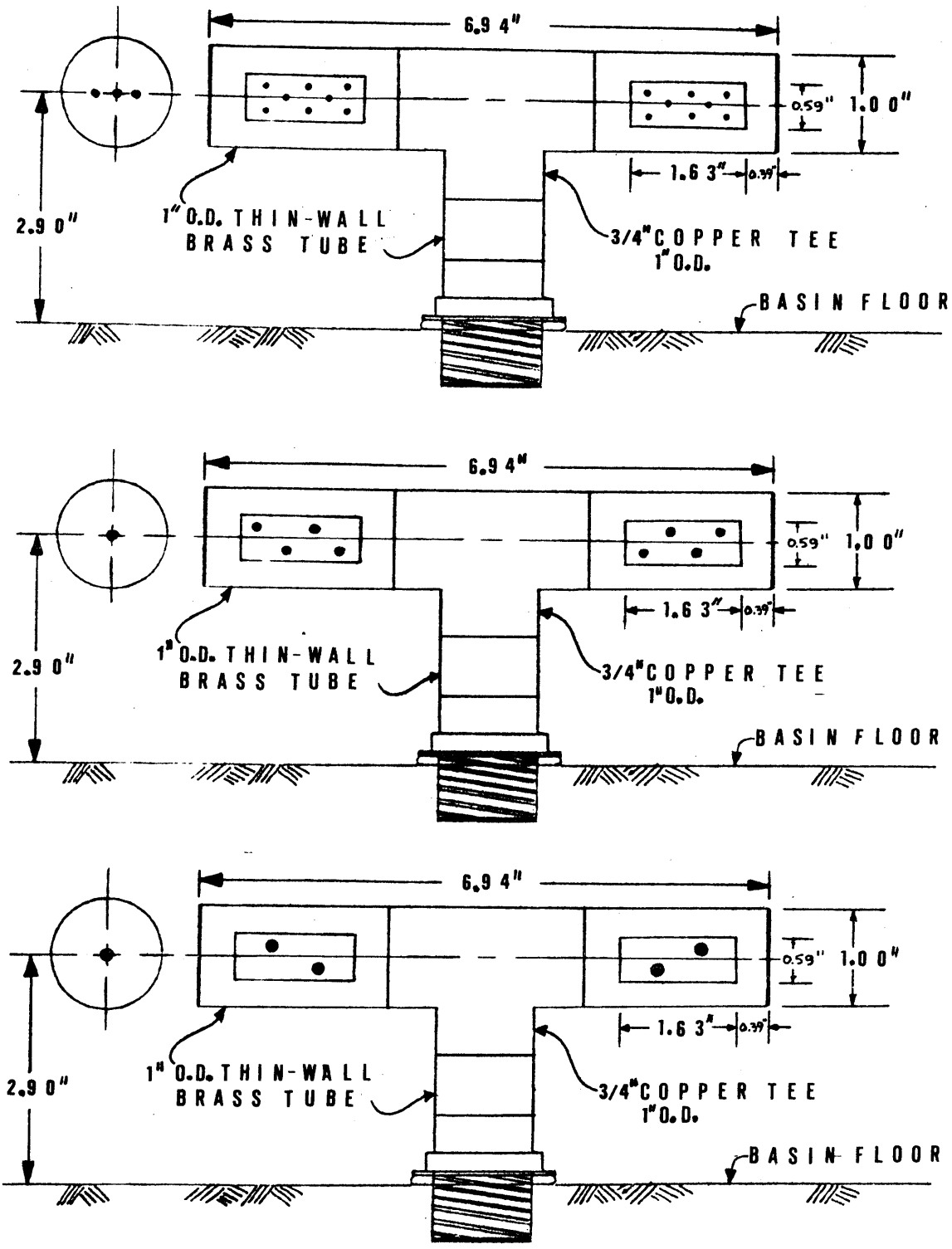

Figure 8: Three Model Quenchers. From Top to Bottom - 35 ports, 17 Ports and 9 Ports. All Quenchers have Total Port Area of 0.46 Square Inches.

have been placed in the basin as shown in Figure 9. Twenty-four probes, placed in five vertical arrays, are located near the quencher to study the near field. The remaining six probes have been placed in three vertical pairs around the far field of the model to document the bulk temperature rise and the extent of induced vertical stratification.

The data acquisition system consists of an Altair 8800B general purpose microcomputer which is used to scan the probes. Probe temperatures can be viewed on a video display terminal, printed on a line printer or stored permanently on a floppy disk storage unit.

On each day for which an experiment was run, probes were calibrated at four different temperatures. At each temperature the average of three thermistor readings was compared with the reading from a mercury thermometer and the difference was input to the computer which developed a third degree polynomial calibration curve for each probe for that day. These polynomials were then used to correct the temperatures as scanned by the data acquisition system. Calibrated accuracy of the thermistor readings is estimated to be $\pm$ 0.1°C.

Associated with each scan, a bulk temperature was computed by a weighted average of the thirty temperature readings. Referring to Figure 9, a weighting factor of 1/8 was associated with each of the six far field probes (cols. F,G and H) and a weighting factor of 1/96 was associated with each of the twenty-four near field probes (cols. A,B,C,D and E.)

3.2.5 Test Procedures

At the beginning of each day thermistors were calibrated using

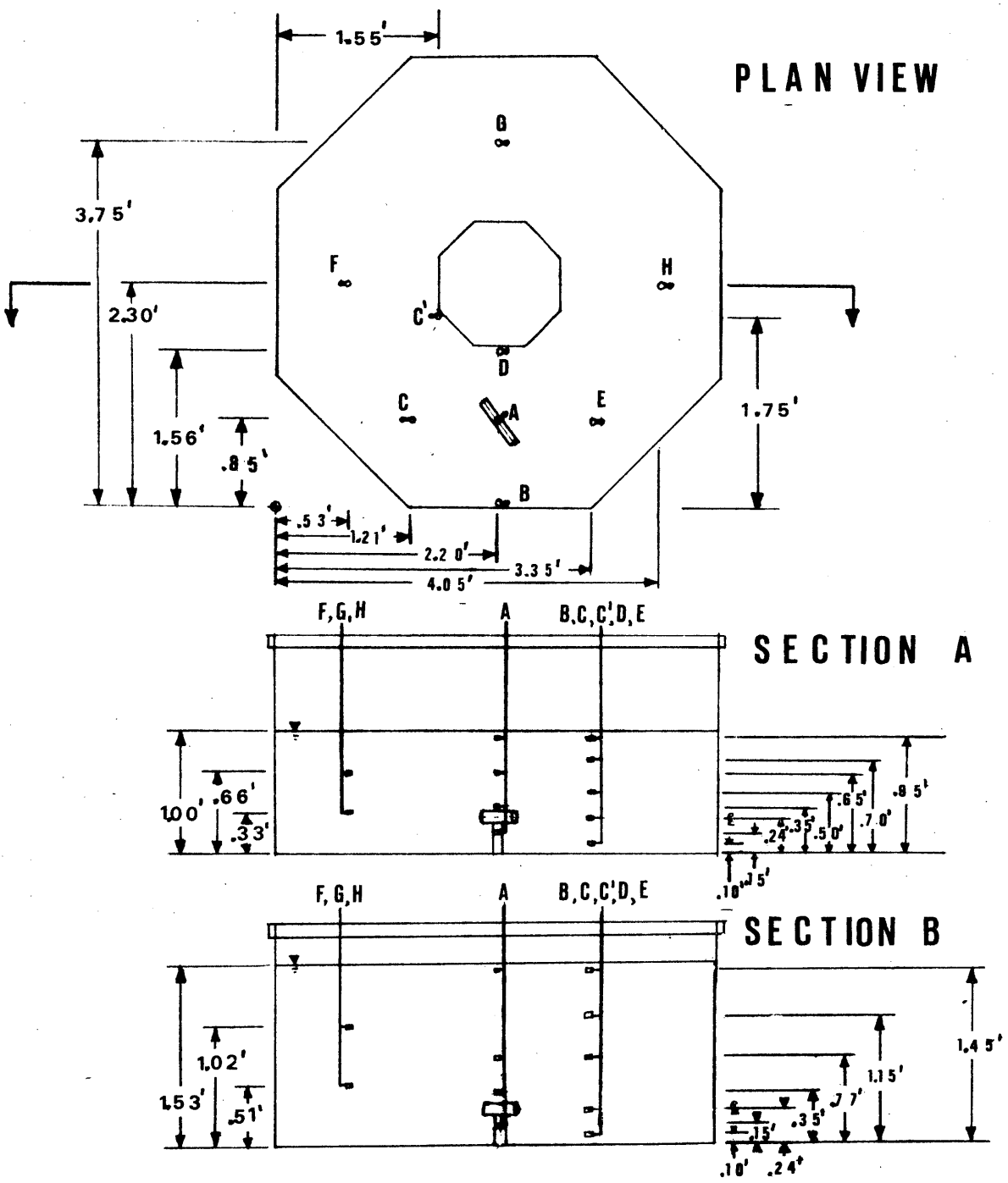

Figure 9: Thermistor Probe Locations: Section A Locations used for H=1.0 Foot
Section B Locations used for H=1.53 Feet
Tree C' used only for $\theta=0°$ Tests.

the procedure described in the previous section. The tank was then emptied, filled with tap water at a temperature of about 25°C, and allowed to come to rest. When still, the basin water level was measured with a point gage (see Figure 6).

Meanwhile steam was flushed through the by-pass system. The start of an experiment was defined as the time at which steam delivery through the quencher began. Steam was delivered at a constant rate of 0.20 lbm/s for a duration of between about 150 secs and about 260 secs (in the model), depending on the water depth, or until temperatures within the basin reached a level of between 45° and 50° C. During the course of the experiment the steam discharge temperature was monitored with the mercury thermometer. For all tests this temperature remained within the range of 124°-126° C.

Thermistors were scanned and the data stored on disk at intervals of between 20 and 30 seconds. Two scans were also taken before the start of steam injection to verify that basin temperatures were initially steady and uniform. Two scans were also taken following the termination of steam injection when the basin was more nearly mixed. This allowed a more accurate computation of the experiment heat budget. All measured temperatures and the computed bulk temperature for each time have been stored in hard copy form.

Following an experiment the water level was measured. Before and after water level and bulk temperature measurements were later used to compute mass and heat budgets to check against the recorded steam flow rate. After an experiment the basin was allowed to cool for approximately

one-half hour prior to the start of the next experiment. In this manner as many as five experiments could be completed in one day.

IV TEST RESULTS

4.1 Program of Tests

Tests were conducted for two purposes: (1) to examine two of the approximations inherent in the scaling analysis and (2) to test the sensitivity of the induced temperature distribution to several parameters which distinguish the Shoreham and LaSalle geometries

The essential variables characterizing each experiment are described in Table 3. Experiments 2-7 are considered the base case tests representing the Shoreham design. Each experiment is characterized by a 35 port quencher (N=35), an 8% fractional area (F_A), an initial water depth of H=17 feet, a quencher location at $\Delta R/W=0.56$ and a quencher orientation of $\theta = 60^o$. See Figure 3. Experiments 2-6 were performed to assess repeatability, while Experiment 7 should be used for comparison with other experiments. (The steam flow rate differs by about 2% between Experiments 2-6 and all of the remaining experiments.)

Experiments 8,9,10 and 14 test the sensitivity to the quencher design (number of ports, N) and to the fractional area of flow resistance F_A. Thus N = 17 and 9 in Experiments 9 and 10 and F_A = 0 and 16% in Experiments 8 and 14. Tests were performed with different N because it was not possible to model the large number of ports in a prototype quencher. The hypothesis to be tested was: results will be insensitive to N in the range $9<N<35$; therefore the 35 port quencher will serve as an acceptable analog of the prototype quencher. Tests were performed with varying fractional area of obstruction because it was concluded that, while far field resistance

TABLE 3

EXPERIMENTAL TEST PROGRAM

Exp. No.	No. of Ports, N	Fractional Area of Flow Resistance, F_A	Initial Pool Depth, H, ft.	Quencher Location $\Delta R/W$	Quencher Orientation θ, ^{o} from tanger
2	35	8	17	0.56	60
3	35	8	17	0.56	60
4	35	8	17	0.56	60
5	35	8	17	0.56	60
6	35	8	17	0.56	60
7	35	8	17	0.56	60
8	35	0	17	0.56	60
9	17	8	17	0.56	60
10	9	8	17	0.56	60
11	35	8	17	0.56	0
12	35	8	26	0.56	60
13	35	8	26	0.56	0
14	35	16	17	0.56	60
15	35	8	26	0.20	0
16	35	8	26	0.76	0
17	35	8	26	0.76	0

Notes:
(1) Exp. 7 parameters correspond to Shoreham Unit 1 pool
(2) Exps. 15, 16 and 17 parameters correspond to LaSalle County pool; inside quencher (Exp. 15), outside quencher (Exps. 16 and 17)
(3) Variables underlined ____ to be compared with base case Exp. 7
(4) Variables underlined _ _ _ to be compared with base case Exp. 13
(5) Exps. 2-6 and 16-17 allow assessment of repeatability

was expected to be small, it might not be scaled properly due to Reynolds number effects. The hypothesis to be tested was: results will be insensitive to F_A in the range $0<F_A<16\%$; therefore flow resistance is not a sufficiently important factor and thus tests conducted with $F_A = 8\%$ (the appropriate prototype value) should be acceptable.

Experiments 11, 12, 13, 15 and 16 explore sensitivity to the three primary variables of water depth, quencher location and quencher orientation which differ between the Shoreham and the LaSalle installations. Thus Exp. 11 uses a quencher orientation of $\theta = 0^o$, Exp. 12 uses a prototype water depth of H = 26 feet, and Exp. 13 uses both $\theta=0^o$ and H = 26 feet. Exp. 15 uses a quencher location of $\Delta R/W = 0.20$ with $\theta = 0$ and H = 26 feet (representing an "inside" quencher at LaSalle) while Exp. 16 uses a quencher location of $\Delta R/W = 0.76$ representing an "outside" quencher at LaSalle. Exp. 17 was performed with the same parameters as Exp. 16 - again to test repeatability.

4.2 Presentation of Results

Temperatures for each experiment are plotted in Figures 10-25. Part a) of each figure documents the spatial temperature distribution at two times while part b) records the time history (in both model and prototype time) of six probes plus the bulk temperature. The probes used in plotting in part b) were selected to provide a representative range of measurement elevation and distance from the quencher (see Figure 9) but not to conform with any precise definition of local-to-bulk temperature difference. If desired, the reader can use the complete set of temperature data recorded in part a) to compute a local-to-bulk temperature difference for each experiment.

a) Spatial Temperature Distribution (See Figure 9 for Precise Probe Locations. Circled Temperatures are Plotted in Part b)

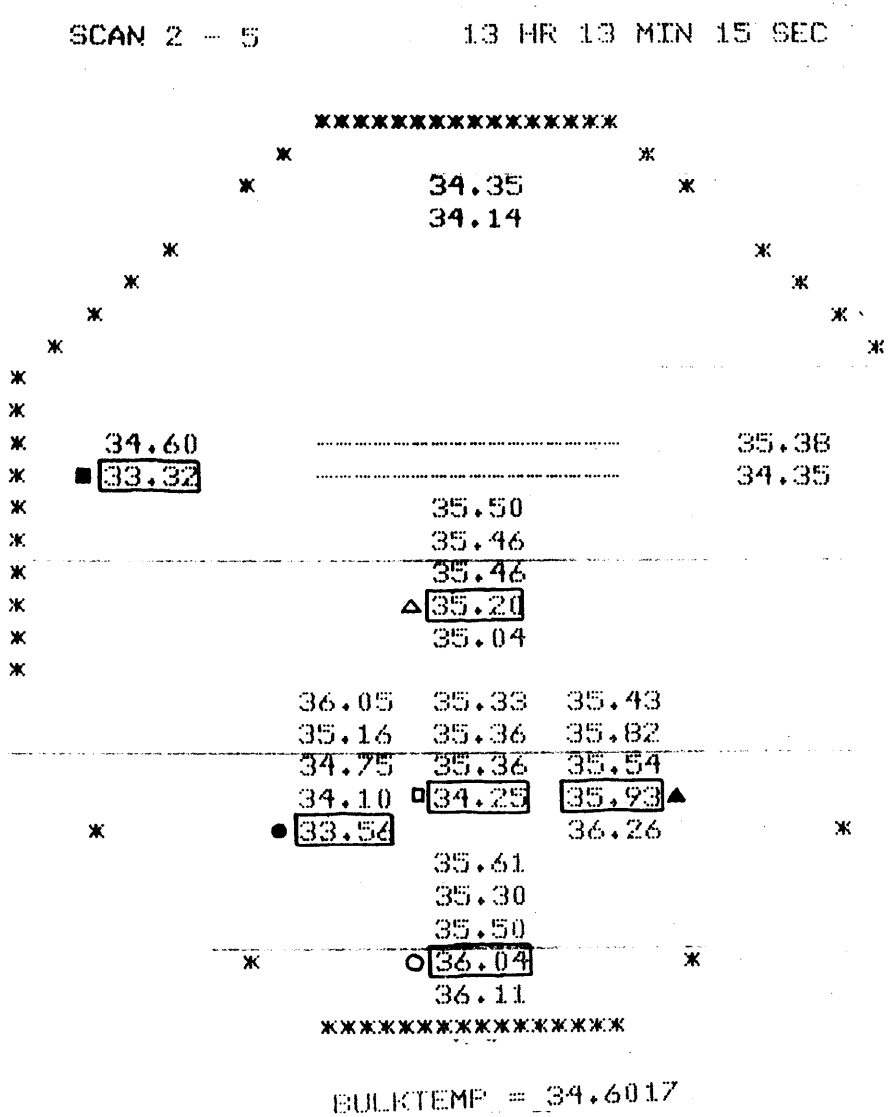

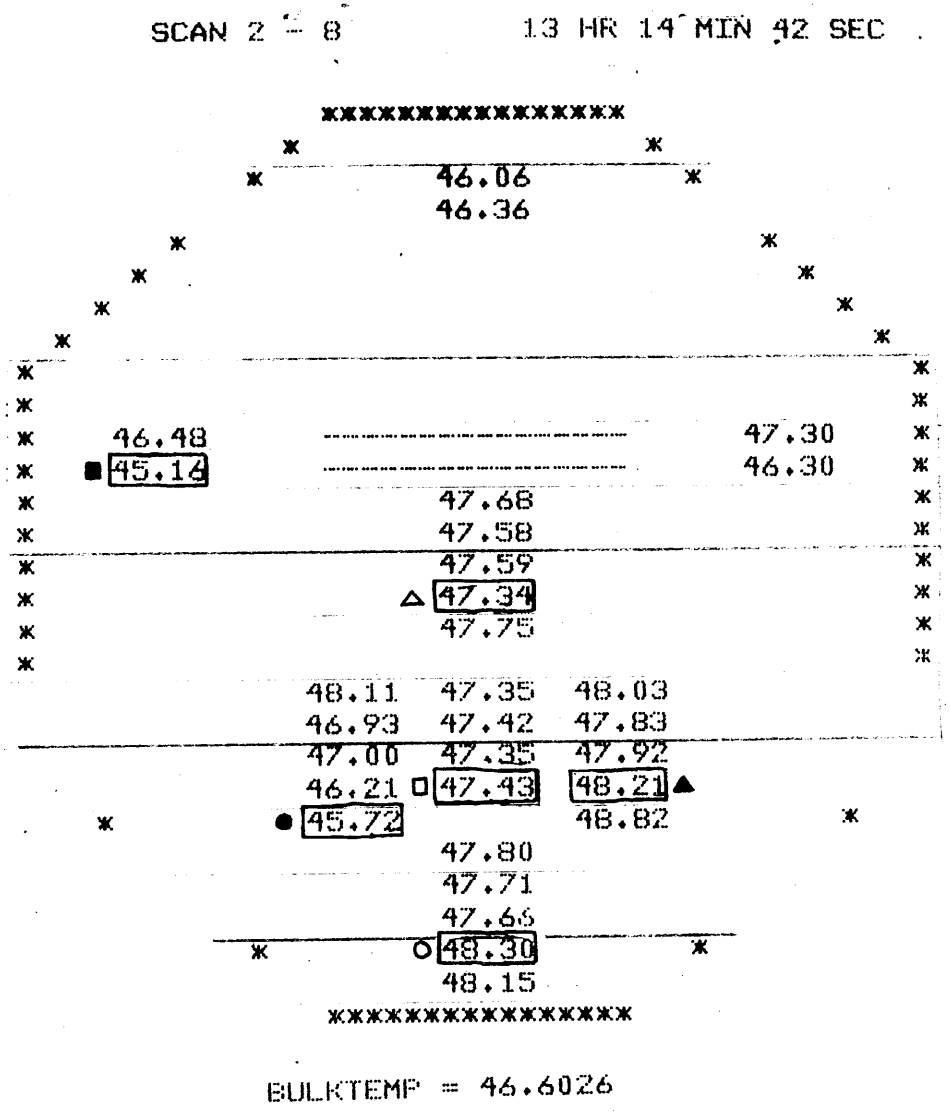

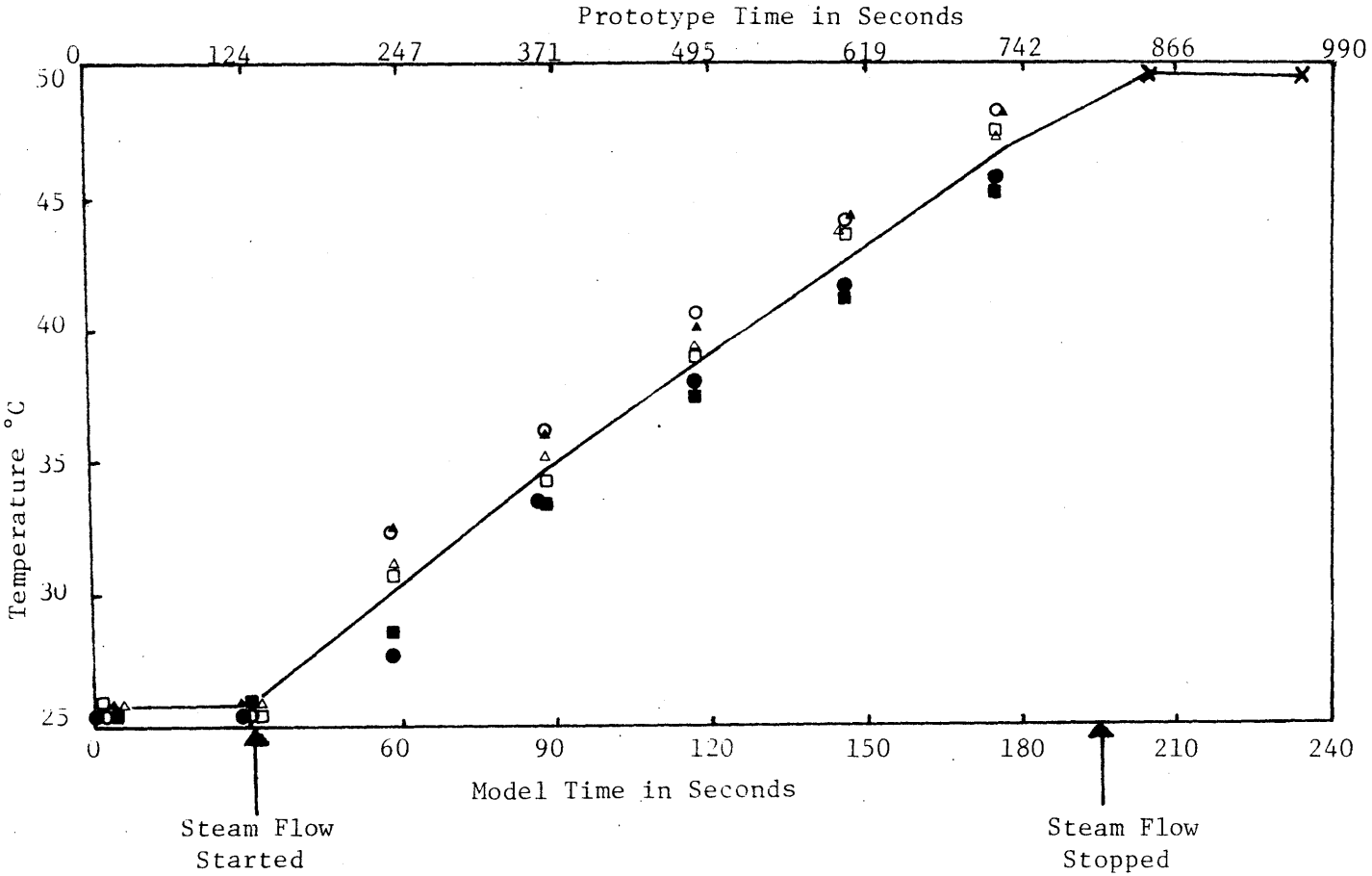

b) Temporal Distribution of Temperature (See Figure 9 and Part a) for Precise Probe Locations)

Figure 10: Results for Experiment 2

a) Spatial Temperature Distribution

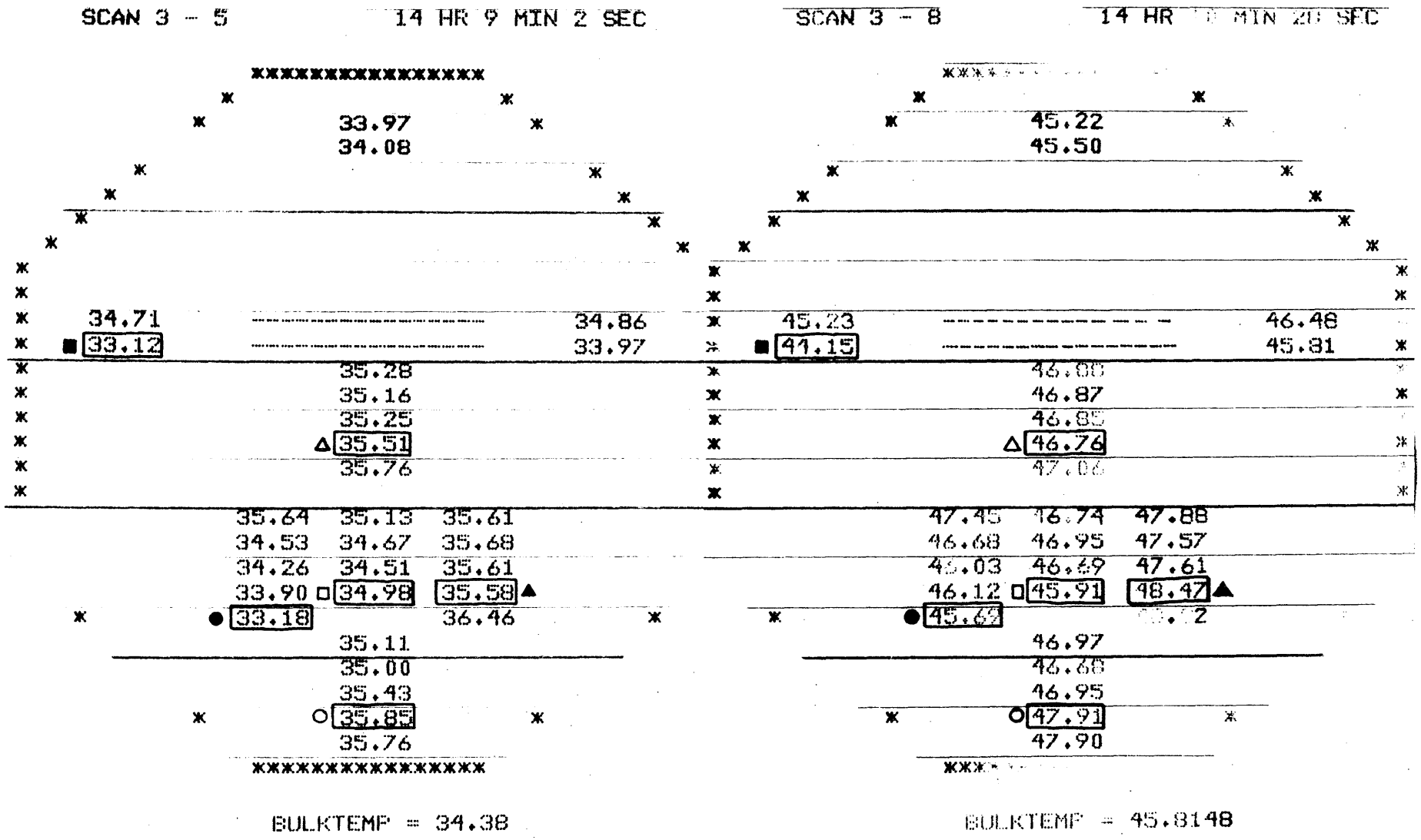

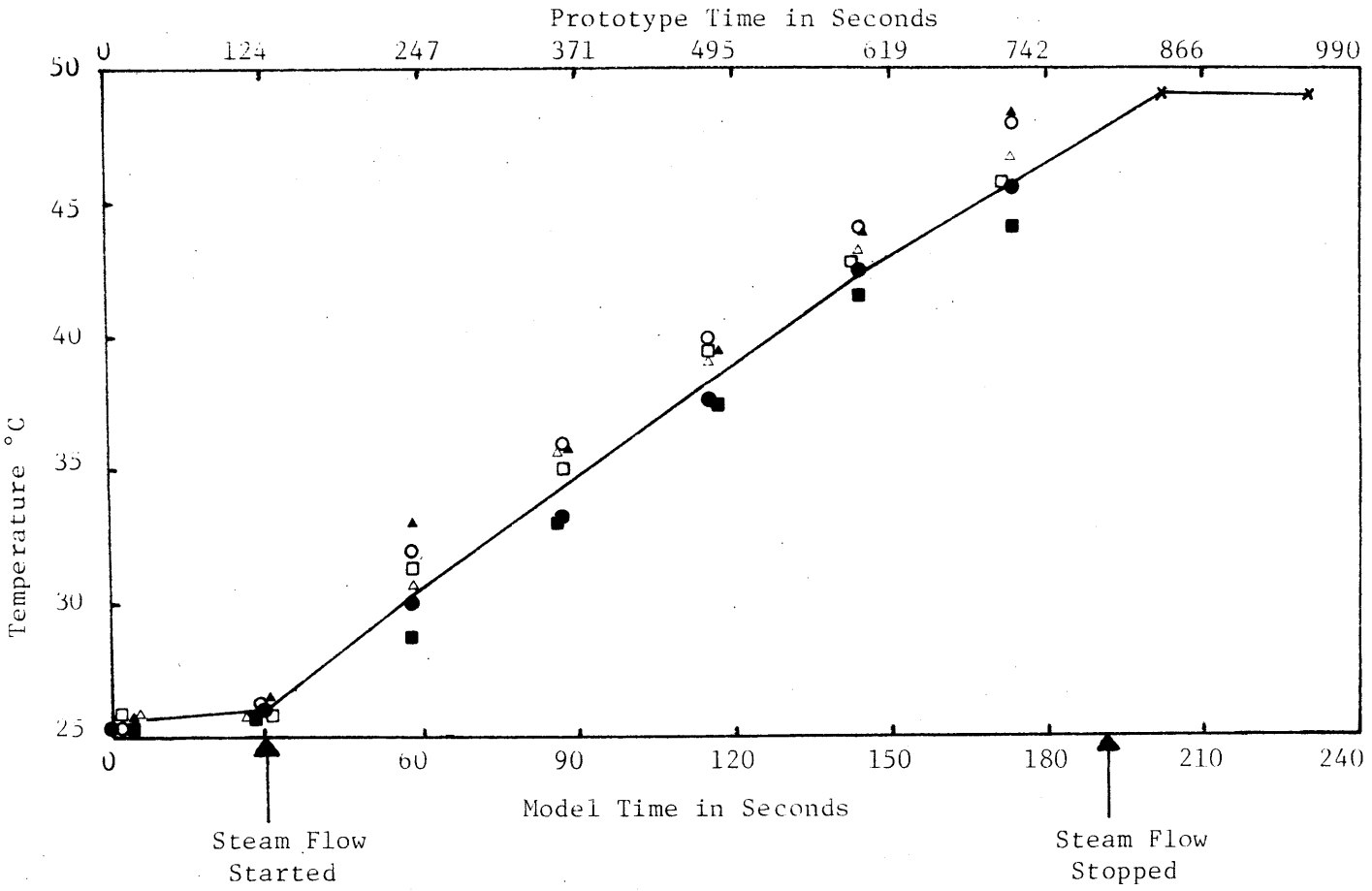

b) Temporal Distribution of Temperature

Figure 11: Results for Experiment 3

a) Spatial Temperature Distribution

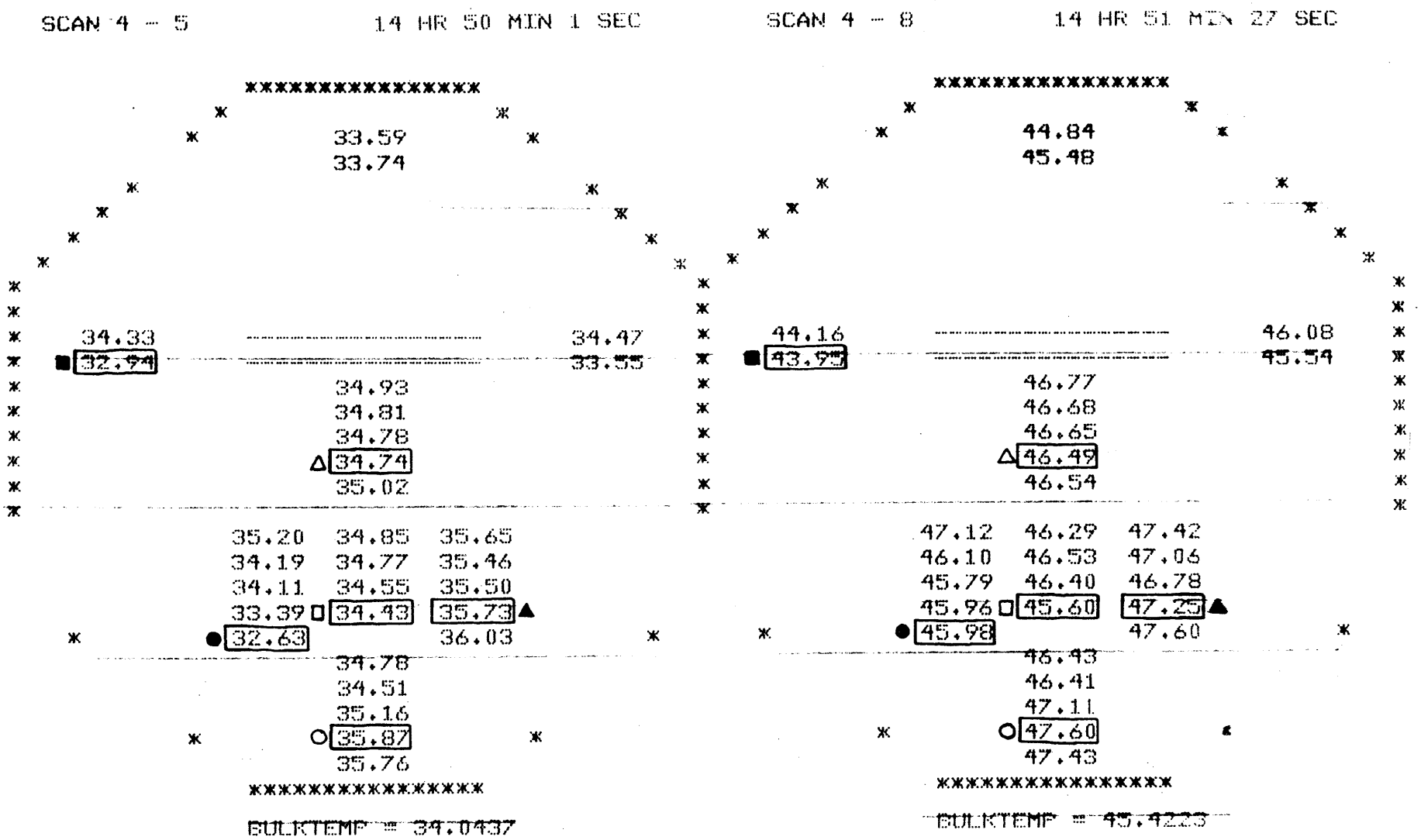

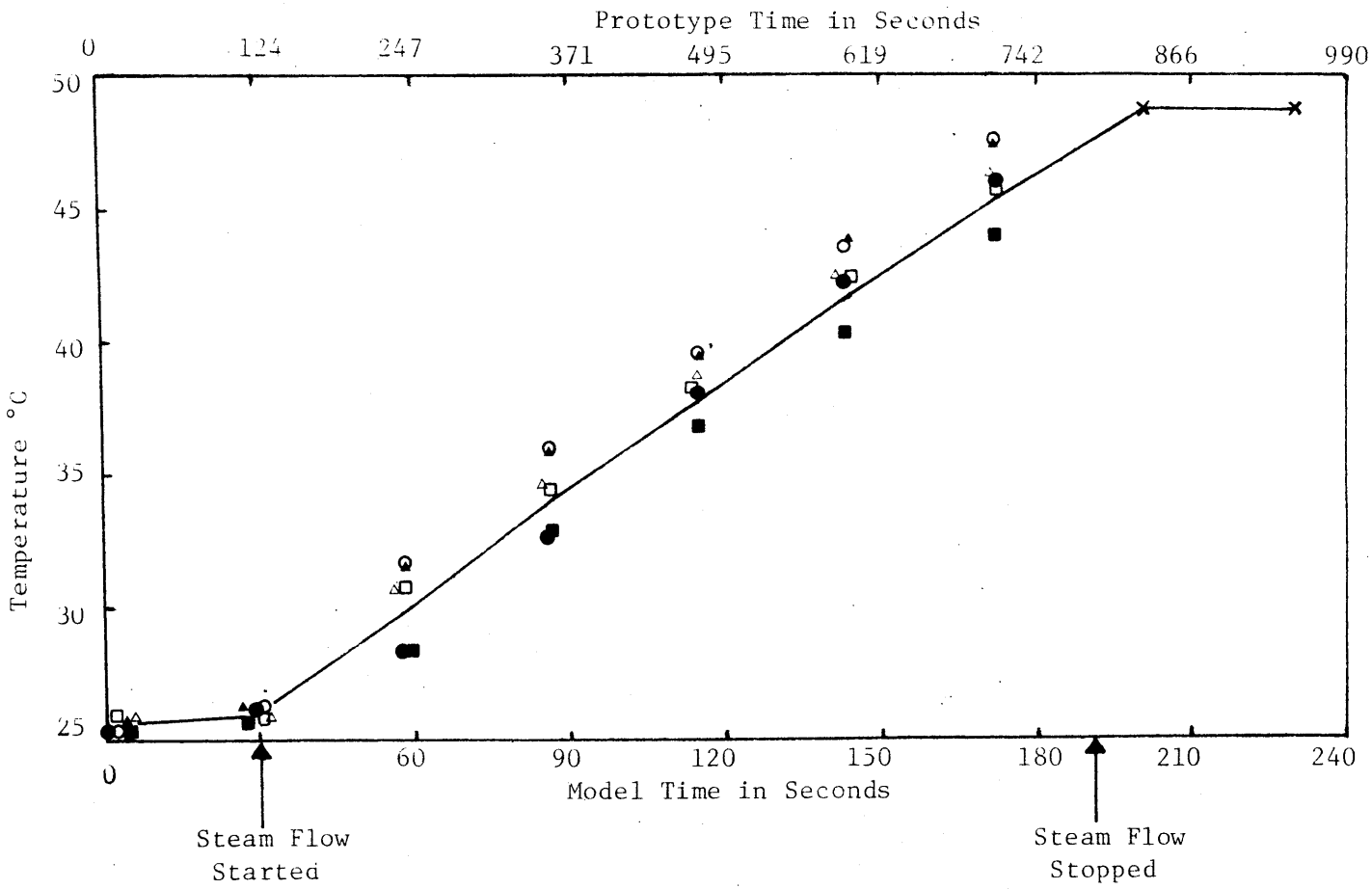

b) Temporal Temperature Distribution

Figure 12: Results for Experiment 4

a) Spatial Temperature Distribution

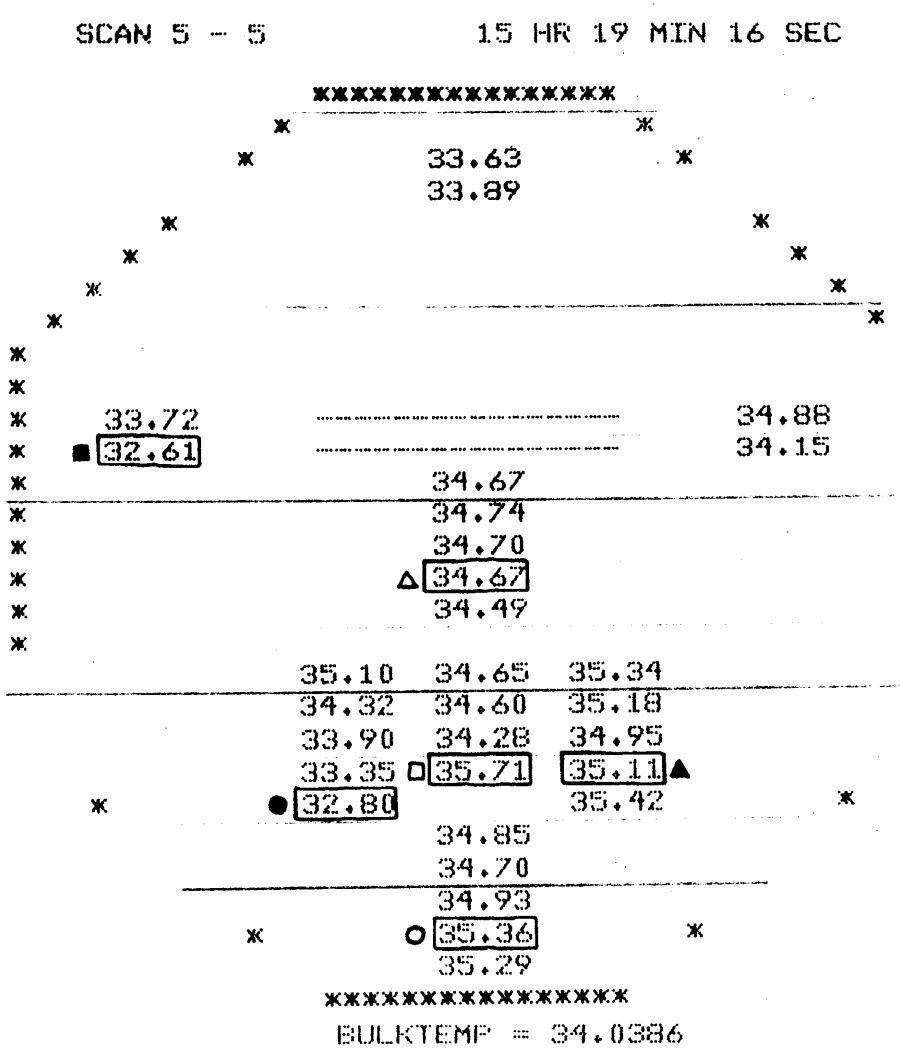

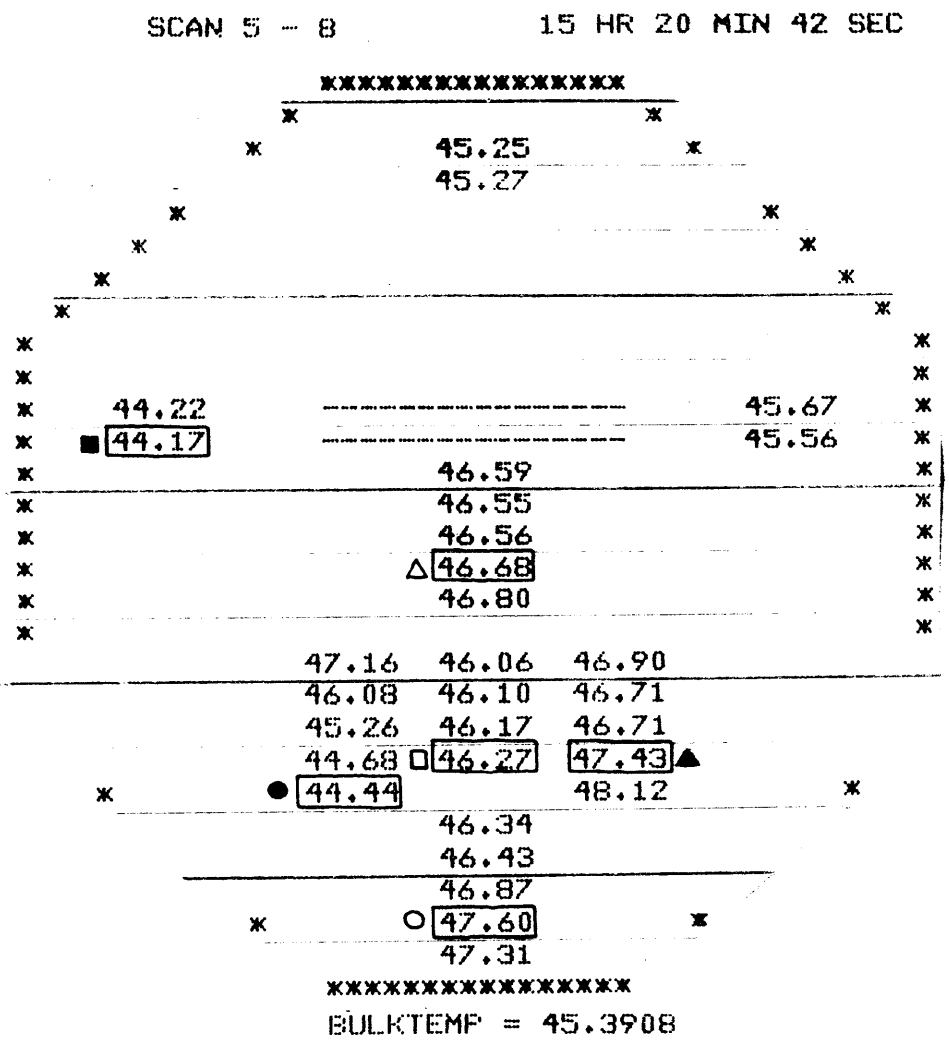

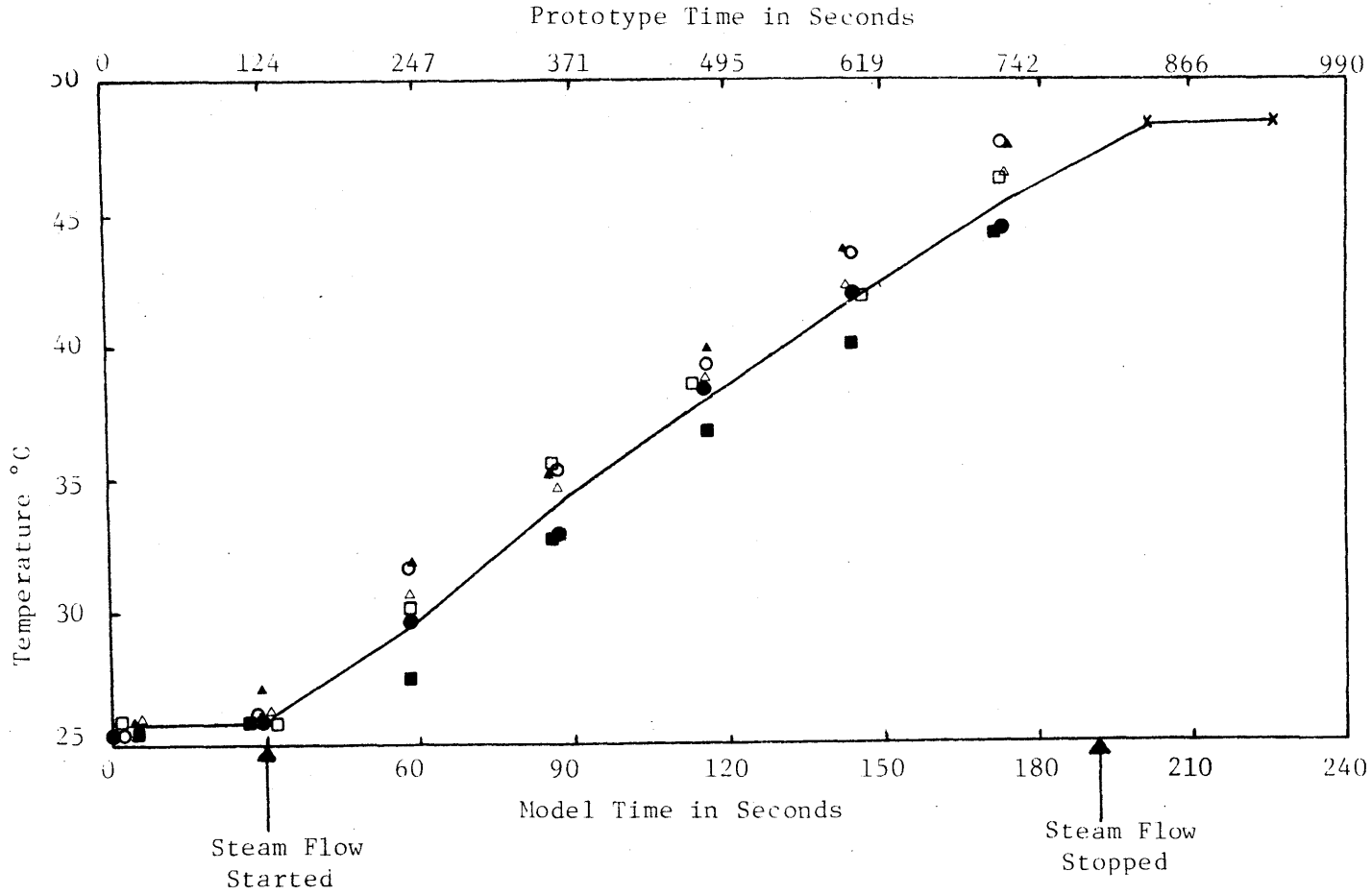

b) Temporal Temperature Distribution

Figure 13: Results for Experiment 5

a) Spatial Temperature Distribution

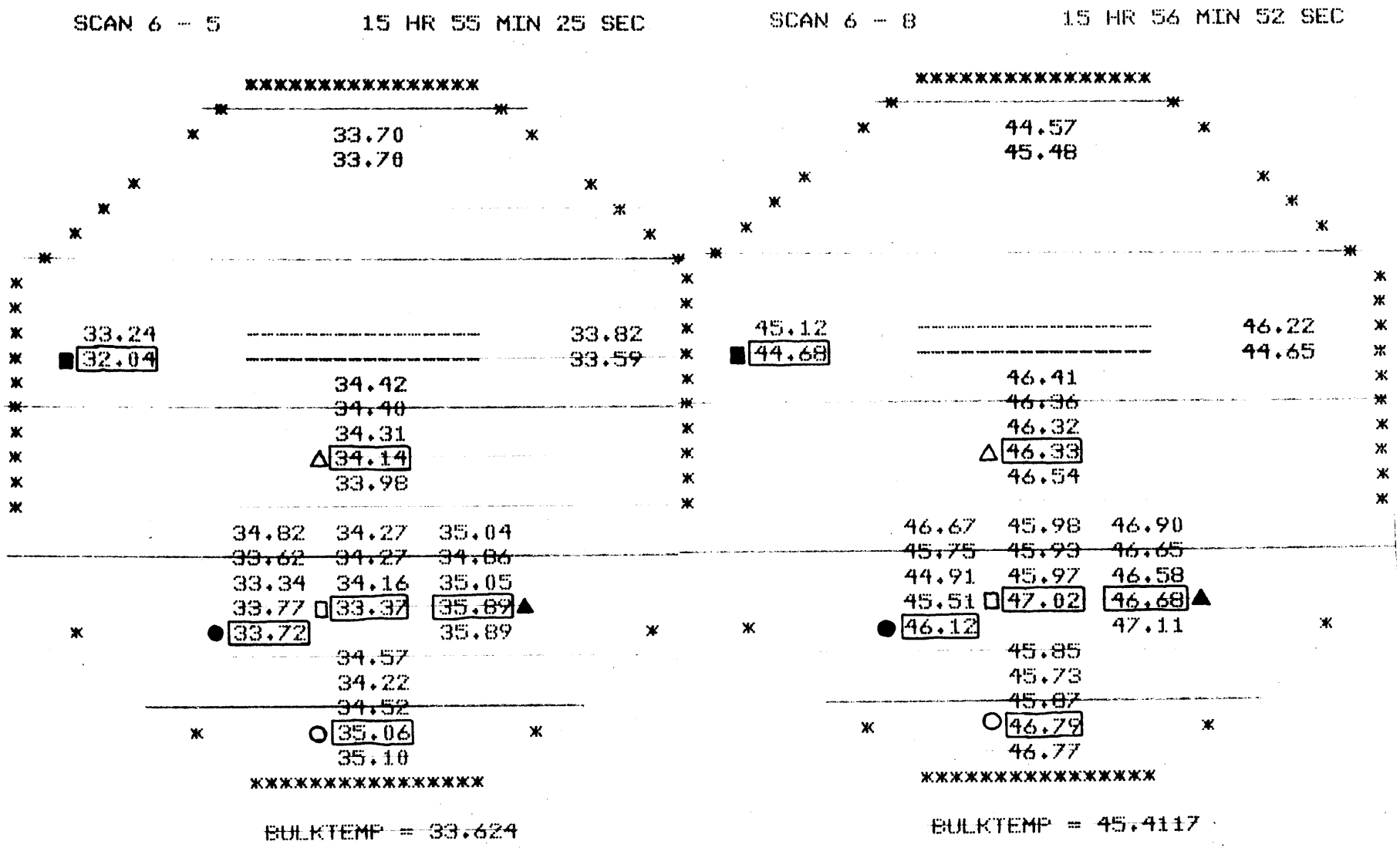

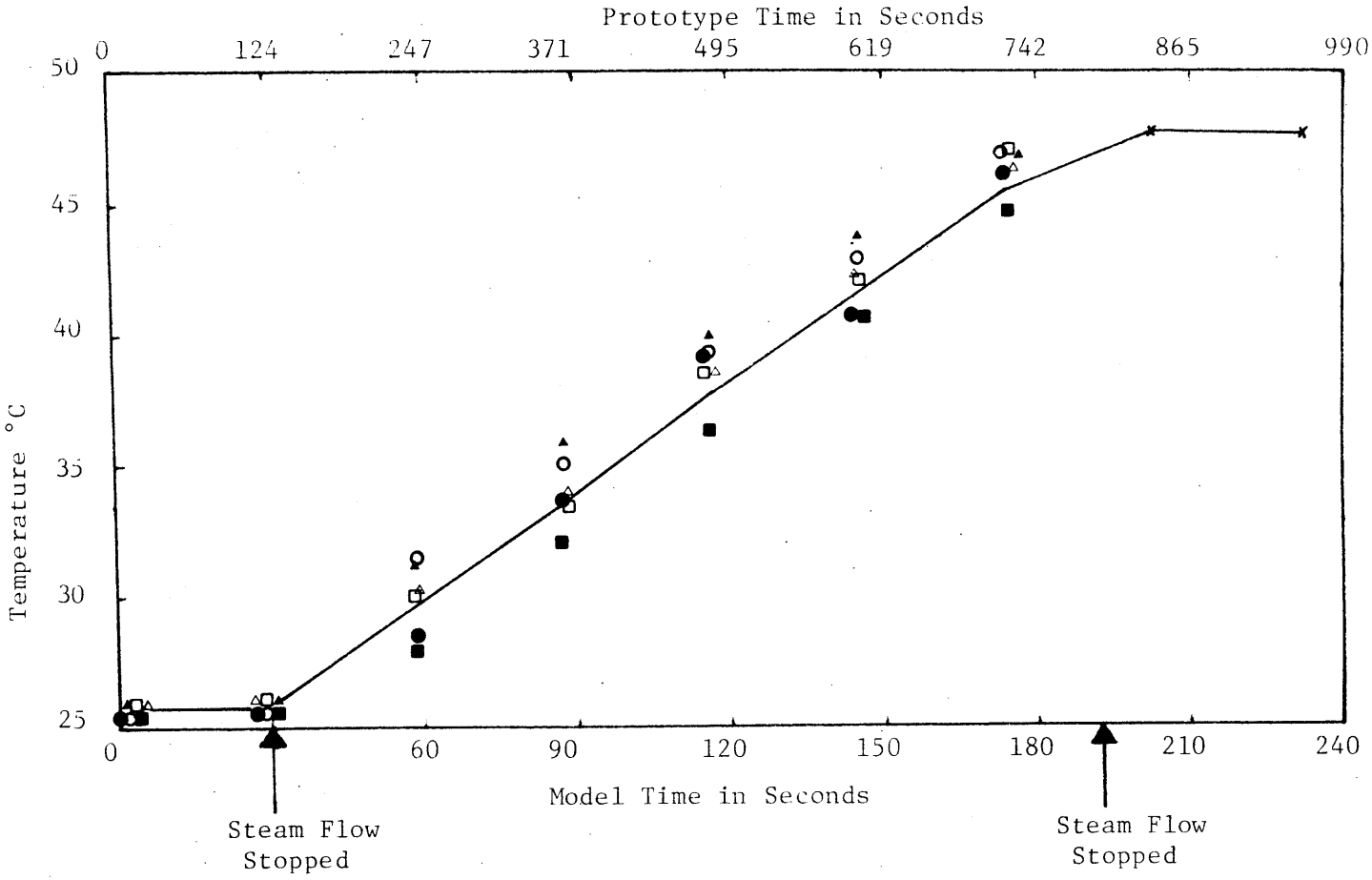

b) Temporal Temperature Distribution

Figure 14: Results for Experiment 6

a) Spatial Temperature Distribution

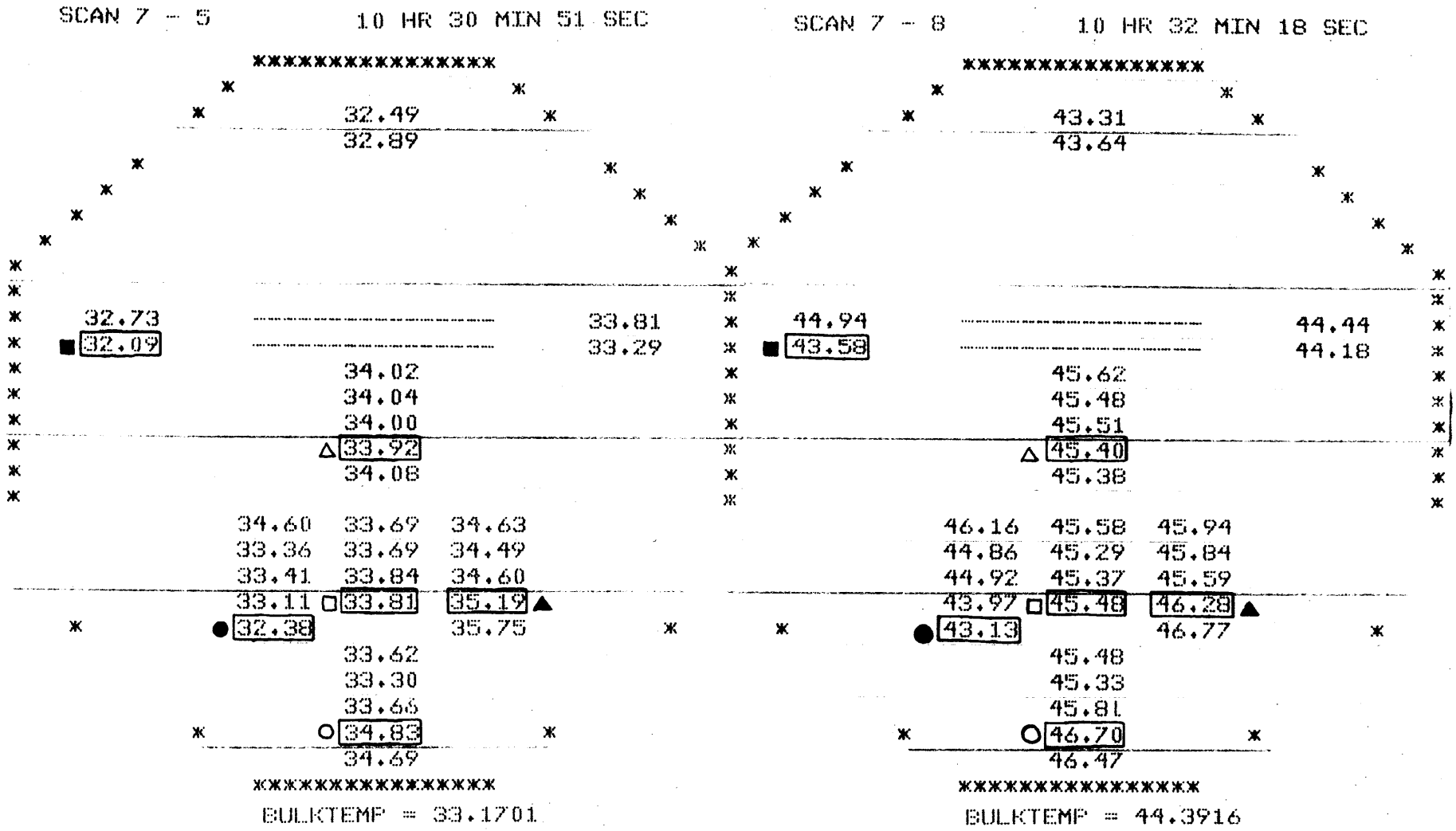

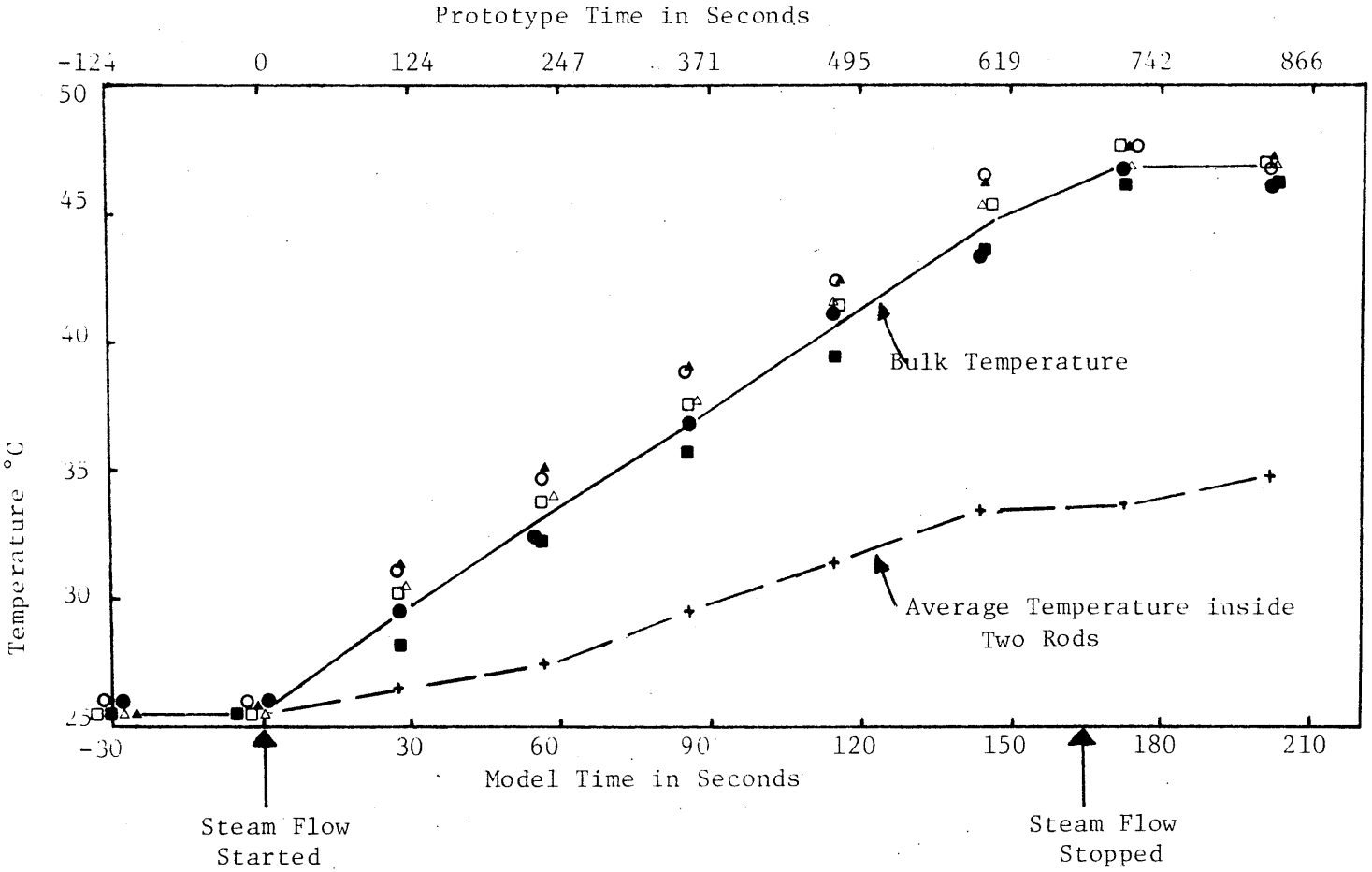

b) Temporal Temperature Distribtuion

Figure 15: Results for Experiment 7

a) Spatial Temperature Distribution

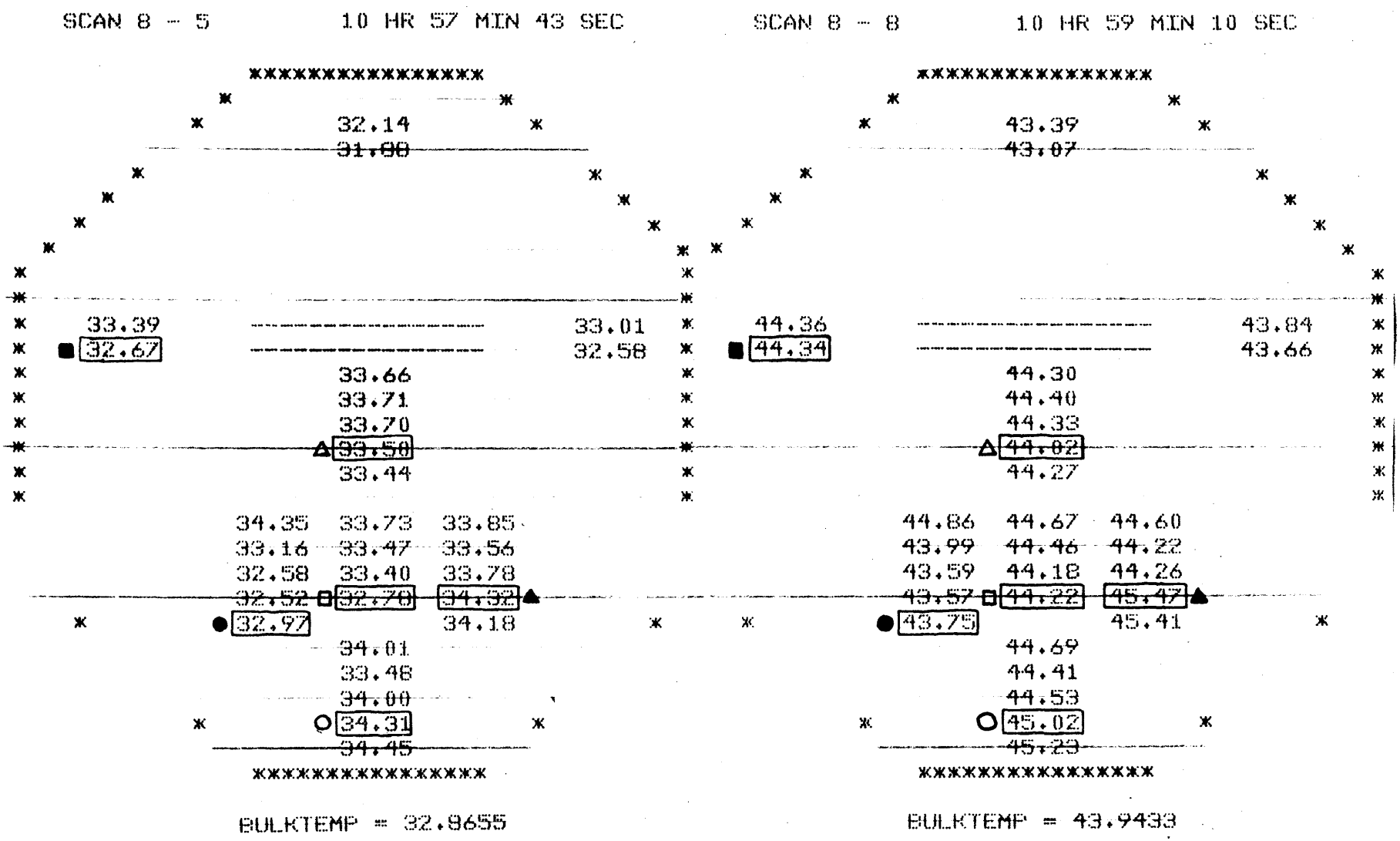

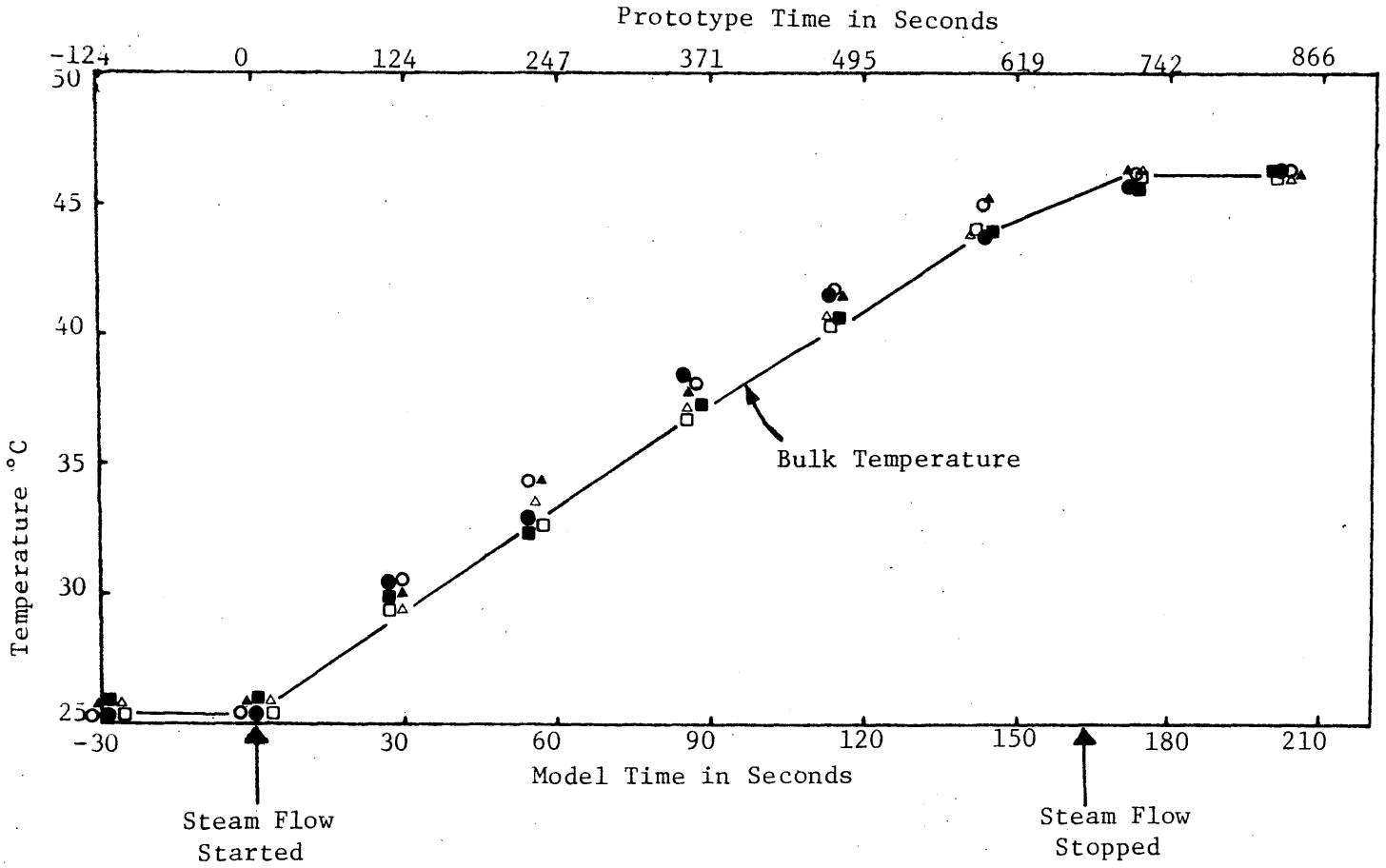

b) Temporal Temperature Distribution

Figure 16: Results for Experiment 8

a) Spatial Temperature Distribution

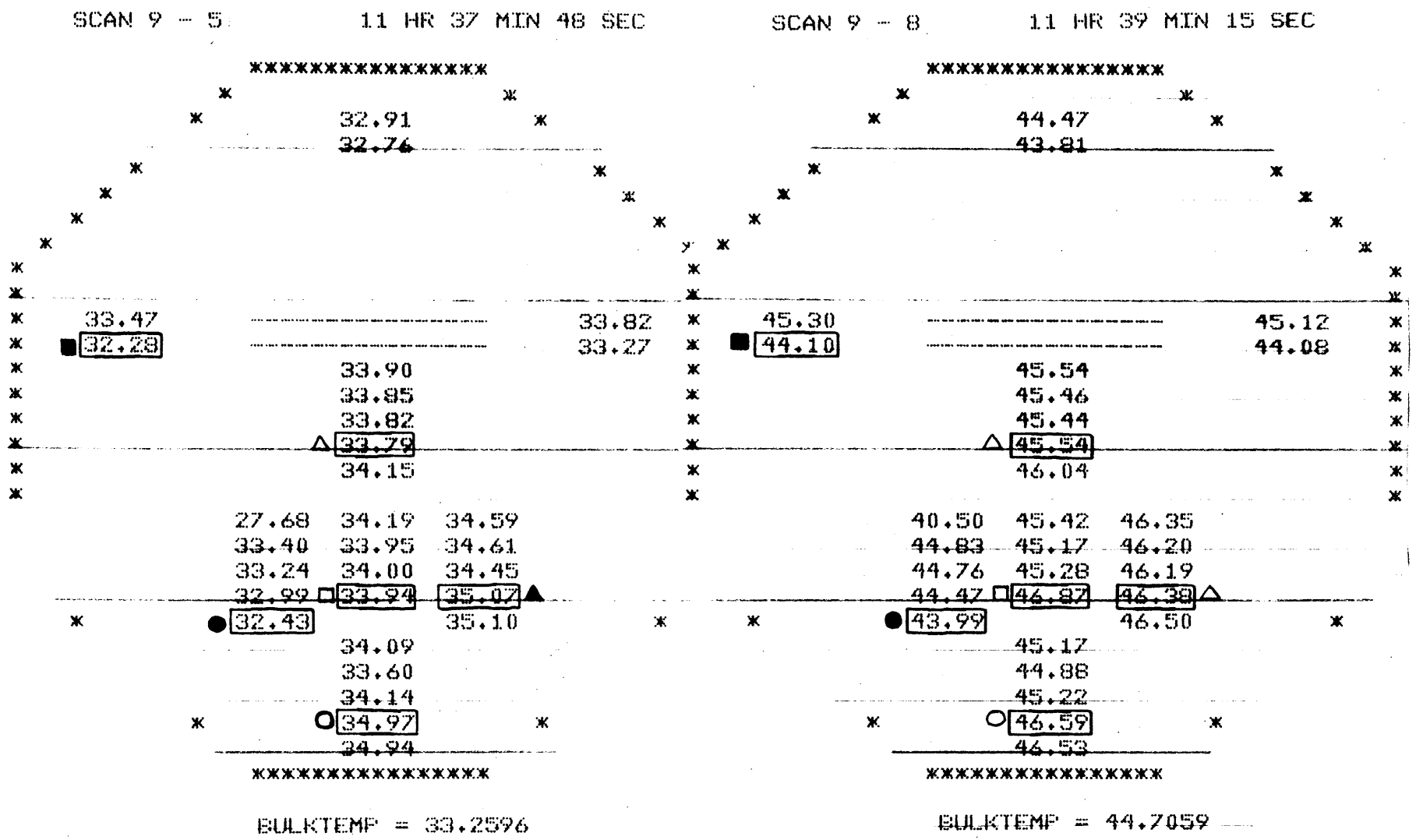

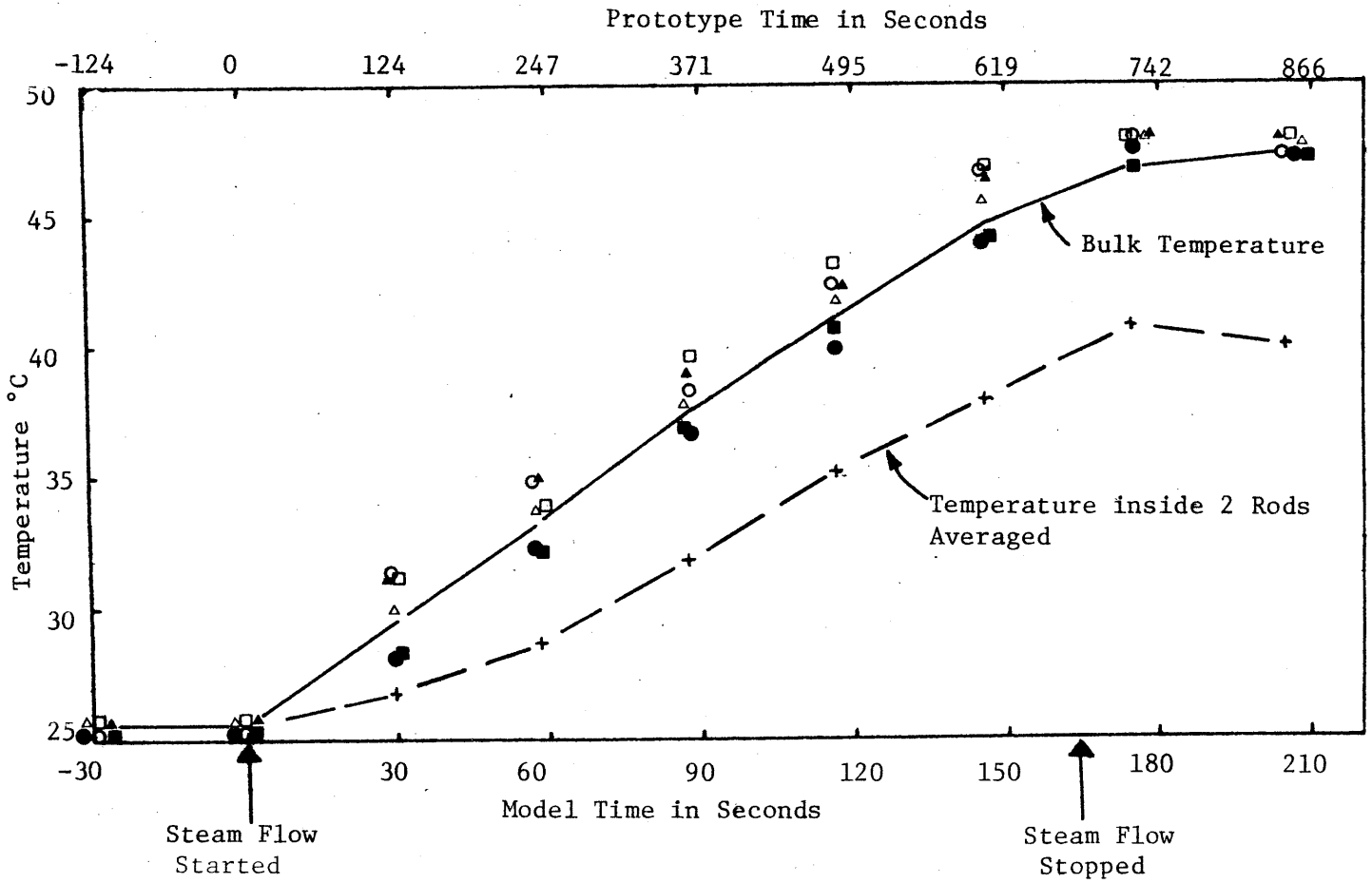

b) Temporal Temperature Distribution

Figure 17: Results for Experiment 9

a) Spatial Temperature Distribution

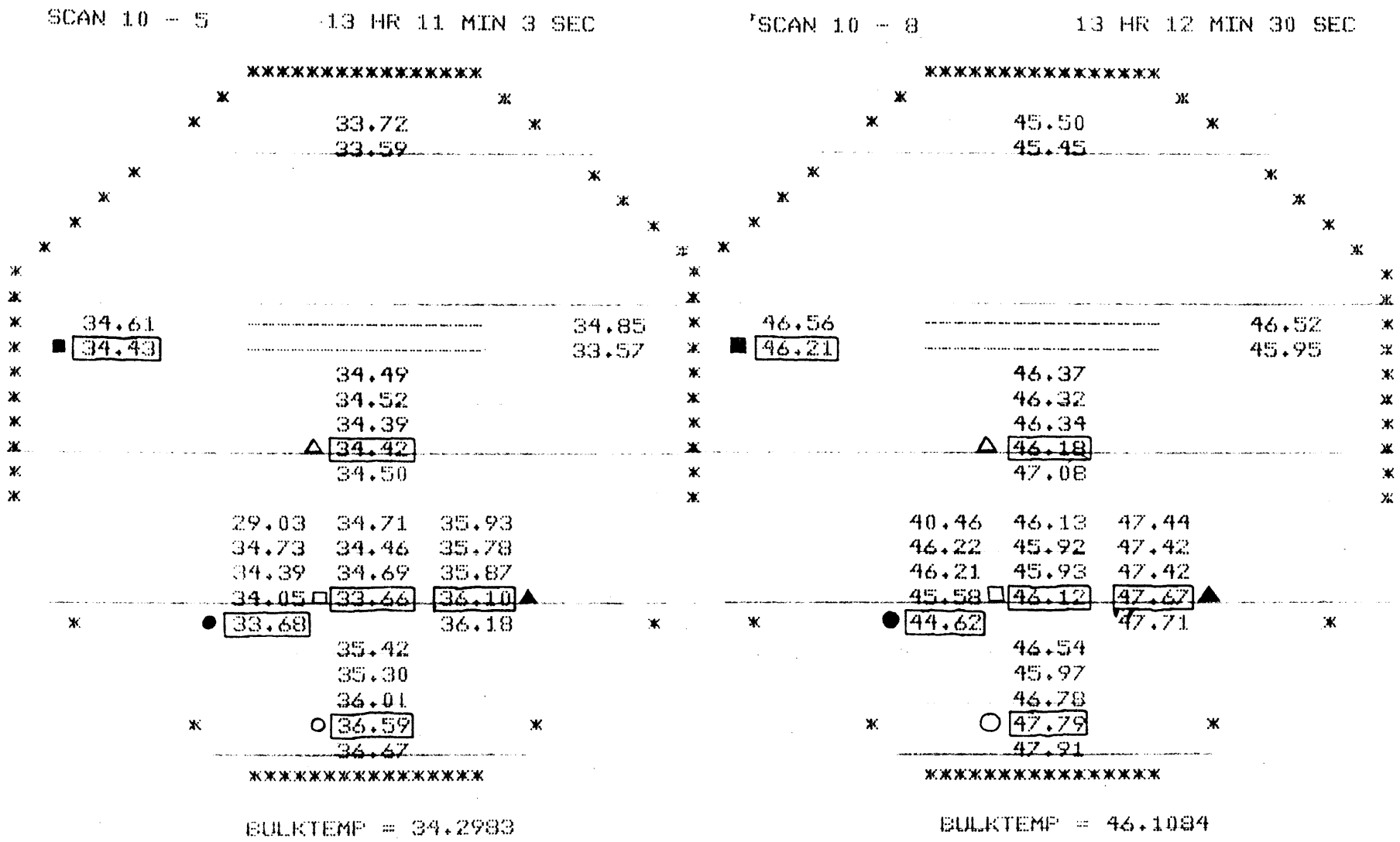

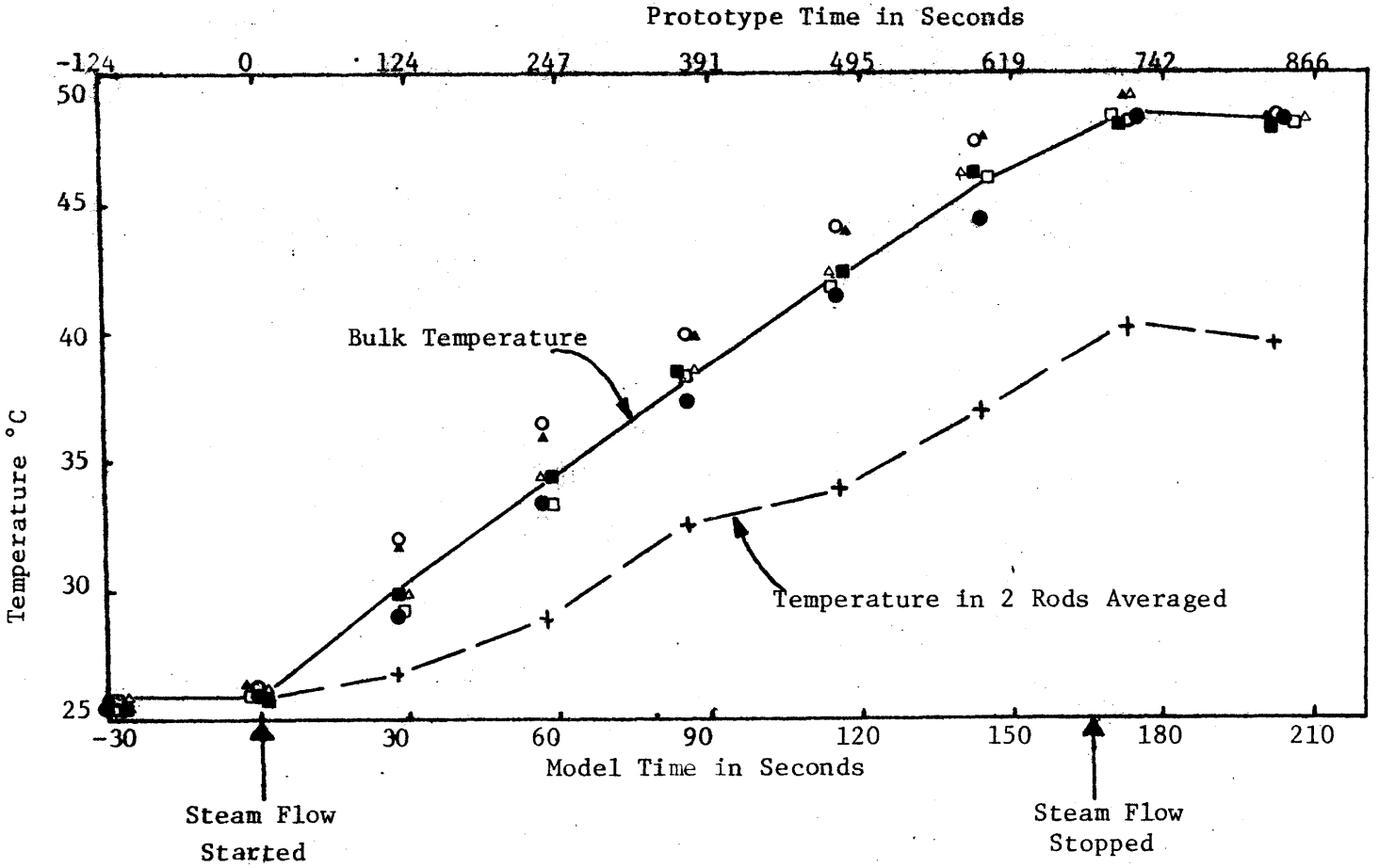

b) Temporal Temperature Distribution

Figure 18: Results for Experiment 10

a) Spatial Temperature Distribution

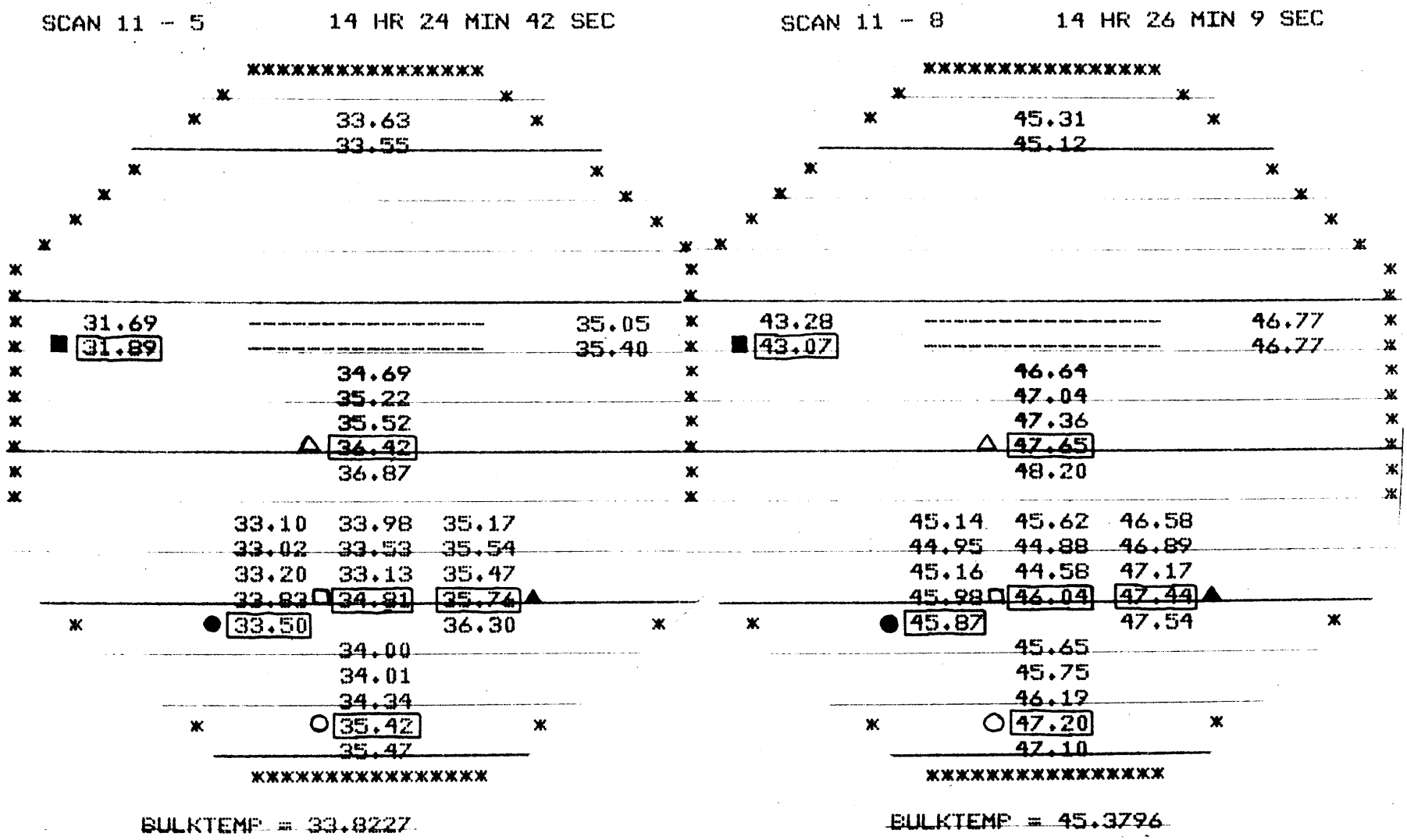

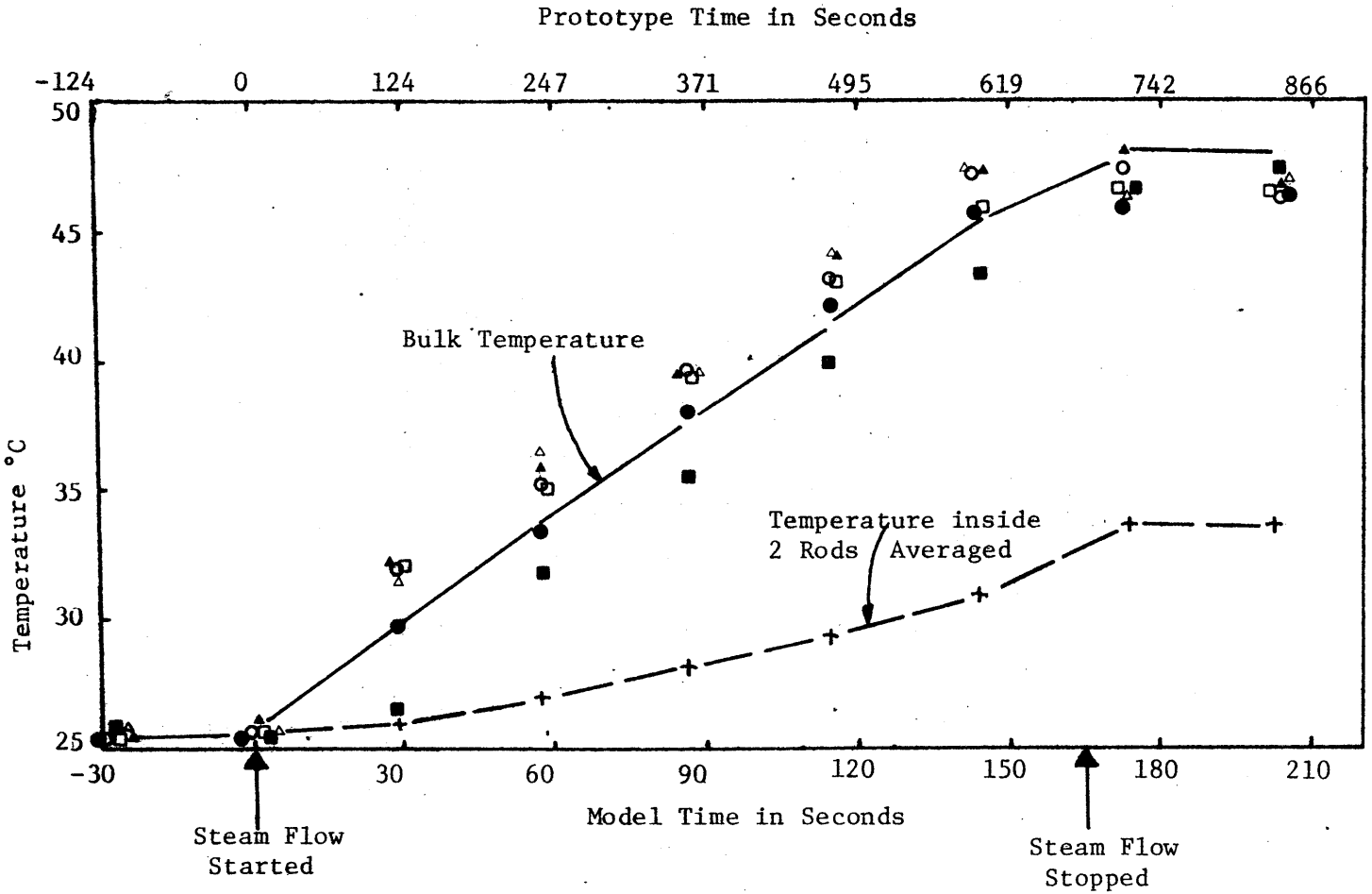

b) Temporal Temperature Distribution

Figure 19: Results for Experiment 11

a) Spatial Temperature Distribution

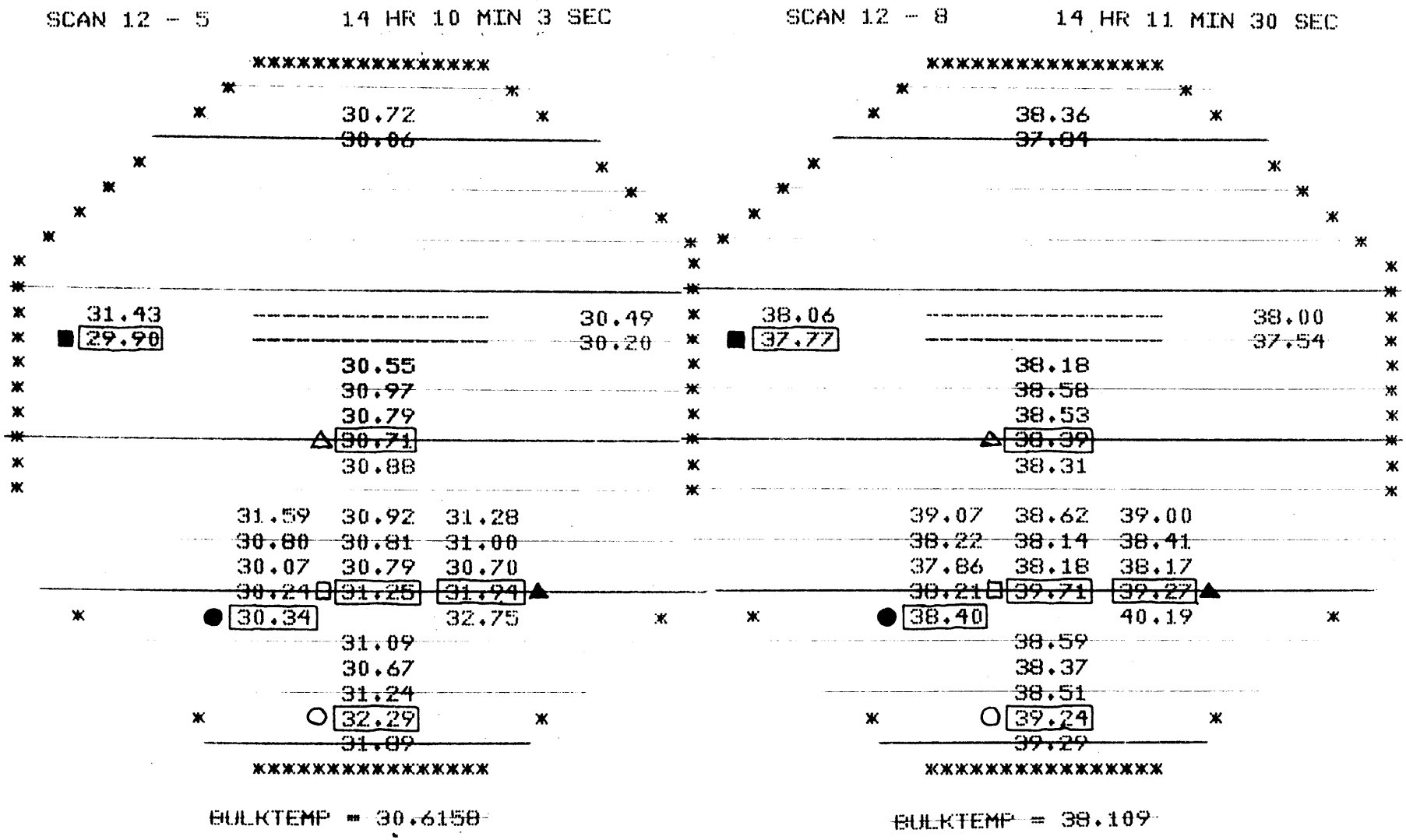

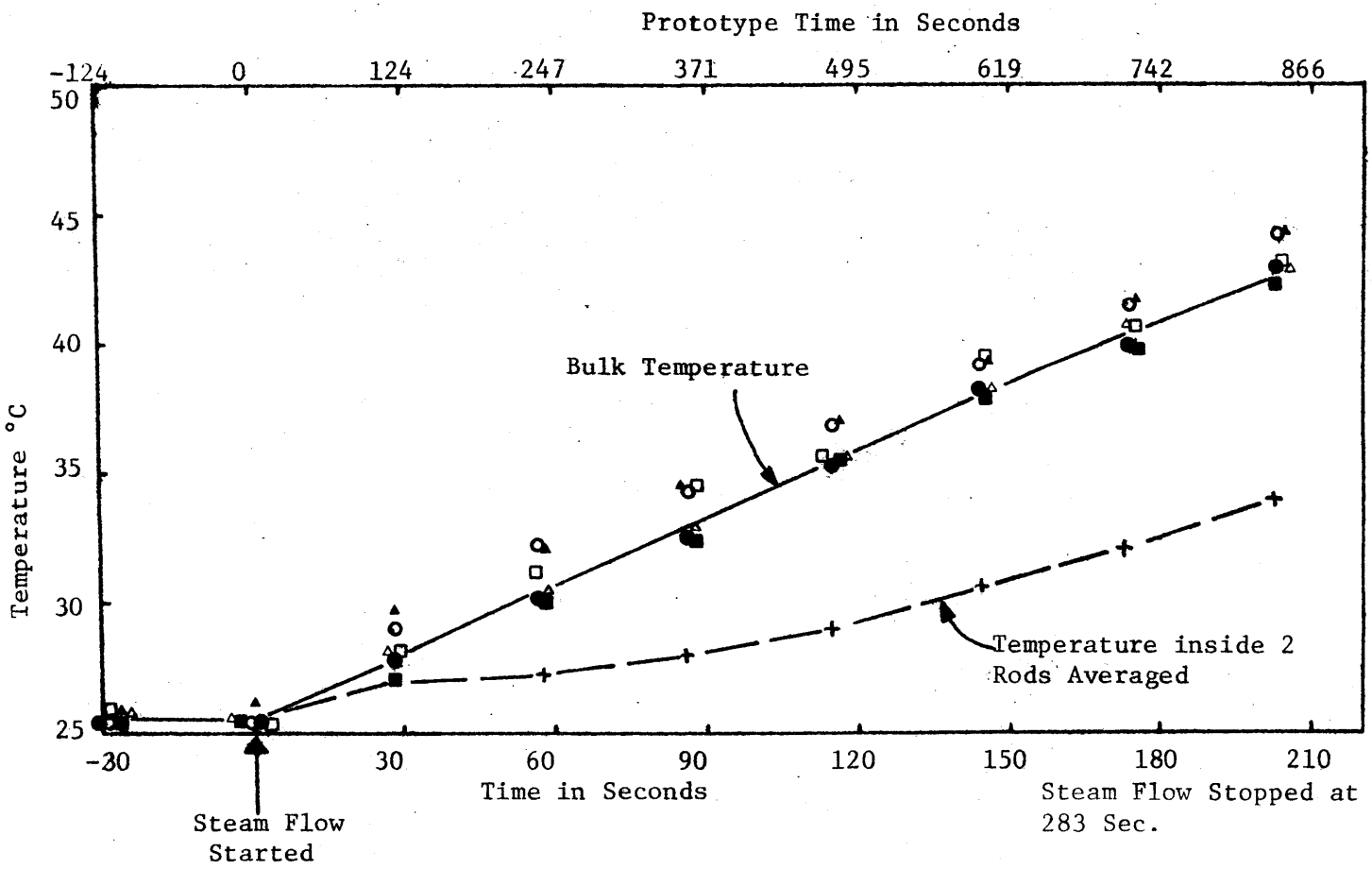

b) Temporal Temperature Distribution

Figure 20: Results for Experiment 12

a) Spatial Temperature Distribution

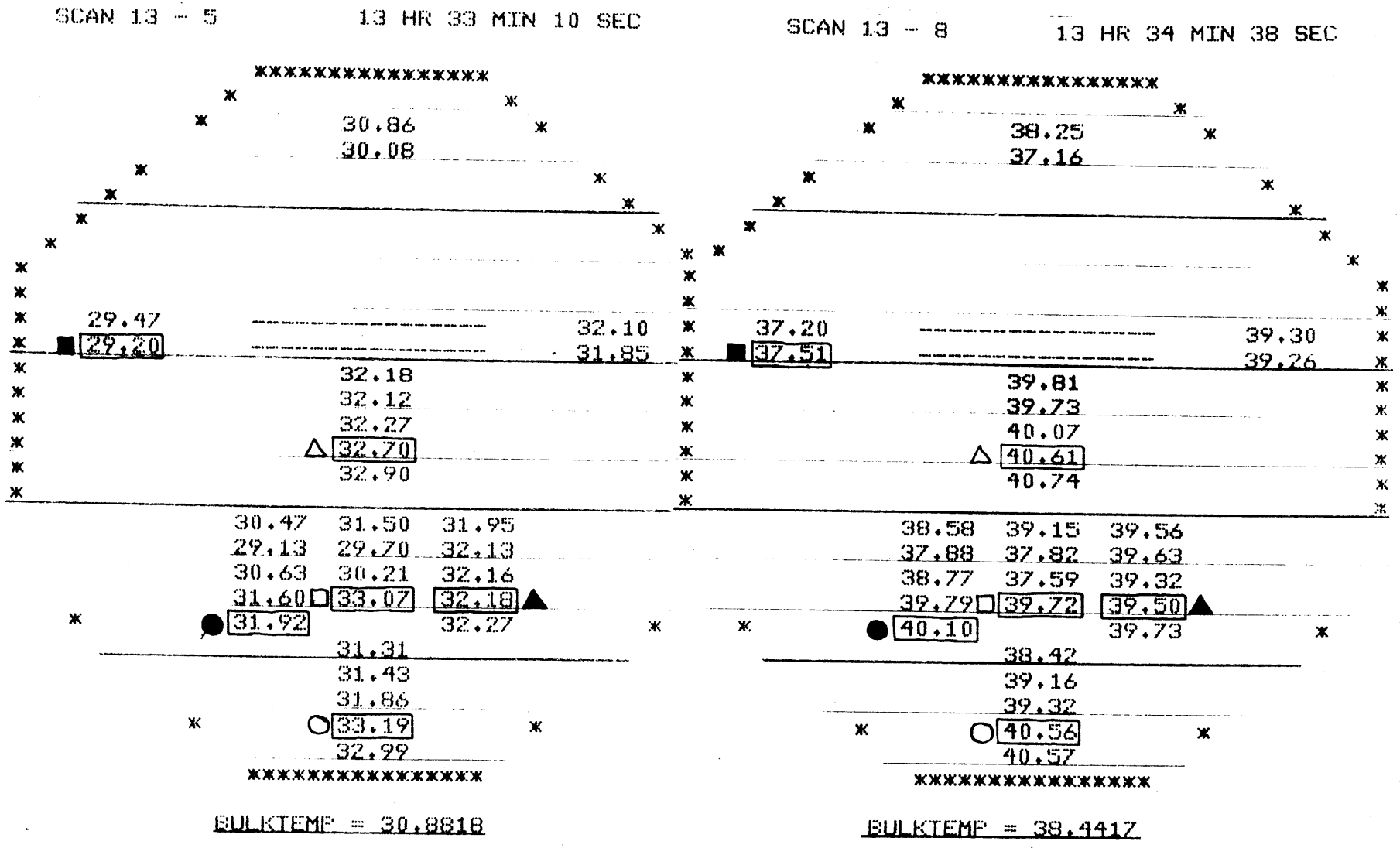

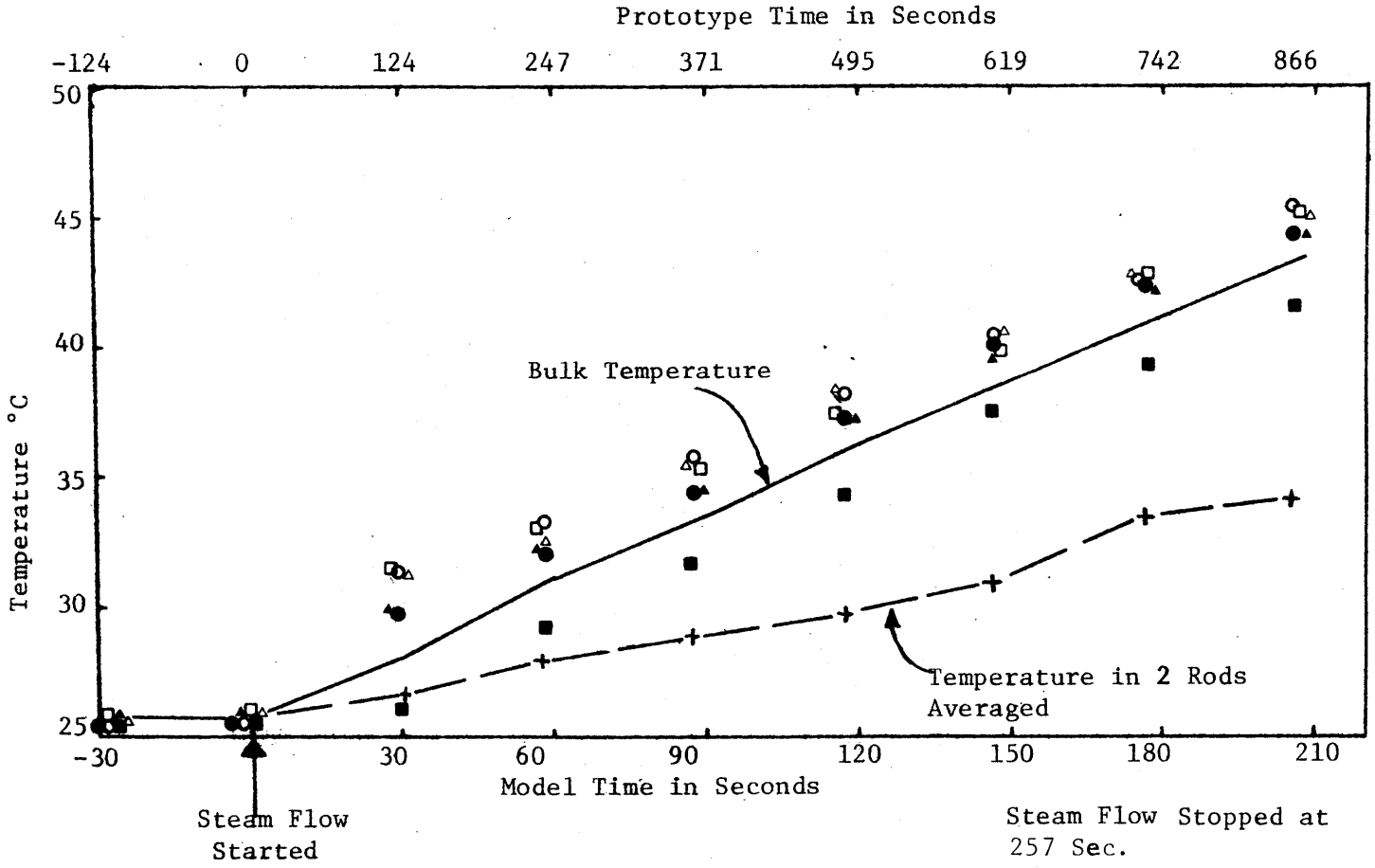

b) Temporal Temperature Distribution

Figure 21 Results for Experiment 13

a) Spatial Temperature Distribution

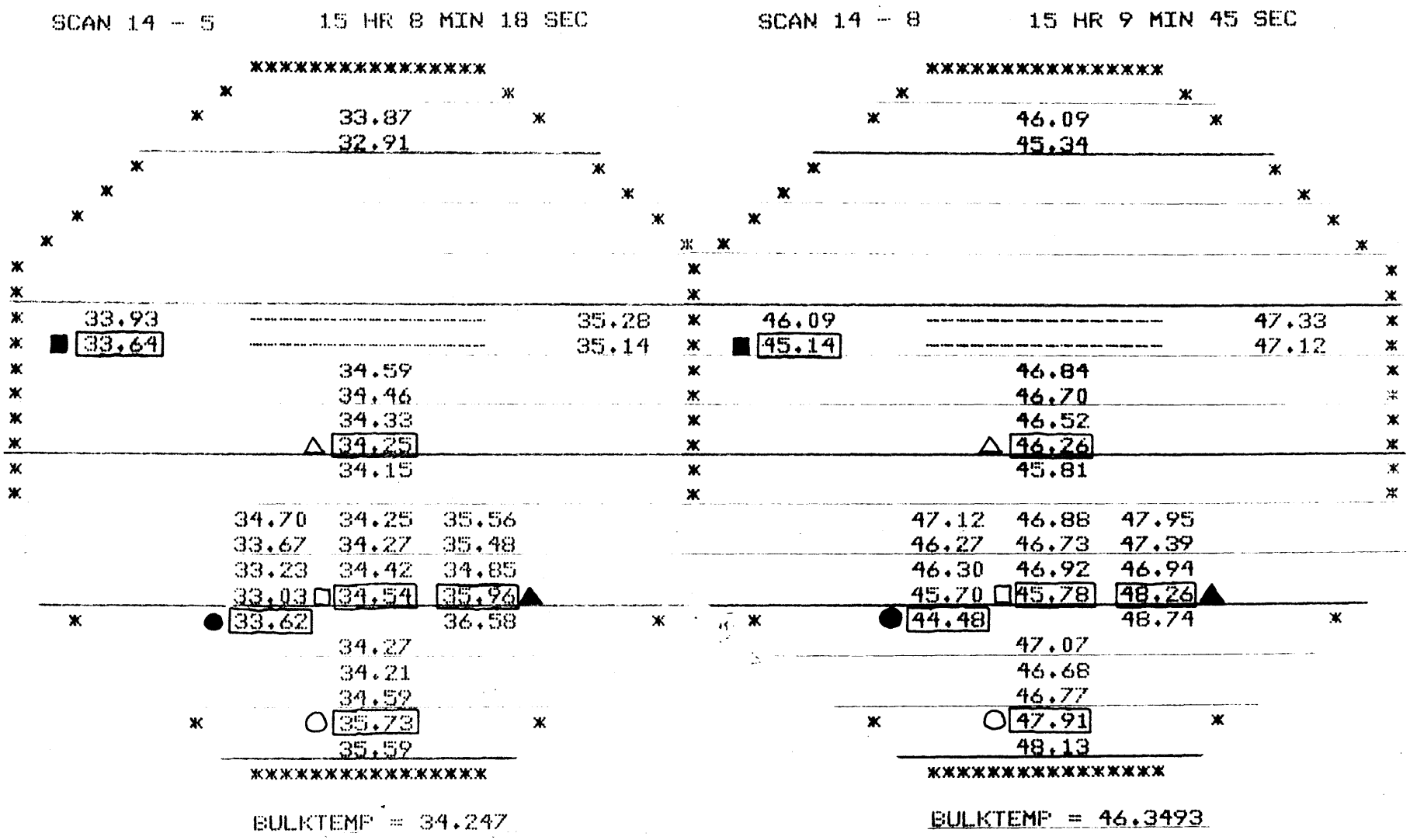

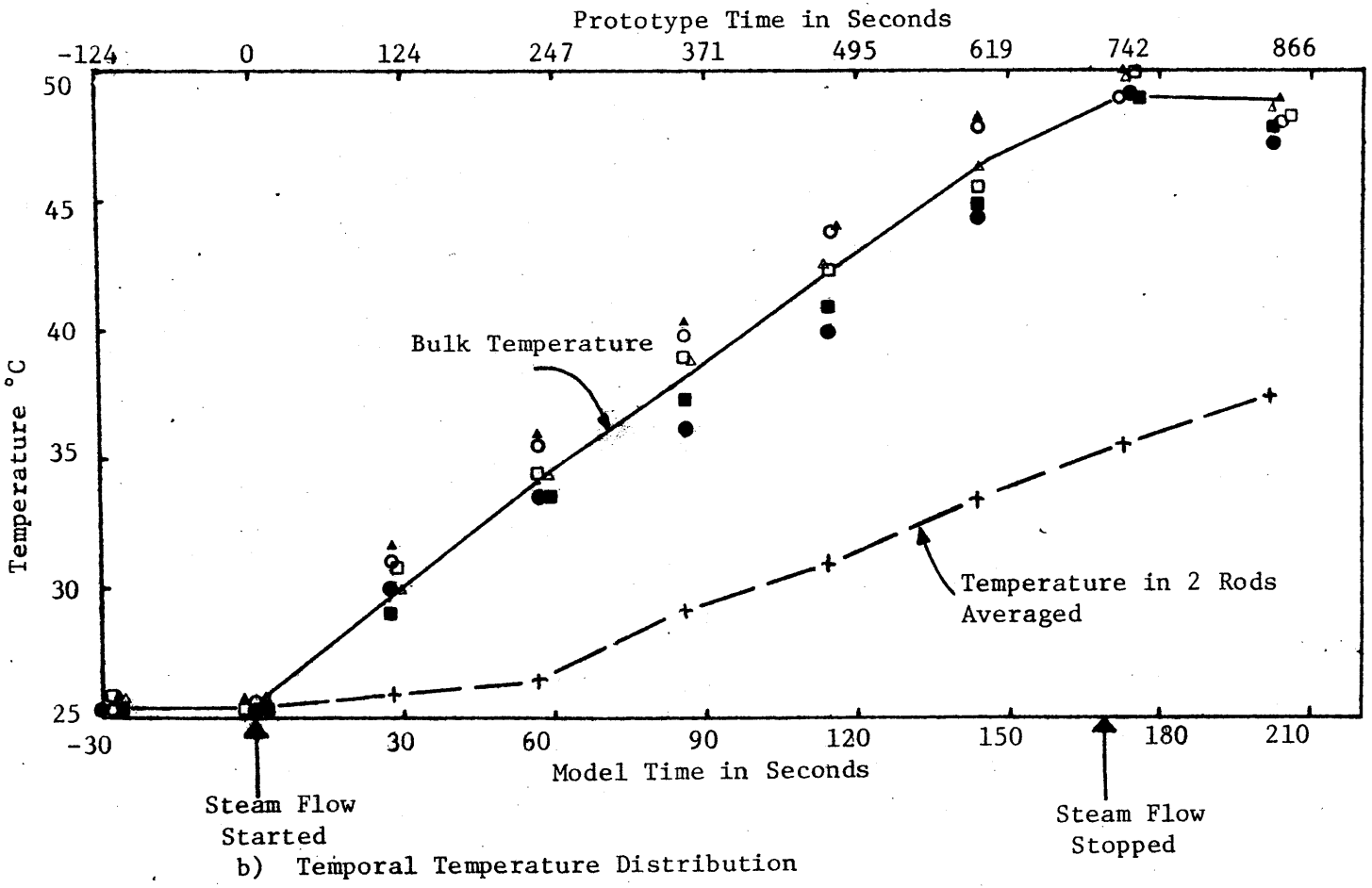

b) Temporal Temperature Distribution

Figure 22: Results for Experiment 14

a) Spatial Temperature Distribution

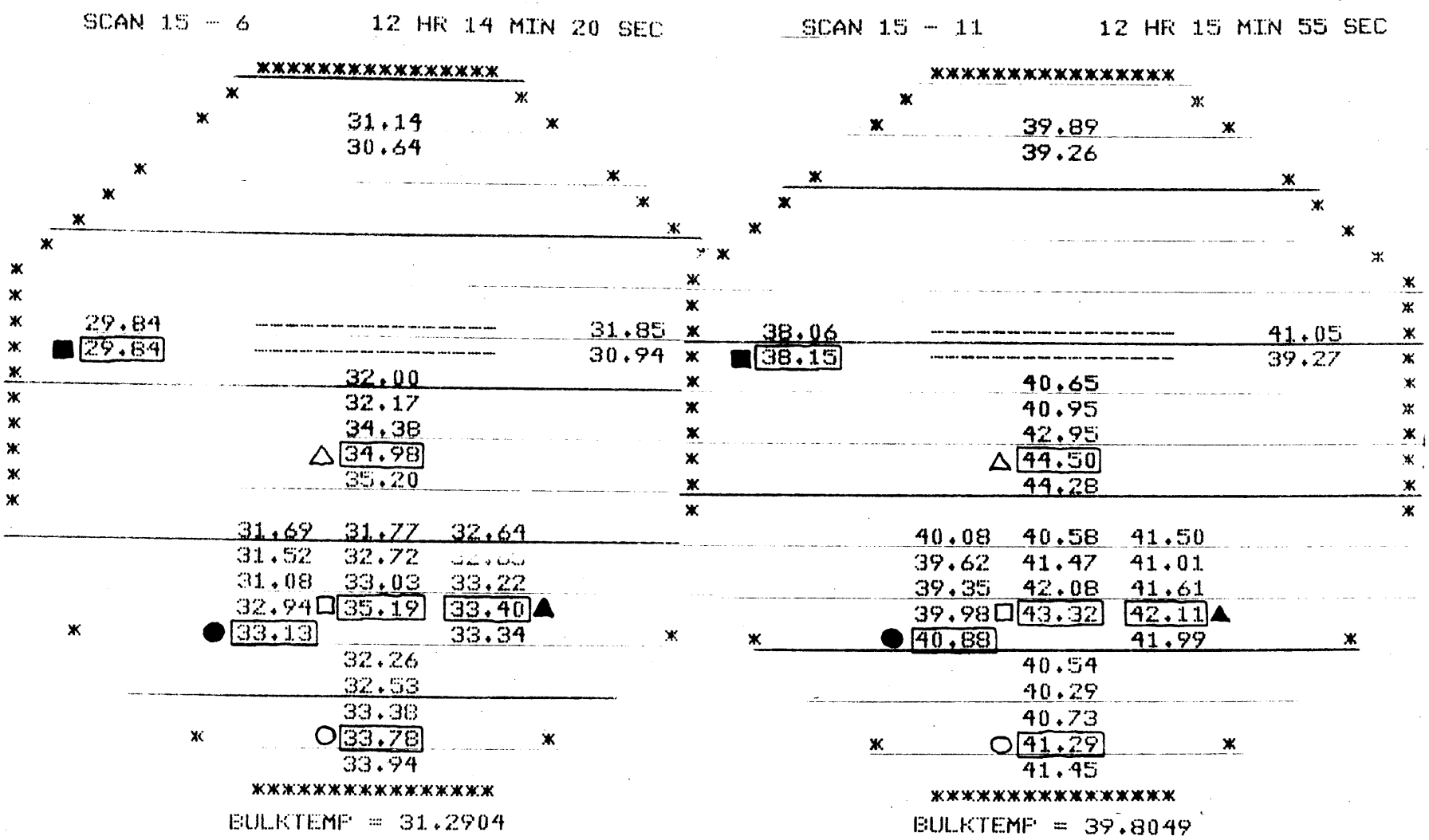

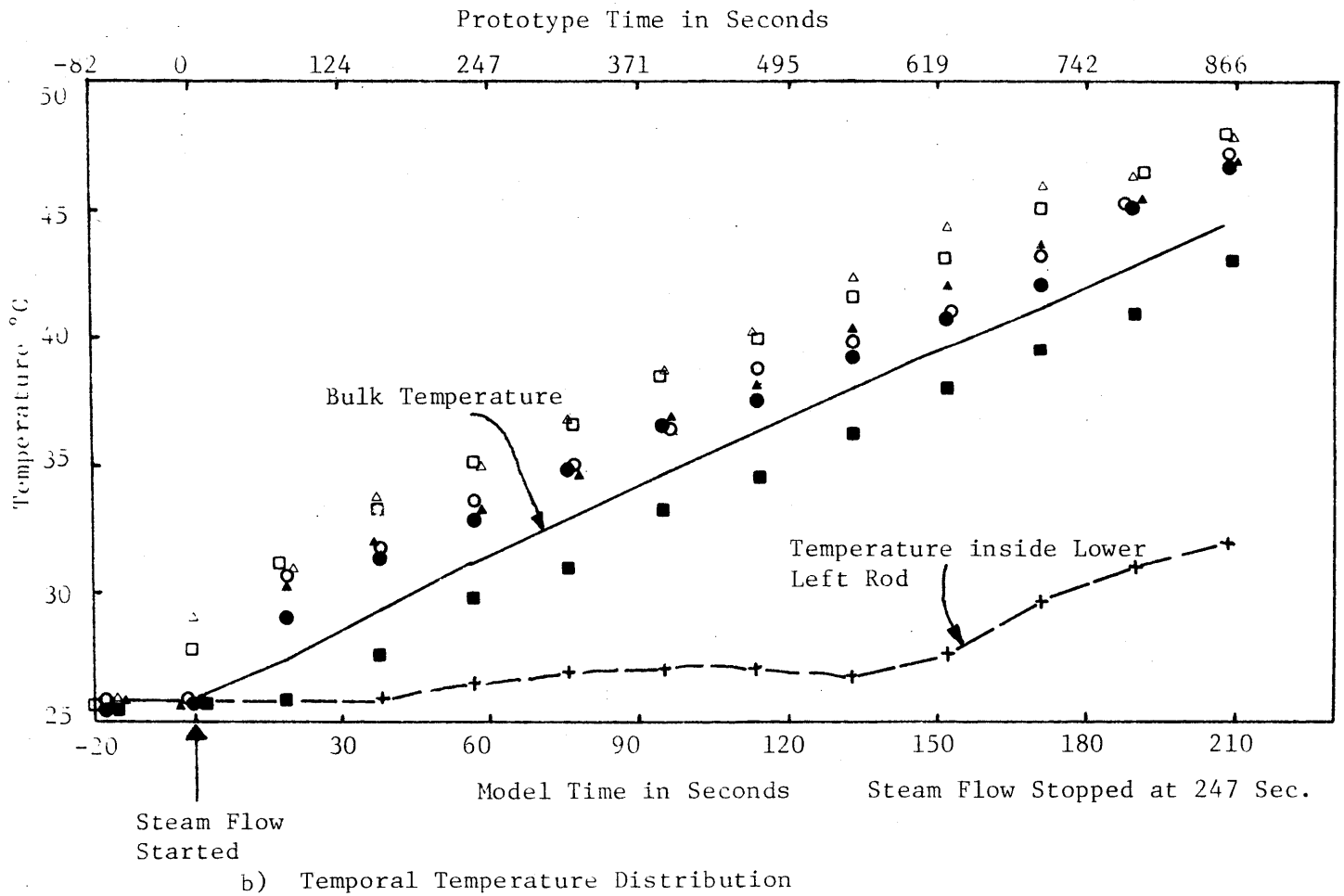

b) Temporal Temperature Distribution

Figure 23: Results for Experiment 15

a) Spatial Temperature Distribution

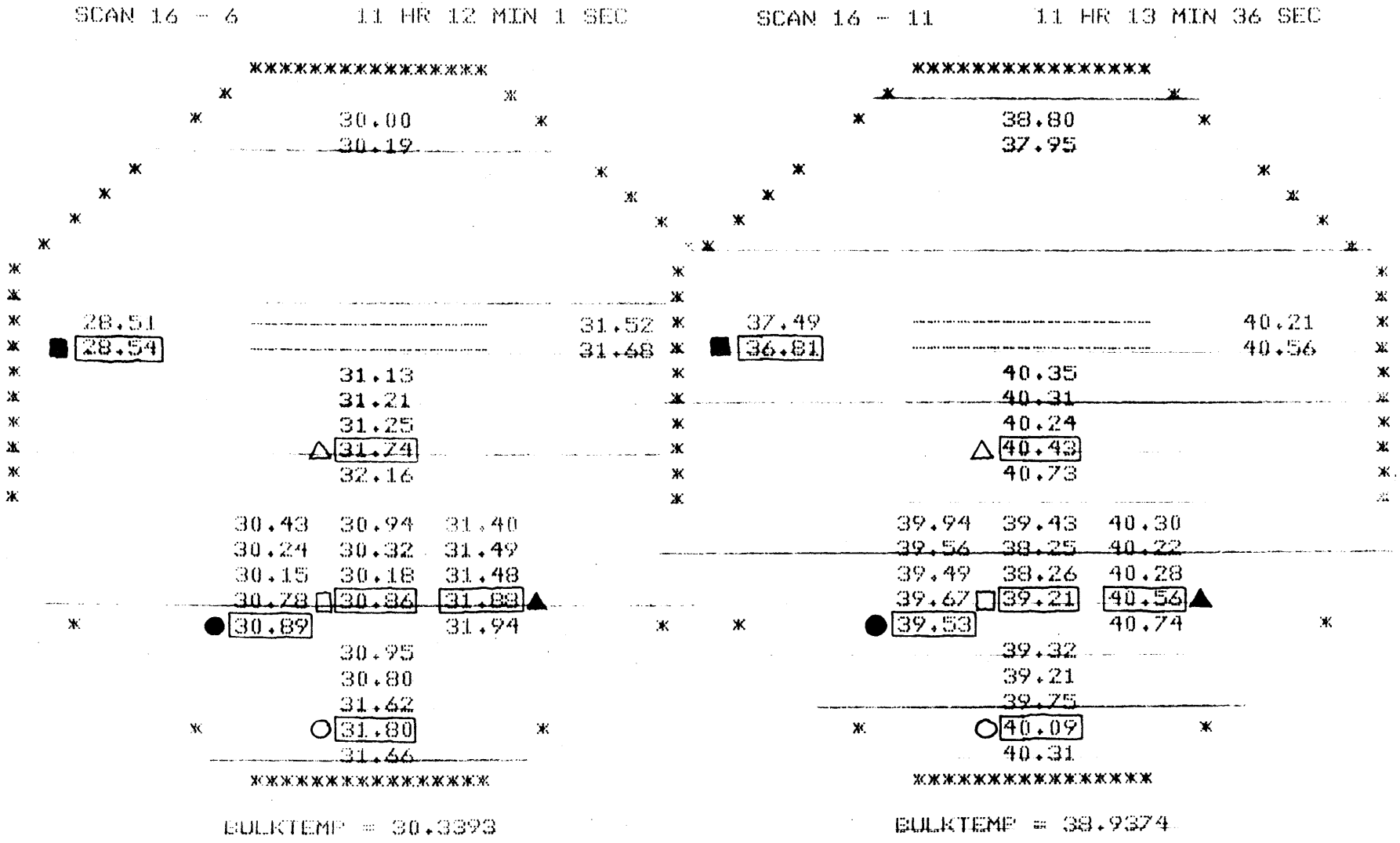

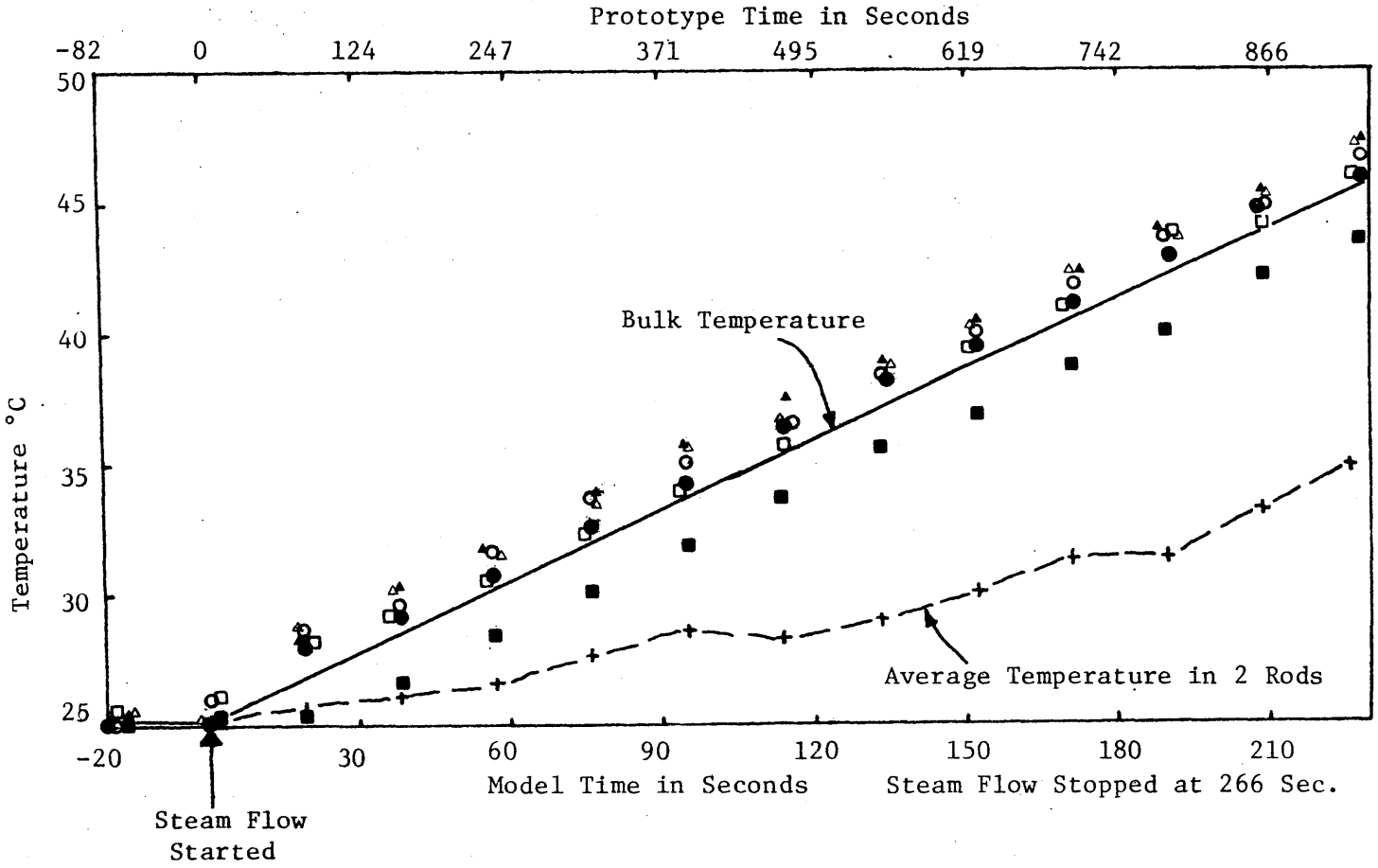

b) Temporal Temperature Distribution

Figure 24: Results for Experiment 16

a) Spatial Temperature Distribution

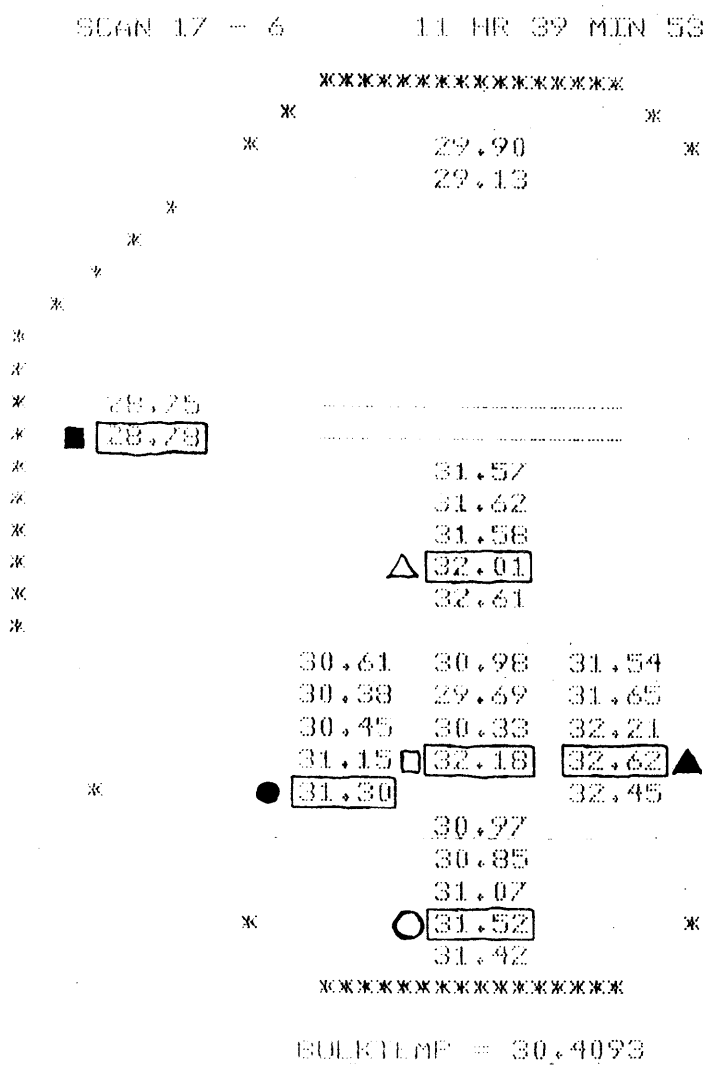

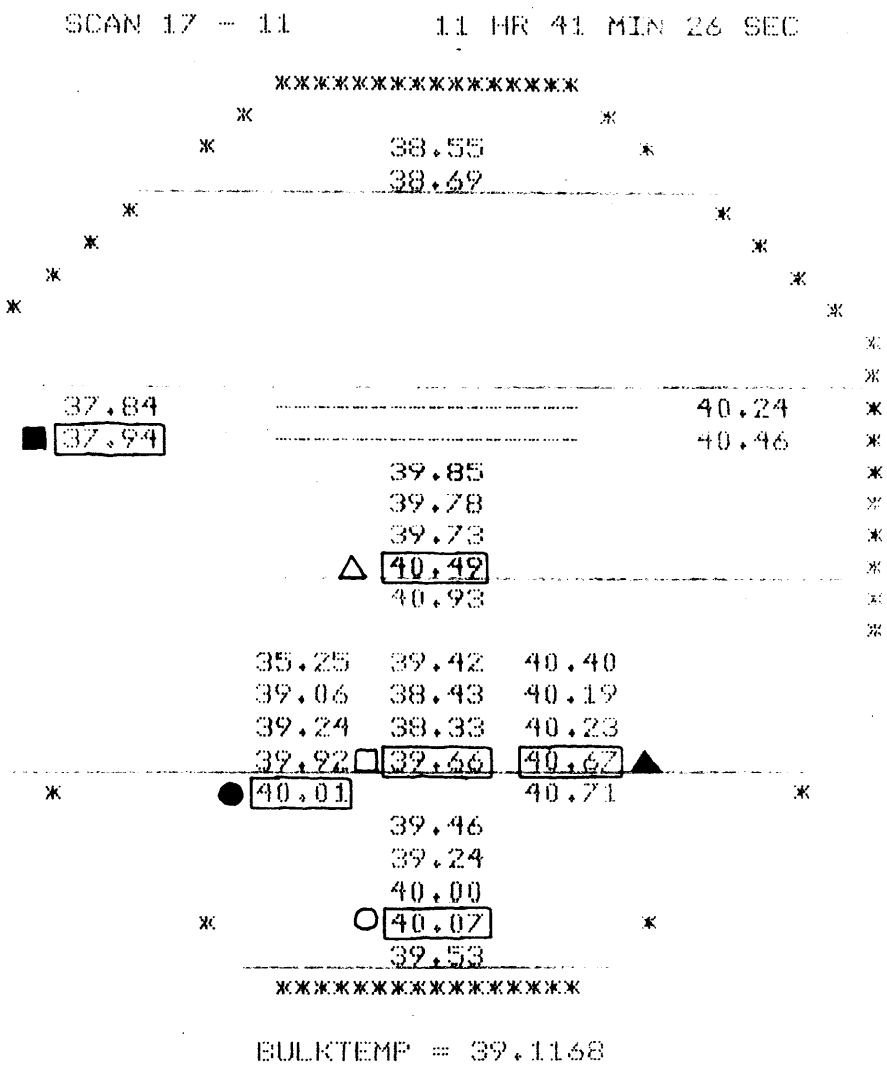

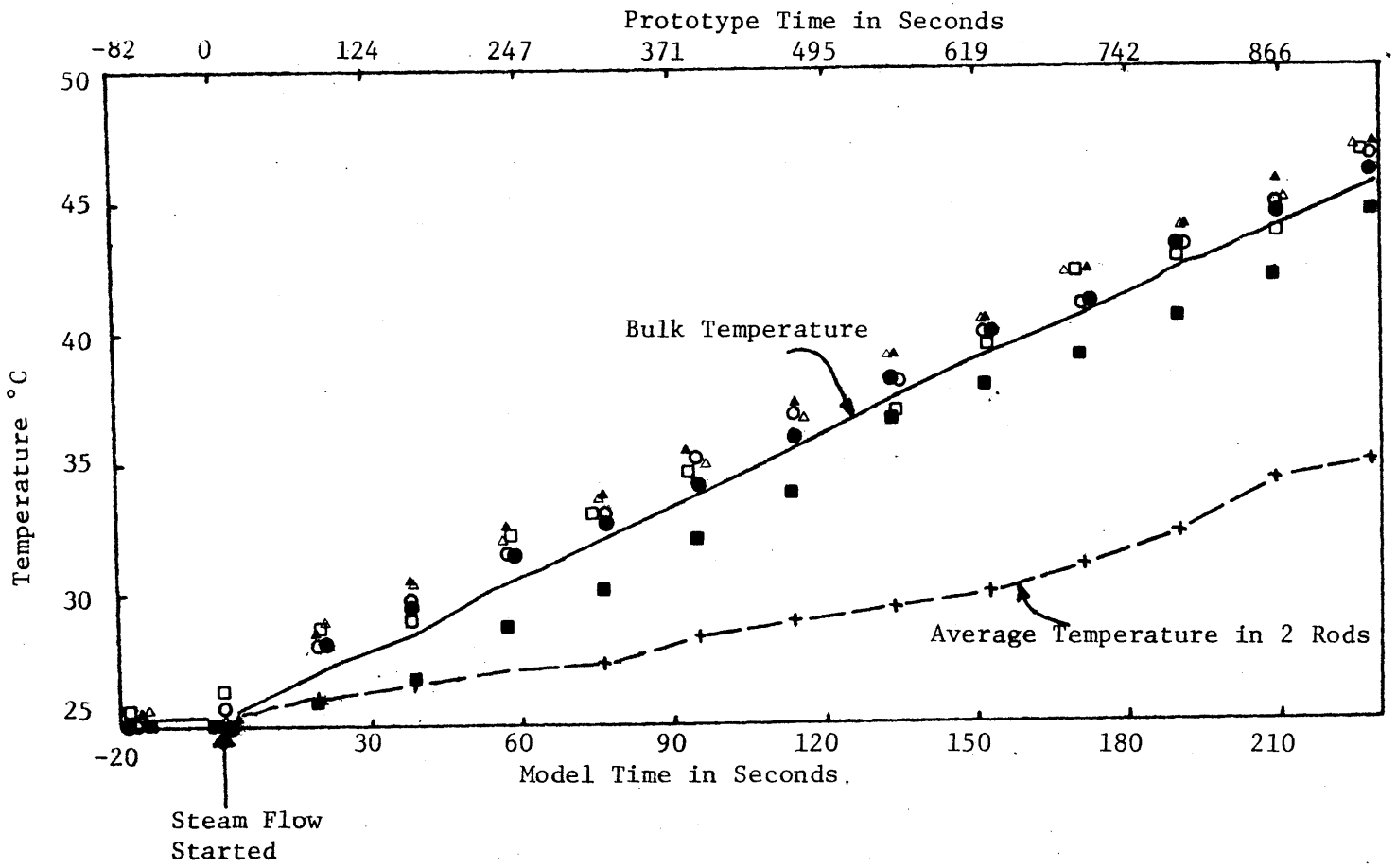

b) Temporal Temperature Distribution

Figure 25: Results for Experiment 17

4.3 Observations and Conclusions

Based on Figures 10-25 , the following observations and conclusions can be made.

1. For any given experiment, the spatial temperature distributions, and thus the range of temperatures, remains fairly constant with time. This allows one to conclude that the range of temperatures recorded over the duration of the experiments (of order 10 to 20 minutes in the prototype) would be representative of temperature ranges occurring at later times assuming that the steam injection rate was constant.

2. Maximum recorded temperatures occur in the near field while minimum temperatures occur in the far field. This reflects the finite time required for buoyancy and momentum driven circulation to advect heat away from the quencher location.

3. There is no significant sensitivity to the number of quencher ports. Experiments 7, 9 and 10, in which the quencher was changed, all show a spatial range in plotted temperature of about 3°C. This insensitivity suggests that the 35 port quencher used in the remaining tests provides an adequate approximation of the prototype quencher.

4. The induced temperature range is somewhat sensitive to the fractional area of flow resistance, varying from about 1.8°C to about 3°C to about 4°C as F_A varies from 0 to 8 to 16% in Experiments 8, 7, and 14. The sensitivity is caused by the increased drag associated with the increased fractional area occupied by columns. However, from observing the flow patterns, it is felt that most of this drag occurs <u>within the near field</u> rather than the far field. Within the near field the

Reynolds numbers are well within the turbulent range in both model and prototype suggesting that the pressure drag will be correctly scaled. Thus the remaining tests which were performed with F_A = 8% should be properly scaled with respect to near field drag. Since far field drag effects are expected to vary with Reynolds number, it is not possible from this comparison to determine the extent of the far field scale effect if any.

5. Increasing water depth from 17 feet to 26 feet (Exp. 7 to Exp. 12) reduces the time rate of change of the bulk temperature rise and reduces slightly the range of temperatures observed at any given time. (The range in temperature for Exp. 12 is about 2.5°C as opposed to about 3°C for Exp. 7). Apparently both reductions are associated with the increased opportunity for dilution allowed by the greater water depth.

6. Changing the quencher orientation to θ=0° (i.e. quencher axis tangent to the pool circumference, ports discharging radially) increases the range of observed temperatures due to poor circulation created by the decrease in jet trajectory. Thus in Exp. 11 the temperature range varies between about 4 and 5 °C as compared with about 3°C for Exp. 7. In Exp. 13 where H=26 feet and θ = 0, the temperature range varied between about 3.5°C and 4°C indicating that the negative effect of quencher orientation more than offset the positive effect of increased water depth.

7. Experiments 15 and 16 were performed with parameters representing the LaSalle installation: H = 26 feet, θ = 0° and $\Delta R/W$ = .20 (Exp. 15) and 0.76 (Exp. 16). The range of temperature for Exp. 15 was between

about 5.5 and 6.5°C - the highest range of any of the experiments and about twice the range in Exp. 7 which represents the Shoreham Station. For Exp. 16 the range was typically between about 3.5 and 4°C. The adverse performance of Exp. 15, in particular, is attributed to the extremely short near field jet trajectory caused by the proximity of the quencher to the inside wall and by the head-on orientation of the discharge ports.

8. The experiments appear highly repeatable. This is born out by comparison of the temperature ranges observed in Exps. 2-6 and 16-17. Within each of these two sets of experiments, temperature ranges vary at most by about 0.5°C. Thus 0.5°C appears to be a reasonable threshold to assign in assessing the significance of the sensitivity observed in the comparison above.

V SUMMARY AND CONCLUSIONS

This report addresses the distribution of induced temperature within a suppression pool caused by steam injection. The problem is first examined theoretically to identify the dominant zones and the approximate circulation and mixing associated with each zone. This analysis is then used to justify the scaling of a physical model to explore more quantitatively the induced temperature distributions.

A 1/17 undistorted scale model employing a steam source was used to conduct sixteen experiments. These tests complement some earlier tests performed at MIT by Soliva (1980) which used a hot water source in place of a steam source. Correct scaling (i.e., the prescription of model steam properties and the interpretation in prototype terms of measured temperatures) is achieved by insuring that the ratio of momentum to buoyancy forces is preserved from model to prototype. By relating the thermal energy of the steam discharge to an induced buoyancy flux of the jet once condensation occurs, this scaling is seen to be equivalent to densimetric Froude scaling.

Experiments were performed for two purposes: (1) to test the adequacy of approximations concerning quencher design and far field basin flow resistance which are inherent in the scaling process and (2) to explore the sensitivity of induced temperatures to geometric differences expected between the Shoreham Unit 1 and the LaSalle County installations. This sensitivity study will help allow prototype data collected at the LaSalle County Site to be applied to the Shoreham Station.

A prototype quencher consists of over 1,000 ports-far more than can be modeled in a sub-scale model. However, induced temperatures were

found to be insensitive to the number of quencher ports in the range $9 \leq N \leq 35$ implying that the thirty-five port quencher used in the majority of tests provides an adequate approximation to the prototype quencher.

Because of uncertainty regarding the scaling of far field flow resistance associated with basin support columns and downcomers, experiments were conducted with varying amounts of model resistance (fractional area of flow restriction between 0 and 16%). Measured temperatures were found to be sensitive to this resistance. However, after viewing the tests it was concluded that the majority of resistance occurs in the near field rather than the far field as originally suspected. Because the near field flow resistance can be accurately scaled it is felt that the subsequent tests performed with a fractional area of obstruction scaled geometrically from the prototype (F_A = 8%) should be reasonably accurate. Moreover, since the objective of the testing is to quantify the sensitivity of spatial temperature distribution to geometric differences between LaSalle and Shoreham, slight distortions are acceptable. They would be expected to affect each test in the same way and to roughly the same degree, leaving comparisons of one test to another relatively unaffected.

The LaSalle Country pool is characterized by a greater initial water depth and a different quencher location and orientation than Shoreham. Experiments show that the range of induced temperatures decreases with the larger water depth but increases with the LaSalle quencher location and orientation. Experiments corresponding to a LaSalle "inside" quencher (located near the reactor pedestal) showed a spatial range of temperatures approximately twice that of the Shoreham quencher. Experiments corresponding

to a LaSalle "outside"quencher (located near the reactor containment wall) showed a spatial range of temperatures approximately 15 to 30% above that for the Shoreham quencher.

It should be emphasized that these conclusions are based merely on a range of observed temperatures and do not relate to any definition of local-to-bulk temperature difference. However, by referring to the complete spatial distribution of measured temperatures for each experiment(refer to part a of Figures 10-25 for typical examples), one could compute such a difference for each experiment.

BIBLIOGRAPHY

Albertson, M.L., Dai, Y.B., Jensen, R.A. and Rouse, H. "Diffusion of Submerged Jets," Trans. ASCE, Vol. 115, 1950.

Daily, J.W. and Harleman, D.R.F., Fluid Dynamics, Addison-Wesley Publishing Co., Inc., Reading, Mass. 1966.

Jirka, G.H., Abraham, G., and Harleman, D.R.F., "An Assessment of Techniques for Hydrothermal Impact Prediction," R.M. Parsons Laboratory for Water Resources and Hydrodynamics, Report No. 203, MIT, 1975.

Jirka, G.H. and Harleman, D.R.F., "The Mechanics of Submerged Multi-port Diffusers for Buoyant Discharges in Shallow Water," R.M. Parsons Laboratory for Water Resources and Hydrodynamics, Report No. 169, MIT 1973.

Ryan, P.J., Harleman, D.R.F., and Stolzenbach, K.D., "Surface Heat Loss from Cooling Ponds," Water Resources Research, Vol. 10, No. 5, Oct. 1974.

Schlichting, H., Boundary Layer Theory, 7 th edition, McGraw Hill, New York, 1979.

Soliva, J-C., "Analytical and Experimental Analysis of Vapor Suppression Pool Mixing and Circulation," S.M. Thesis, Dept. of Civil Engineering, M.I.T., July 1980.

Stanford, L.E. and Webster, C.C., "Energy Suppression and Fission Product Transport in Pressure-Suppression Pools," Oak Ridge National Laboratory, Report No. ORNL-TM-3448, 1972.

Ungate, C.D., Harleman, D.R.F., and Jirka, G.H., "Mixing of Submerged Turbulent Jets at Low Reynolds Numbers," R.M. Parsons Laboratory for Water Resources and Hydrodynamics, Report No. 197, MIT, 1975.

Wright, S.J., "Mean Behavior of Buoyant Jets in a Crossflow," Journal of the Hydraulics Division, ASCE, Vol. 103, HY5, May, 1977.

Yevdjevich, V.M., "Diffusion of Slot Jets with Finite Length-Width Ratios," Hydraulic Papers, Colorado State University, Ft. Collins, Colorado, No. 2, 1966.

LIST OF FIGURES

LIST OF TABLES

LIST OF SYMBOLS

A	discharge (total) cross-sectional area
B	discharge kinematic buoyancy flux
b	discharge "slot" width (2-D plane source representation)
C_D	drag coefficient associated with basin obstacles
c	speed of sound in fluid
c	specific heat of water
D	discharge jet diameter (axisymmetric source representation)
D	diameter of basin obstacle
E	discharge energy flux
F, F_{Drag}	drag force on basin obstacle
$F_{Boundary}$	boundary friction force
F_{Tot}	total force
$\mathbb{F}$	discharge densimetric Froude number
$\mathbb{F}_{HC}$	a densimetric Froude number based on boundary resistance used to compute densimetric exchange flow
F_A	fraction of basin area occupied by resistance rods
f_e	equivalent bottom friction factor including cyclinder drag
f_o	bottom friction factor
G	discharge mass rate
g	acceleration of gravity
H	water depth
h	fluid enthalpy
Δh	enthalpy difference between discharge and ambient fluid
k	kinematic water surface heat exchange coefficient
L	far field channel length used in computation of densimetric exchange flow
L_m	near field channel length
ℓ	characteristic jet dimension
$\mathbb{M}$	discharge Mach number
M	discharge kinematic momentum flux

N	number of far field obstacles (support columns and downcomers)
Q	discharge flow rate
$\mathbb{R}$	Reynolds number
ΔR	radial position of quencher within basin
S	dilution
s	coordinate along jet trajectory
T	temperature
T_i	initial basin temperature
Y	discharge jet submergence
t	time
u	discharge velocity
v	ambient flow velocity
W	basin width
$\vec{x}$	spatial coordinates
x	basin wetted perimeter
α	fluid thermal diffusivity
β	coefficient of thermal expansion
ε	bottom roughness length
θ	horizontal angle between quencher axis and pool tangent
ρ	fluid density
$\Delta\rho$	density difference between ambient fluid and discharge
ν	fluid kinematic viscosity

Additional subscripts

bulk	bulk denotes bulk temperature
c	denotes end of condensation zone
i	denotes an individual downcomer or support column
m	denotes model value
p	denotes prototype value
r	denotes ratio between model and prototype
s	denotes (steam) source
w	denotes water source
o	denotes (equivalent water) source
1,2,3,4,5	denotes zone of analysis